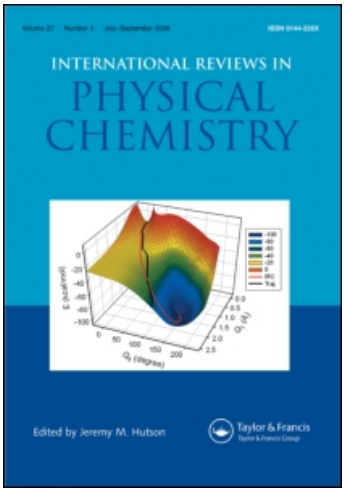

International Reviews in Physical Chemistry
Publication details, including instructions for authors and subscription information:
http://www.informaworld.com/smpp/title~content=t713724383

Dynamical processes in the lowest-excited triplet metal-to-ligand charge transfer states of ruthenium and osmium diimine complexes in crystals

Hans Riesen; Lynne Wallace; Elmars Krausz

Online publication date: 26 November 2010

To cite this Article Riesen, Hans , Wallace, Lynne and Krausz, Elmars(1997) 'Dynamical processes in the lowest-excited triplet metal-to-ligand charge transfer states of ruthenium and osmium diimine complexes in crystals', International Reviews in Physical Chemistry, 16: 3, 291 — 359
To link to this Article: DOI: 10.1080/014423597230217
URL: http://dx.doi.org/10.1080/014423597230217

INTERNATIONAL REVIEWS IN PHYSICAL CHEMISTRY, 1997, VOL. 16, NO. 3, 291–359

Dynamical processes in the lowest-excited triplet metal-to-ligand charge transfer states of ruthenium and osmium diimine complexes in crystals

by HANS RIESEN†, LYNNE WALLACE and ELMARS KRAUSZ

Research School of Chemistry, The Australian National University, Canberra, ACT 0200, Australia

This review presents a detailed description of the lowest-excited states in ruthenium(II) and osmium(II) diimine complexes, based on extensive studies of their optical spectra in crystalline environments. Deuteration, and Zeeman and Stark effects provide a wealth of incisive results. The transferred charge in the lowest-excited triplet metal-to-ligand charge transfer states is localized on a single ligand in ruthenium(II) diimine complexes and the excitation exchange interaction between equivalent metal–ligand subunits is $< 0{\cdot}5\ cm^{-1}$. Localization gives rise to subtle effects, such as small Stokes shifts, in spectra. The lowest-excited states of osmium(II) diimine complexes in crystals with low inhomogeneous broadening are well described as coherent intramolecular excitons with excitation exchange interactions in the range from 2 to 30 cm^{-1}.

1. Introduction

The spectral, photophysical and photochemical properties of $[Ru(bpy)_3]^{2+}$ (bpy = 2,2′-bipyridine) and $[Os(bpy)_3]^{2+}$ have been the subject of many studies over the last two decades (DeArmond and Carlin 1981, Kalyanasundaram 1982, Meyer 1984, Ferguson *et al.* 1985, Juris *et al.* 1988, Krausz and Ferguson 1989). Novel applications of the $[Ru(bpy)_3]^{2+}$ complex and its derivatives have been found in analytical chemistry (Downey and Nieman 1992) and in solar energy conversion (Grätzel 1991). The nonlinear optical properties of $[Ru(bpy)_3]^{2+}$ have also received some interest (Dhenaut *et al.* 1995).

The driving force for many studies has been the fundamental question as to whether the transferred charge in the luminescent lowest-excited triplet metal-to-ligand charge transfer (^{3}MLCT) states in the $[Ru(bpy)_3]^{2+}$ and $[Os(bpy)_3]^{2+}$ complexes is delocalized over all three ligands or localized on a single ligand on the electronic timescale. In the latter case, stochastic *intramolecular* excitation energy transfer occurs in the characteristically long-lived lowest-excited ^{3}MLCT states.

It is well accepted that the lowest-excited ^{3}MLCT states in $[Ru(bpy)_3]^{2+}$ and $[Os(bpy)_3]^{2+}$ are localized in *solutions* and *frozen glasses* (Bradley *et al.* 1981, Forster and Hester 1981, Smothers and Wrighton 1983, Caspar *et al.* 1984, Gex *et al.* 1987, Krause 1987, Caroll and Brus 1987, Kato *et al.* 1989, Danzer and Kincaid 1990, Malone and Kelley 1991, Danzer *et al.* 1993, Striplin and Crosby 1994, Pogge and Kelley 1995). Strong evidence has been obtained from excited state resonance Raman (ERR) experiments (Bradley *et al.* 1981, Smothers and Wrighton 1983, Danzer and Kincaid 1990). Notably, the same ERR frequencies were observed for the mono-bpy complex *fac*-$XRe(CO)_3(bpy)$ with X = Cl or Br as for the $[Ru(bpy)_3]^{2+}$ complex

† Author for correspondence.

0144–235X/97 $12·00

(Smothers and Wrighton 1983). The ERR work has also been performed in frozen glasses (Caroll and Brus 1987) where again the same frequencies were observed. It then follows that the primary localization in solution cannot be due to a solvent relaxation process.

Evidence for a localized description was also provided by the work on $[Ru(bpy)(CN)_4]^{2-}$ (Kato *et al.* 1989). This mono-bpy complex shows very similar energy separations of the three lowest-excited ^{3}MLCT states as the tris-bpy complex.

Inhomogeneous broadening of optical excitations is a general phenomenon in condensed matter. A spread of transition energies arises from variations of the local environments of individual chromophores. The inhomogeneous width is usually many orders of magnitude larger than the homogeneous line width. The inhomogeneous broadening in solutions and glasses of metal-to-ligand charge transfer (MLCT) transitions can be in the order of 1000 cm^{-1}. Importantly, each *individual* ligand in a metal tris-diimine complex has an independently different environment. We term this variation at the molecular level nanoheterogeneity. For example, such nanoheterogeneity gives rise to large low symmetry fields in the spectroscopy of the $^2E \leftarrow {}^4A_2$ transition of the nominally trigonal $[Cr(bpy)_3]^{3+}$ in amorphous hosts (Riesen and Krausz 1992).

As a consequence of the nanoheterogeneity, the energies of MLCT transitions to each ligand in an individual $[Ru(bpy)_3]^{2+}$ complex differ. Since the lowest-excited states are localized in solutions and glasses, the inhomogeneous width determines an upper limit for the excitation exchange interaction β (Zewail *et al.* 1982) between the metal–ligand subunits. β must be considerably smaller than the inhomogeneous spread (see section 2). The transferred charge would be delocalized over all ligands if the excitation exchange interaction β was comparable to or larger than the inhomogeneous width.

By using laser spectroscopies, we have gained a detailed and consistent understanding of the lowest-excited ^{3}MLCT states in ruthenium and osmium diimine complexes. Introductions to laser based techniques such as luminescence line narrowing and spectral-hole burning have been presented by Yen and Selzer (1981), Friedrich and Haarer (1984), MacFarlane and Shelby (1987), Moerner (1988), Völker (1989), and Riesen and Krausz (1993a). Stark effects and isotope shifts in particular provided direct evidence for the nature of the lowest-excited states. In this review we provide a summary of published work as well as presenting significantly improved and illustrative unpublished data.

2. Basic theoretical concepts

2.1. *Exciton coupling*

A phenomenological description of weak coupling between metal–ligand subunits in the lowest-excited ^{3}MLCT states of $[M(L)_3]^{2+}$ (L = diimine) complexes is provided by using an exciton formalism. In the following we neglect effects of vibronic coupling. Useful introductions to exciton theory have been presented by Craig and Walmsley (1968), Davidov (1962), Burland and Zewail (1979), Zewail *et al.* (1982) and Broude *et al.* (1985). The basis functions for an intramolecular exciton description are given in equation (1) where ϕ_i is the wavefunction of the metal–ligand subunit i. The asterisk denotes the excited metal–ligand subunit.

$$\Phi_1 = |\phi_1^* \phi_2 \phi_3|, \quad \Phi_2 = |\phi_1 \phi_2^* \phi_3|, \quad \Phi_3 = |\phi_1 \phi_2 \phi_3^*|. \tag{1}$$

The electronic Hamiltonian describing a single exciton level is then given by equation (2)

$$\mathscr{H} = \mathscr{H}_1 + \mathscr{H}_2 + \mathscr{H}_3 + \mathscr{V} \tag{2}$$

where $\mathscr{H}_1$, $\mathscr{H}_2$ and $\mathscr{H}_3$ are the Hamiltonians of the individual metal–ligand subunits with

$$\langle \Phi_i | \mathscr{H}_i | \Phi_i \rangle = \varepsilon_i. \tag{3}$$

β is the matrix element of the interaction potential $\mathscr{V}$ between two subunits.

$$\langle \Phi_1 | \mathscr{V} | \Phi_2 \rangle = \langle \Phi_1 | \mathscr{V} | \Phi_3 \rangle = \langle \Phi_2 | \mathscr{V} | \Phi_3 \rangle = \beta. \tag{4}$$

Using the basis set and the Hamiltonian given in equations (1) and (2), respectively, the secular equation (5) follows

$$\begin{array}{c} \quad \Phi_1 \quad\quad \Phi_2 \quad\quad \Phi_3 \\ \left\{ \begin{vmatrix} \varepsilon_1 - \lambda & \beta & \beta \\ \beta & \varepsilon_2 - \lambda & \beta \\ \beta & \beta & \varepsilon_3 - \lambda \end{vmatrix} \right\} \end{array} = 0. \tag{5}$$

For identical ligands ($\varepsilon_1 = \varepsilon_2 = \varepsilon_3$) eigenvectors and eigenvalues λ of the secular equation (5) are given in (6) and (7)

$$\Psi_A = (1/3^{1/2})(\Phi_1 + \Phi_2 + \Phi_3) \quad \text{with the energy } \varepsilon + 2\beta, \tag{6}$$

$$\Psi_{E_\pm} = \mp(1/3^{1/2})(\Phi_1 + \exp[\pm i2\pi/3]\,\Phi_2 + \exp[\pm i4\pi/3]\,\Phi_3)$$
$$\text{with the energy } \varepsilon - \beta. \tag{7}$$

The subscripts A and $E_\pm$ refer to irreducible representations in the D_3 point group.

Upon deuteration of all n hydrogen atoms of a diimine ligand i the ^{3}MLCT transition energy associated with this particular ligand, ε_i, shifts to higher energy by Δ_n. If only p hydrogen atoms are exchanged by deuterium (partial deuteration) a partial shift $\Delta_p \approx (p/n)\,\Delta_n$ results. This isotopic shift is of course associated with differences of the zero point energies. Vibrational frequencies of the reduced ligand (in the ^{3}MLCT state) in general shift to lower energy and hence upon deuteration the difference of the sum of zero point energies between the ground state and the excited state increases that is to say there is a blue shift.

It is possible to synthesize complexes in which one, two or three ligands have the same degree of deuteration. In a specifically deuterated complex which has one deuterated ligand the *lowest-energy* exciton becomes confined to the two protonated ligands if $|\beta|$ is much smaller than the deuteration shift. Correspondingly, the exciton becomes localized on the protonated ligand in a system with two deuterated ligands. These cases are schematically portrayed in figure 1.

When the excitation exchange interaction β is of the same order of magnitude as, or larger than the deuteration shift, specific deuteration will not lead to full localization of the exciton.

The effects of nanoheterogeneity (see above) are taken into account by allowing the diagonal energies ε_i in the equation (5) to vary *independently*. This static diagonal disorder effectively breaks the symmetry of the nominally trigonal system. If this disorder is substantially larger than the excitation exchange interaction β, the ^{3}MLCT excitons become localized.

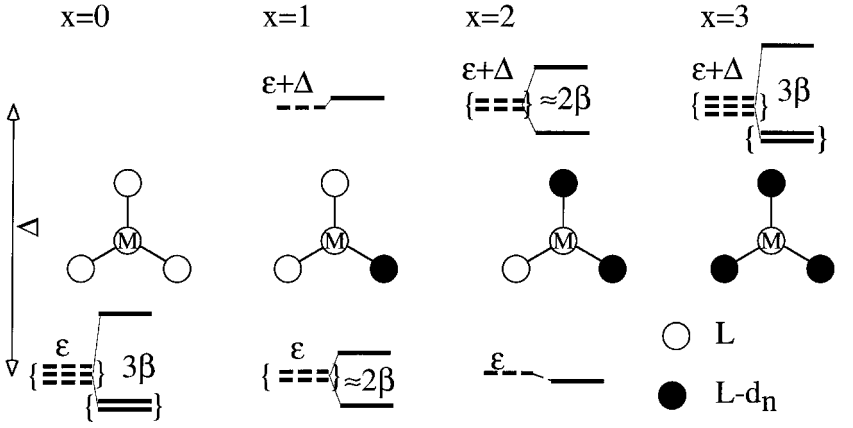

Figure 1. Localization of an *intramolecular* ^{3}MLCT exciton in the series of specifically deuterated complexes $[M(L)_{3-x}(L\text{-}d_n)_x]$ (x = 0–3) (L = diimine). The deuteration shift Δ_n is 9 times larger than the excitation exchange interaction β. Parentheses indicate degenerate levels. The levels for $\beta = 0$ are shown as dashed lines.

An important parameter is the ratio of the excitation exchange interaction and the diagonal disorder, which is approximated by the inhomogeneous line width Γ_ε. This ratio can be used to estimate the lower limit for the coherence η_c of the exciton in a trigonal $[M(L)_3]^{2+}$ system according to following equation (Zewail *et al.* 1982).

$$\eta_c = \frac{3\beta}{\Gamma_\varepsilon}. \tag{8}$$

The exciton is localized when $\eta_c \ll 1$.

The ^{3}MLCT transitions to one ligand lie at significantly higher energy in some crystal systems (see sections 3 and 4). In this case the lowest-excited ^{3}MLCT states involve the two crystallographically equivalent ligands only. The exciton formalism then reduces to the simplest case of the mini-exciton (Botter *et al.* 1976). The basis functions and the secular equation are given by

$$\Phi_1 = |\phi_1^* \phi_2|, \ \Phi_2 = |\phi_1 \phi_2^*| \tag{9}$$

and

$$\begin{array}{cc} \Phi_1 & \Phi_2 \\ \begin{pmatrix} \varepsilon_1 - \lambda & \beta \\ \beta & \varepsilon_2 - \lambda \end{pmatrix} & = 0 \end{array} \tag{10}$$

with the eigenvalues $\lambda_\pm$

$$\lambda_\pm = \frac{\varepsilon_1 + \varepsilon_2}{2} \pm \frac{[(\varepsilon_1 + \varepsilon_2)^2 + 4\beta^2]^{1/2}}{2} \tag{11}$$

and the eigenvectors Ψ_+, Ψ_-

$$\begin{aligned} \Psi_+ &= \cos\gamma\Phi_1 + \sin\gamma\Phi_2, \\ \Psi_- &= \sin\gamma\Phi_1 - \cos\gamma\Phi_2, \end{aligned} \tag{12}$$

where $\tan 2\gamma = 2\beta/(\varepsilon_2 - \varepsilon_1)$.

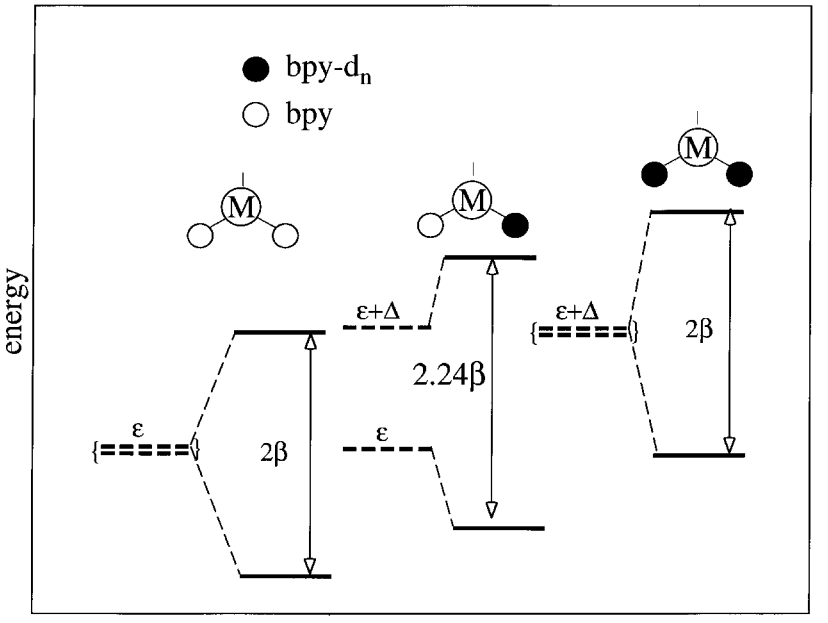

Figure 2. Deuteration effects on the energies of the Davidov components of an intramolecular ^{3}MLCT exciton in a system with two equivalent ligands. The solid lines are for $\beta = \Delta$. The dashed lines are for $\beta = 0$.

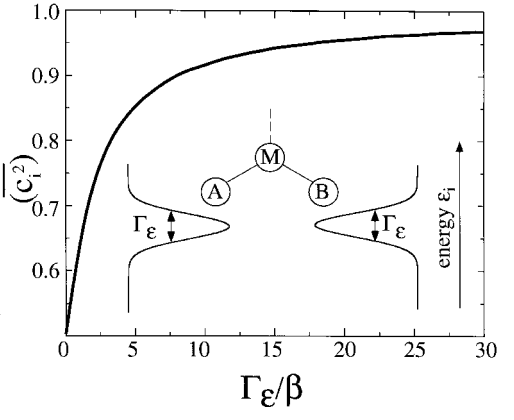

Figure 3. Degree of localization of the lowest-energy ^{3}MLCT exciton in a system with two equivalent ligands as a function of the ratio Γ_ε/β. Independent Gaussian distributions of the energies ε_i of the two ligands with equal centre frequency and widths Γ_ε are assumed. $\overline{c_i^2}$ is the probability that the transferred electron is on the ligand with the lower energy ε_i.

It is possible to have one or both crystallographically equivalent ligand(s) deuterated. In a system which has one of the crystallographically equivalent ligands deuterated, the *lowest-energy* exciton becomes localized on the protonated ligand if $|\beta|$ is much smaller than the deuteration shift. In figure 2 we show the situation when the excitation exchange interaction β is equal to the deuteration shift Δ. In this case the lowest-energy level moves to higher energy by approximately half the full deuteration shift when one of the equivalent ligands is deuterated.

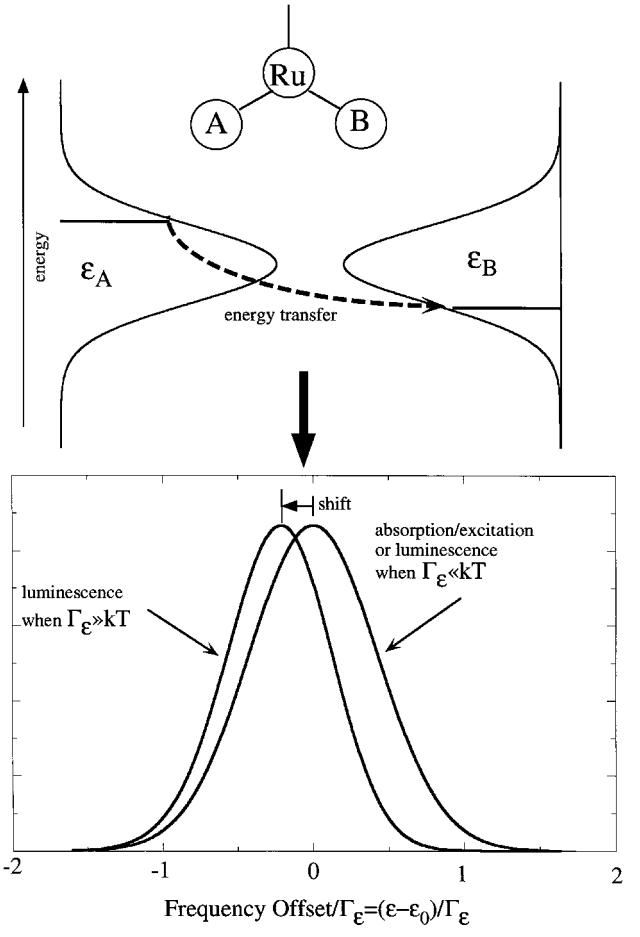

Figure 4. Effect of intramolecular ^{3}MLCT energy transfer on the position and line width of the electronic origin in luminescence for a complex with two equivalent ligands. Independent Gaussian distributions for $\varepsilon_{A,B}$ of ligands A and B were assumed to calculate the lineshapes in the lower panel (see text).

2.2. *Spectral consequences of localization and nanoheterogeneity*

As is discussed above for the trigonal case, nanoheterogeneity can lead to localization of excitons. Figure 3 illustrates this localization process for the mini-exciton which is described in the secular equation (10). Independent (non-correlated) Gaussian distributions with width Γ_ε are taken for the diagonal energies ε_A and ε_B. When $\Gamma_\varepsilon/\beta = 7{\cdot}5$ the probability c_1^2 (given as the average of the square of the amplitude of the wavefunction) of finding the transferred electron on the lower-energy ligand is $\approx 0{\cdot}9$ at lowest temperature. We consider this to be a localized case, that is to say the excited states are localized if the excitation exchange interaction is about seven times smaller than the static diagonal disorder.

Stochastic intramolecular transfer of localized excitation energy from one subunit to the crystallographically equivalent subunit is fast compared to the luminescence lifetimes. Interactions of a fraction of a wavenumber provide transfer rates of the order of magnitude of or greater than 1×10^9 s^{-1}.

Fast intramolecular excitation energy transfer has important consequences in the

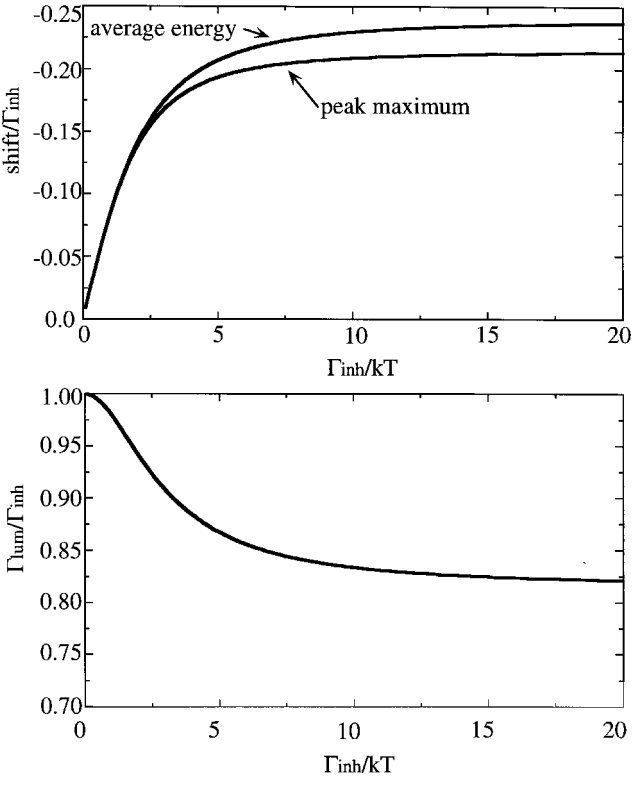

Figure 5. Effects of intramolecular energy transfer on the peak position and the line width. The upper panel shows the shift of the average energy and the peak maximum of the electronic origin in luminescence of a complex with two equivalent ligands as a function of the ratio of the inhomogeneous distribution Γ_{inh} and the temperature T. The lower panel shows the corresponding dependence of the line width of the origin in non-selectively excited luminescence. Independent Gaussian distributions of width Γ_{inh} are assumed for $\varepsilon_{A,B}$.

spectroscopy of localized ^{3}MLCT states ($\beta \ll \Gamma$). Firstly, the luminescence decays as a single exponential. Secondly, small apparent Stokes shifts result between origin features observed in excitation and luminescence, since the ^{3}MLCT excitation energy flows to the ligand with the lowest energy, ε_i, at lowest temperature. This situation can be readily modelled. The distributions of the energies ε_i, of the two metal–ligand subunits are described by independent Gaussians of width $\Gamma_\varepsilon = \Gamma_{inh}$ and centre frequency ε_0. The lineshape as a function of the temperature of the electronic origin in luminescence is then given by

$$f(\varepsilon, T) = N \exp\left[-4 \ln 2 \left(\frac{\varepsilon - \varepsilon_0}{\Gamma_\varepsilon}\right)^2\right] W(\varepsilon, T), \tag{13}$$

where N is a normalization factor and

$$W(\varepsilon, T) = \int_{-\infty}^{\infty} \exp\left[-4 \ln 2 \left(\frac{y - \varepsilon_0}{\Gamma_\varepsilon}\right)^2\right] \frac{\exp\left[-\dfrac{\varepsilon - \varepsilon_0}{kT}\right]}{\exp\left[-\dfrac{\varepsilon - \varepsilon_0}{kT}\right] + \exp\left[-\dfrac{y - \varepsilon_0}{kT}\right]} \mathrm{d}y. \tag{14}$$

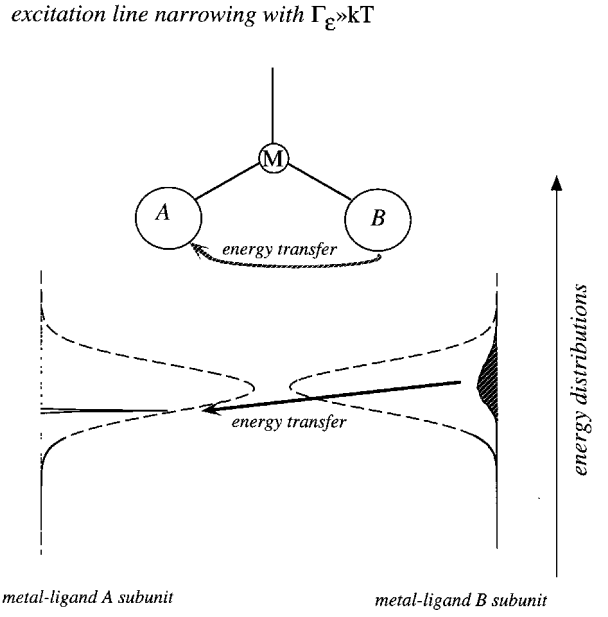

Figure 6. Schematic representation of excitation line narrowing experiments for localized ^{3}MLCT transitions in a system with two equivalent ligands (A and B). The ^{3}MLCT transitions to the third ligand are assumed to be significantly higher in energy. The ^{3}MLCT transition of ligand A is narrowed by selectively monitoring the luminescence. The shaded area highlights the distribution of the ^{3}MLCT excitations of ligand B which are deactivated by intramolecular excitation energy transfer to A when $\Gamma_\varepsilon \gg kT$. ^{3}MLCT energies of A and B are independent.

When $\Gamma_\varepsilon \gg kT$ the following limit is obtained for $f(\varepsilon, T)$

$$f(\varepsilon, \Gamma_\varepsilon \gg kT) = N \exp\left[-4 \ln 2 \left(\frac{\varepsilon - \varepsilon_0}{\Gamma_\varepsilon}\right)^2\right] \operatorname{erfc}\left[\frac{(\varepsilon - \varepsilon_0)\, 2(\ln 2)^{1/2}}{\Gamma_\varepsilon}\right], \qquad (15)$$

where erfc is the complementary error function.

The high temperature limit converges to the original Gaussian distribution. Figure 4 shows the lineshape in the two limits $\Gamma_\varepsilon \gg kT$ and $\Gamma_\varepsilon \ll kT$. Figure 5 presents the dependence of the observed full width at half maximum in luminescence Γ_{lum}, the peak maximum and the average energy of the origin in luminescence as a function of Γ_ε/kT. The curves in figures 4 and 5 are calculated by using equations (13) and (14). The calculations illustrated in figure 5 show that at lowest temperature a small Stokes shift of the electronic origin of $\approx 0{\cdot}2\Gamma$ between luminescence and absorption results. The full width at half maximum of the origin is reduced in luminescence by $\approx 20\%$ in comparison with measurements made in absorption or excitation.

2.3. *Line narrowing experiments in localized transitions*

The combined action of intramolecular ^{3}MLCT excitation energy transfer and nanoheterogeneity gives rise to characteristic features in excitation and luminescence line narrowing experiments. It is possible to observe distinct ^{3}MLCT transitions to the three ligands in a trigonal lattice or to both ligands in a lattice with two crystallographically equivalent ligands.

We discuss here the latter case in more detail. Either of the two crystallographically equivalent ligands can have its ^{3}MLCT transitions at lower/higher energy. Figure 6

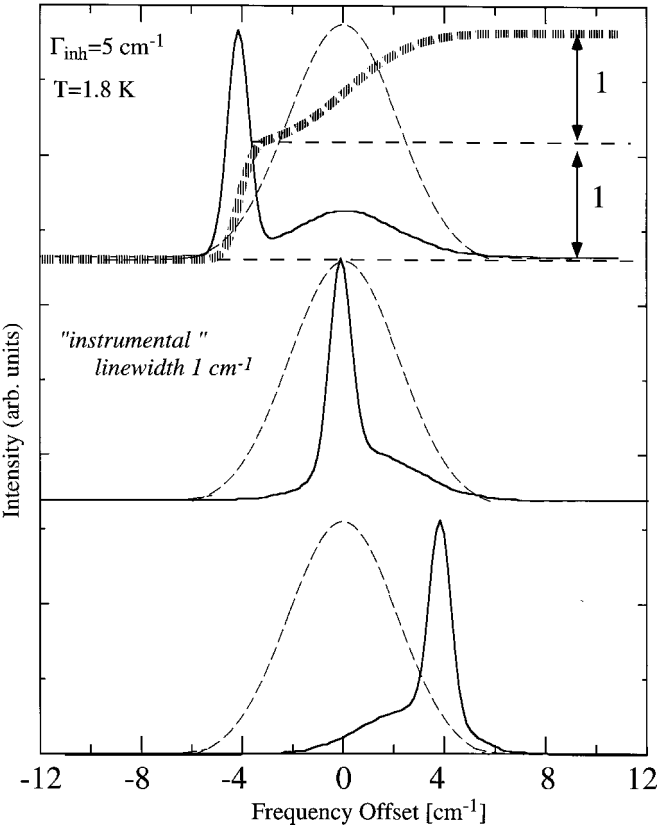

Figure 7. Simulated excitation line narrowing spectra of a localized ^{3}MLCT transition in a system with two equivalent ligands. The luminescence is monitored at (top) the low edge, (centre) the centre and (bottom) the high edge of the inhomogeneously broadened line. The inhomogeneous distribution and the integral of one of the simulated spectra are indicated by dashed lines. Independent Gaussian distributions are assumed for $\varepsilon_{A,B}$.

shows the case where the ^{3}MLCT transition to ligand A has arbitrarily been chosen to lie at low energy. In an excitation line narrowing experiment we observe a narrowed feature due to ligand A whose ^{3}MLCT transition is directly excited. The broader feature is due to ligand B in the (non-correlated) crystallographically equivalent position. Ligand B transfers its ^{3}MLCT excitation energy to ligand A after being excited, for the cases when its ^{3}MLCT transition is higher in energy. The width of the broader feature reflects the lack of correlation of the energies of the two subunits.

Figure 7 shows simulated excitation line narrowing experiments for three wavelengths at which the luminescence is monitored. When the emission is detected at the red edge of the inhomogeneous distribution of the luminescence, the intensity ratio of the narrowed to the broad feature approaches 1:1. Similar behaviour is predicted for three equivalent ligands, but with different statistics. In this latter case the ^{3}MLCT transition of one ligand is resonantly observed and the other two ligands lead to a broad feature with twice the intensity of the narrowed feature when the luminescence is measured at the red edge of the inhomogeneous distribution of the luminescence origin.

Excitation line narrowing experiments can provide an upper limit for the excitation

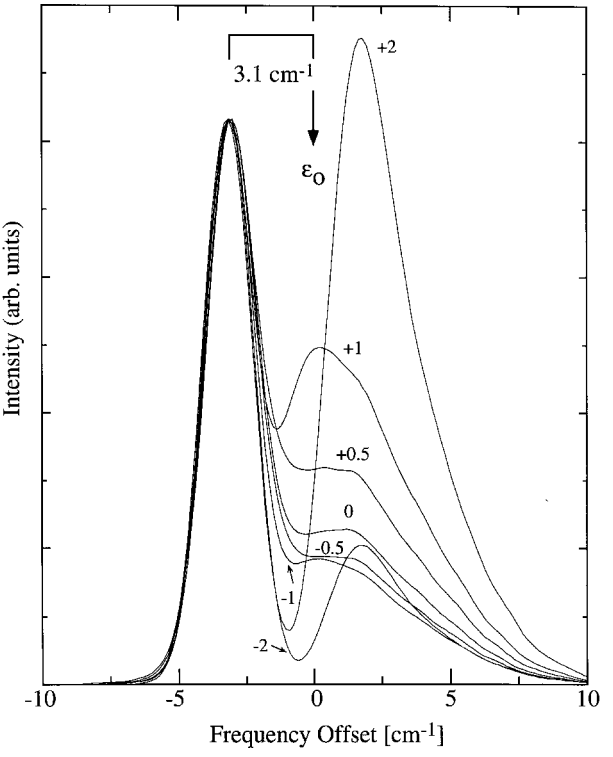

Figure 8. Simulations of narrowed excitation spectra in a system with two equivalent ligands. Values of β are indicated. Other parameters are $\Gamma_m = 1{\cdot}2\ cm^{-1}$, $T = 1{\cdot}8$ K, $\Gamma_{laser} = 1{\cdot}1\ cm^{-1}$, $\Gamma_{inh} = 3{\cdot}5\ cm^{-1}$. The luminescence is monitored $3{\cdot}1\ cm^{-1}$ to lower energy of the centre frequency ε_0 of the distribution. The frequency offset is relative to ε_0.

exchange interaction β. This is illustrated in figure 8 for the case of two equivalent ligands. The following assumptions were taken in these simulations; diagonal energies ε_i of the two metal–ligand subunits are non-correlated and described by Gaussian distributions of width Γ_s, intramolecular energy transfer leads to thermalization of all levels (Boltzmann distribution), the energies ε_i(I), ε_i(II) and ε_i(III) (i = A or B) on one metal–ligand subunit are well correlated. The instrumental widths of the monochromator and the laser are provided by Gaussians of width Γ_m and Γ_{laser}. The Gaussian distributions of the non-correlated energies ε_A and ε_B are then generated by a random generator. About 40 000 calculations were accumulated in order to achieve adequate convergence.

When $\beta \neq 0$ the eigenvalues and eigenvectors are determined using equations (11) and (12) in each calculation. The transition intensities are calculated from the eigenvectors. The transition dipoles were arbitrarily assumed to lie in the metal–ligand plane and perpendicular to the metal–ligand directions. Reversing the sign of β in this calculation has the same effect as taking the transition dipoles to lie parallel to the metal–ligand directions. Figure 8 illustrates that the exciton splitting becomes relevant for $|\beta| \geqslant \Gamma_{inh}/3$ where two well separated transitions start to emerge. Naturally, if $|\beta| \geqslant \Gamma_{inh}$ two distinct transitions are also observed in *non-selective* spectroscopy.

Results complementary to those in excitation line narrowing are obtained in luminescence line narrowing. In particular, for excitation at the high energy side of an

origin, one predicts a narrowed feature due to the ligand whose ^{3}MLCT state is directly excited and a broad feature due to the ligand in the crystallographically equivalent position, whose ^{3}MLCT state is fed by intramolecular excitation transfer from the primarily excited ligand. In time resolved luminescence line narrowing experiments the intramolecular excitation transfer can then be observed by measuring the kinetics of the narrowed and the broad feature (see section 5.4).

3. Crystal structures

3.1. $[Ru(bpy)_3](PF_6)_2$

The room temperature crystal structure of racemic $[Ru(bpy)_3](PF_6)_2$ was reported by Rillema *et al.* (1979). The $P\bar{3}c1$ structure preserves the inherent D_3-32 symmetry of the $[Ru(bpy)_3]^{2+}$ cation. There is only a single D_3 $[Ru(bpy)_3]^{2+}$ chromophoric site because the two enantiomeric cations per unit cell are inversion related.

A low temperature structure for $[Ru(bpy)_3](PF_6)_2$ was subsequently reported by Biner *et al.* (1992). A phase change occurs on cooling. At about 190 K the crystal symmetry remains trigonal but the unit cell triples to form the spacegroup P31c. The old tertiary axes become the new secondary axes. The structure modulation consists of small relative rotations of the $[Ru(bpy)_3]^{2+}$ units about their threefold axes giving rise to three inequivalent sites in the asymmetric unit, each of C_3-3 symmetry.

Direct spectroscopic observation of the three sites, energetically separated by ≈ 40 cm^{-1}, has been previously made by doping the crystal with $[Os(bpy)_3]^{2+}$ (Braun *et al.* 1989). Fast *intermolecular* energy transfer processes ensures that the luminescence in the neat $[Ru(bpy)_3](PF_6)_2$ material is dominated by the lowest-energy $[Ru(bpy)_3]^{2+}$ site at low temperatures.

3.2. $[Zn(bpy)_3](ClO_4)_2$ *and* $[Ru(bpy)_3](ClO_4)_2$

Racemic $[Ru(bpy)_3](ClO_4)_2$ and racemic $[Zn(bpy)_3](ClO_4)_2$ are isomorphous and crystallize in the monoclinic spacegroup $C2/c$ with 4 formula units per unit cell (Harrowfield and Sobolev 1994, Krausz *et al.* 1995). The structure can be described as a commensurate modulation of an idealised structure of $P\bar{3}c1$ spacegroup symmetry. In this structure two equivalent cations of D_3-32 symmetry are *c*-glide related. The structural modulation preserves one third of the *c*-glide operations and lowers the site symmetry of the cation to C_2-2. All cations are still equivalent but within a single cation one bpy ligand lies about the symmetry axis (the crystal *b* axis) while the other two ligands are equivalent, being related by the symmetry axis. The two pyridine halves of each of these latter ligands are not equivalent. Figure 9 shows a projection of a layer of the $[Ru(bpy)_3](ClO_4)_2$ structure down the *c* axis. An adjacent layer is *c*-glide related, Ru and Cl atoms being approximately on the *c* glide perpendicular to the *b* axis. The quasi-trigonal axis of the cation is within 1° of the *c* axis.

The bite angles and bond lengths are similar for all three ligands, Ru–N1 2·063(5), Ru–N2 2·062(5), Ru–N3 2·054(5) Å, N1–Ru–N2 78·8(2)°, N3–Ru–N3 78·5(3)°. However, the distinct ligand has a moderately different anion environment in comparison with the crystallographically equivalent ligands. This leads to a difference in MLCT transition energies.

The energy difference between the charge-transfer transitions to the two crystallographically equivalent ligands and the crystallographically distinct ligand due to the crystallographic variations can be estimated by a point charge calculation. The

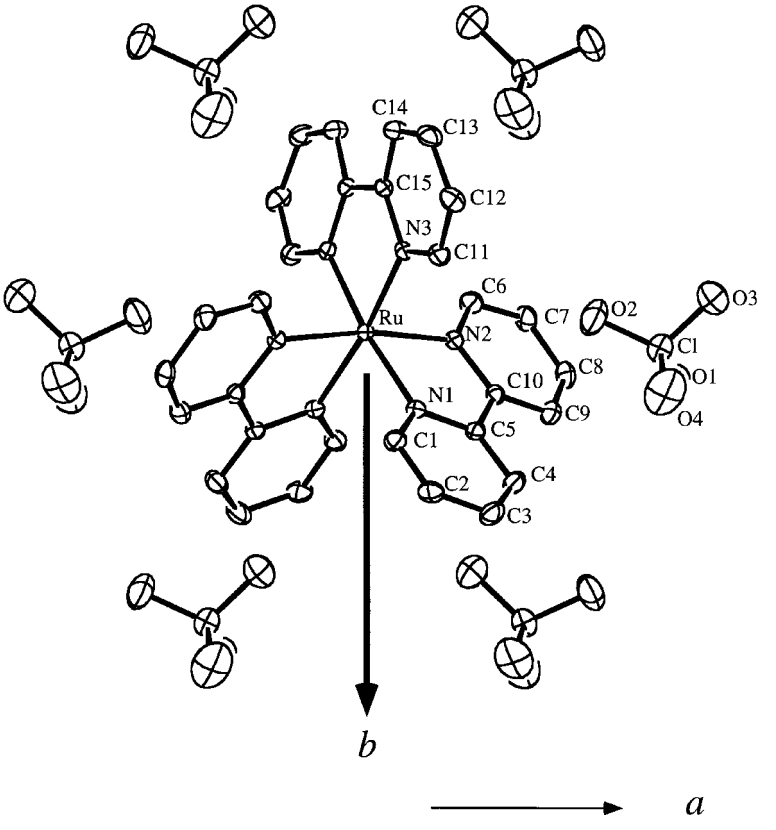

Figure 9. Projection of a layer of the $[Ru(bpy)_3](ClO_4)_2$ structure down the crystal c axis.

potential energy of an electron on the nitrogen atom with coordinate r is approximated by equation (16) where R_i is the coordinate of an outer sphere ion with charge $-Z_i e$ ($Z_i < 0$ and $Z_i > 0$ for positive and negative charges, respectively)

$$V_c = \sum^{i} \frac{Z_i e^2}{|r - R_i|}. \tag{16}$$

In $[Ru(bpy)_3](ClO_4)_2$ the potential energy for an electron on the nitrogen N3 of the distinct ligand is estimated to be ≈ 2000 cm^{-1} higher in energy in comparison with N1 and N2 of the crystallographically equivalent ligands (Riesen *et al.* 1996b). The corresponding difference for the $[Zn(bpy)_3](ClO_4)_2$ lattice is similar.

This simple point charge calculation provides an upper limit for the energy difference of the charge-transfer processes between the two positions as it assumes a dielectric constant of unity. If the dielectric constant of the free electron gas of 2·3 is used, an energy difference of about 900 cm^{-1} is calculated. These estimates also apply to the $[Os(bpy)_3]^{2+}$ chromophore which has similar metal–nitrogen bond lengths (Constable *et al.* 1989, Richter *et al.* 1991).

The $[Ru(bpy)_3](PF_6)_2$ material undergoes a phase transition at 190 K, tripling the unit cell to form a modulated structure. The C2/c perchlorate salts have already locked into a modulated structure at room temperature. Consequently, any further phase transition is very unlikely. A measurement of the unit cell dimension at 170 K

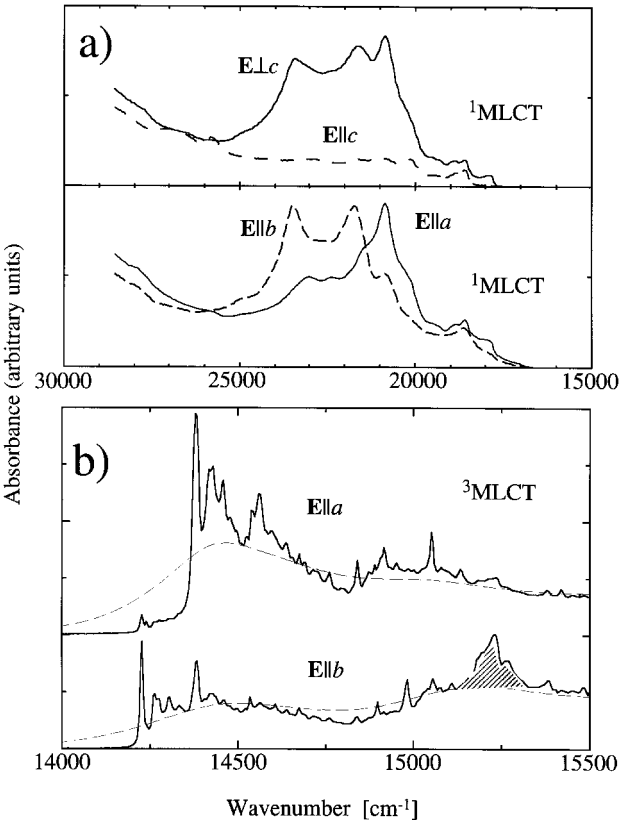

Figure 10. Polarized absorption spectra of $[Ru(bpy)_3]^{2+}$ doped in $[Zn(bpy)_3](ClO_4)_2$ and $[Os(bpy)_3]^{2+}$ in $[Ru(bpy)_3](ClO_4)_2$ at 10 K in the regions of the (*a*) ^{1}MLCT and (*b*) ^{3}MLCT transitions.

has confirmed that no phase change had occurred by this temperature (Krausz *et al.* 1995).

The C2/c structure manifests itself in polarized absorption spectra (Krausz *et al.* 1995). A substantial dichroism is observed in the metal–ligand plane due to the fact that the ligands are not equivalent. This dichroism is illustrated in figure 10 for the ^{1}MLCT region of $[Ru(bpy)_3]^{2+}$ doped in $[Zn(bpy)_3](ClO_4)_2$ and the ^{3}MLCT region of $[Os(bpy)_3]^{2+}$ doped in $[Ru(bpy)_3](ClO_4)_2$. In the ruthenium(II) system most of the intensity is found in the metal–ligand plane. The natural polarization for a charge-transfer transition lies indeed along the metal–ligand direction.

The substantial dichroism in the metal–ligand plane ($\mathbf{E} \| a, \mathbf{E} \| b$) can also be easily observed with a polarizing microscope. If all ligands were equivalent no dichroism would ensue. That is to say spectra taken with $\mathbf{E} \| a$ and $\mathbf{E} \| b$ would be identical.

A key consequence of the crystallographic inequivalence of ligand positions in the C2/c structure is the fact that complexes $[M(bpy)_{3-x}(L')_x]^{2+}$ with $x = 1, 2$ (M = Ru, Os; L′ = bpy-$d_{n=2,4,6,8}$ with both pyridines deuterated equivalently; L′ = 2,2′-bipyrazine; L′ = 3,3′-bipyridazine etc.) can enter the lattice in two ways as is shown in figure 11. In the $x = 1$ system one third of the complexes enter the lattice with the L′ ligand in the distinct position and two thirds of the complexes enter the lattice with L′ in one of the crystallographically equivalent positions. In the $x = 2$ system one third

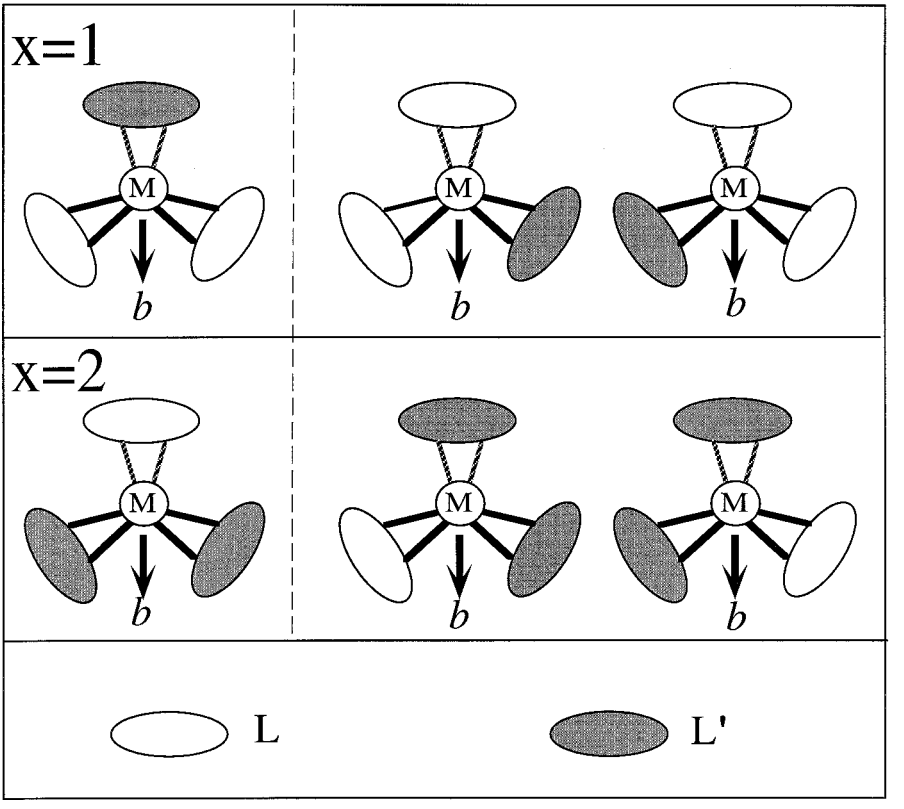

Figure 11. The two ways by which a $[M(L)_{3-x}(L')_x]^{2+}$ complex with $x = 1, 2$ can enter the $[Zn(bpy)_3](ClO_4)_2$ lattice.

of the complexes enter the lattice with the L′ ligands in the crystallographically equivalent positions and two thirds of the complexes enter the lattice with one of the L′ ligands in the distinct position.

4. Probing the C2/c structure of $[Zn(bpy)_3](ClO_4)_2$ by spectroscopy

Optical spectroscopy can be used to probe the inequivalence of the two positions for the ligand in the C2/c crystal structure of racemic $[Zn(bpy)_3](ClO_4)_2$. Dopants of the general formula $[M(bpy)_2(L')]^{2+}$ can enter the lattice with the statistics discussed above. The ligand L′ should structurally be as similar as possible to bpy to avoid problems of miscibility. Furthermore, the π* acceptor orbital of L′ should have a significantly lower energy than that of bpy in order to ensure that its lowest-excited ^{3}MLCT states are invariably lower. Suitable probes are $[M(bpy)_2(bprid)]^{2+}$ (bprid = 3,3′-bipyridazine) and $[M(bpy)_2(bpz)]^{2+}$ (bpz = 2,2′-bipyrazine) with M = Ru, Os. In these systems two ^{3}MLCT luminescences occur, arising from the L′ ligand in either position. The energy difference of the ^{3}MLCT state of L′ in the two positions is thus directly obtained from the spectra.

The low-temperature luminescence spectrum in the region of the electronic origins of $[Ru(bpy)_2(bprid)]^{2+}$ in $[Zn(bpy)_3](ClO_4)_2$ is shown in figure 12. The luminescence consist of a superposition of two spectra. The other three complexes $[Ru(bpy)_{3-x}(bprid)_x]^{2+}$ with $x = 0, 2, 3$ show a *single* luminescence spectrum (Riesen *et al.* 1995a). The intensity ratio of the two spectra in the $x = 1$ system establishes that the

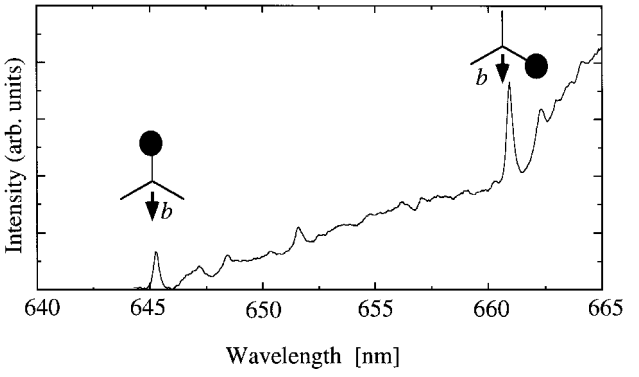

Figure 12. Luminescence spectrum of $[Ru(bpy)_2(bprid)]^{2+}$ in $[Zn(bpy)_3](ClO_4)_2$ at $\approx$ 2 K in the region of the electronic origins. The position of the bprid ligand relative to the crystal *b* axis is indicated for the two emissions.

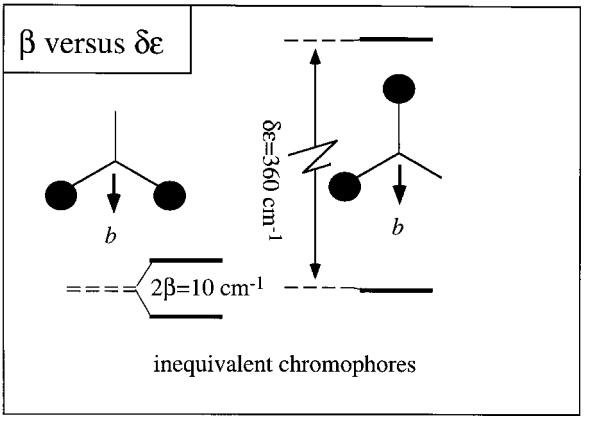

Figure 13. Quenching of the effects of the excitation exchange interaction with the inequivalence of subunit excitation energies. The diagram is shown for $\beta = 5\ cm^{-1}$ and $\delta\varepsilon = 360\ cm^{-1}$.

higher energy emission is due to the complexes which have the bprid ligand in the crystallographically distinct position. Correspondingly, the lower energy emission occurs when the complex enters the lattice with the bprid ligand in either of the crystallographically equivalent positions.

The energy difference of the lowest-excited ^{3}MLCT state of the bprid ligand in the two positions is $\approx 360\ cm^{-1}$. This is in accord with the estimated energy difference provided by the point charge model (see section 3) which, though performed for the $[Ru(bpy)_3](ClO_4)_2$ system, is likely to also provide a valid estimate for the bprid and the bpz ligands.

In the $[Ru(bpy)(bprid)_2]^{2+}/[Zn(bpy)_3](ClO_4)_2$ system, intramolecular excitation energy transfer ensures that the luminescence is dominated by ^{3}MLCT emission from a bprid ligand in the crystallographically equivalent position. This bprid ligand can have either a bpy or a bprid ligand in the other equivalent position. If the excitation exchange interaction β between the Ru-bprid subunits was significant, there would be two sets of luminophores. This is illustrated in figure 13 for an assumed value of

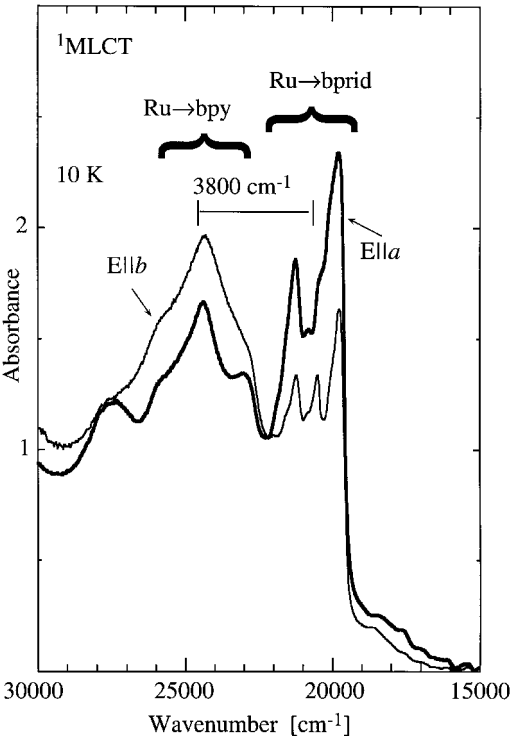

Figure 14. Polarized absorption spectra of $[Ru(bpy)_2(bprid)]^{2+}$ in $[Zn(bpy)_3](ClO_4)_2$ at 10 K. The energy separation of the baricentres of the two ^{1}MLCT regions involving the bprid and the bpy ligands is indicated.

$\beta = 5$ cm^{-1}. As only one luminescence feature is observed in the experiment, β must be significantly less than the inhomogeneous width of the electronic origins (≈ 5 cm^{-1}).

The gradual blue shift of the luminescence spectra of $[Ru(bpy)_{3-x}(bprid)_x]^{2+}/[Zn(bpy)_3](ClO_4)_2$ from $x = 1$ to $x = 3$ has been attributed to the stabilization of the dπ orbitals (Crutchley and Lever 1982, Kitamura *et al.* 1983, Rillema *et al.* 1983, Riesen *et al.* 1995a). An energy difference of the π^* orbitals of the bprid and bpy ligands of ≈ 3700 cm^{-1} can be extrapolated from these shifts. Figure 14 shows the absorption spectrum of the $x = 1$ system in the ^{1}MLCT region. Transitions involving the bprid ligand and the bpy ligands are well separated. The energy difference of the baricentres of the two singlet regions is about 3800 cm^{-1} in agreement with the above estimate.

Two spectra are also observed in the luminescence of the complexes $[Ru(bpy)_2(bpz)]^{2+}$ and $[Ru(bpy\text{-}d_8)_2(bpz)]^{2+}$ in the $[Zn(bpy)_3](ClO_4)_2$ host (figure 15) (Riesen *et al.* 1996a). The π^* orbital of bpz is ≈ 3000 cm^{-1} lower in energy in comparison with that of bpy. The energy difference between the ^{3}MLCT origins I involving the bpz ligand in the two positions is ≈ 258 cm^{-1}. The intensity ratio of the higher to lower emission is $\approx 1:2$ again reflecting the statistics outlined in figure 11.

We have also measured the emission and excitation spectra of $[Os(bpy\text{-}d_8)_2(bprid)]^{2+}$ in the $[Zn(bpy)_3](ClO_4)_2$ host. From the emission spectra an energy difference of the two positions for the bprid ligand of ≈ 600 cm^{-1} is obtained (Wallace 1996).

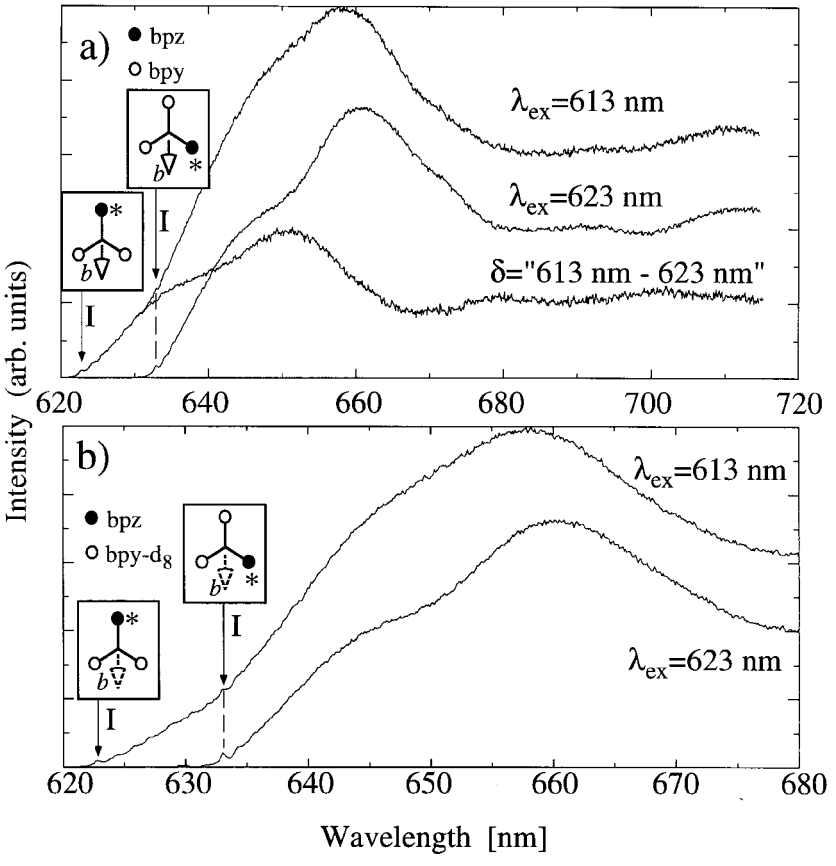

Figure 15. Luminescence spectra of (*a*) $[Ru(bpy)_2(bpz)]^{2+}$ and (*b*) $[Ru(bpy\text{-}d_8)_2(bpz)]^{2+}$ in $[Zn(bpy)_3](ClO_4)_2$ at 1·8 K. Excitation wavelengths λ_{ex} are indicated. Origins are assigned to the two possible orientations of the bpz ligand with respect to the crystal *b* axis.

5. Localized ^{3}MLCT states in ruthenium diimine systems

In this section we review the characteristics of the three lowest-excited electronic states of ruthenium diimine systems. The electronic origins of these states are denoted as I, II and III. In $[Ru(bpy)_3]^{2+}$ doped in $[Zn(bpy)_3](ClO_4)_2$ energy spacings are ΔE_{I-II} = 8·7 cm^{-1} and $\Delta E_{I-III} \approx 62$ cm^{-1}. In this system the origins II and III are ≈ 80 and ≈ 500 times more intense than origin I, respectively. Origin I of $[Ru(bpy)_3]^{2+}$ in $[Zn(bpy)_3](ClO_4)_2$ has an oscillator strength of only $\approx 10^{-8}$ and thus all three lowest-energy origins are weak. The oscillator strength of origin I is comparable to that of the ^{3}LC origin of $[Rh(bpy)_3]^{3+}$ (Komada *et al.* 1986). Thus it may not be surprising that the excitation exchange interaction is small in the lowest-excited ^{3}MLCT states. In all the ruthenium diimine systems investigated, we have found that $\beta \ll \Gamma_g$; that is to say (see section 2.1) the lowest-excited states are localized. The following subsections illustrate the application of a wide range of experiments which probe the localized nature of the three lowest-excited states.

5.1. *Deuteration effects in the electronic origins*

Electronic origins of delocalized states shift gradually in energy as a function of the deuteration degree of a molecule. In most cases, a blue shift occurs since excited state

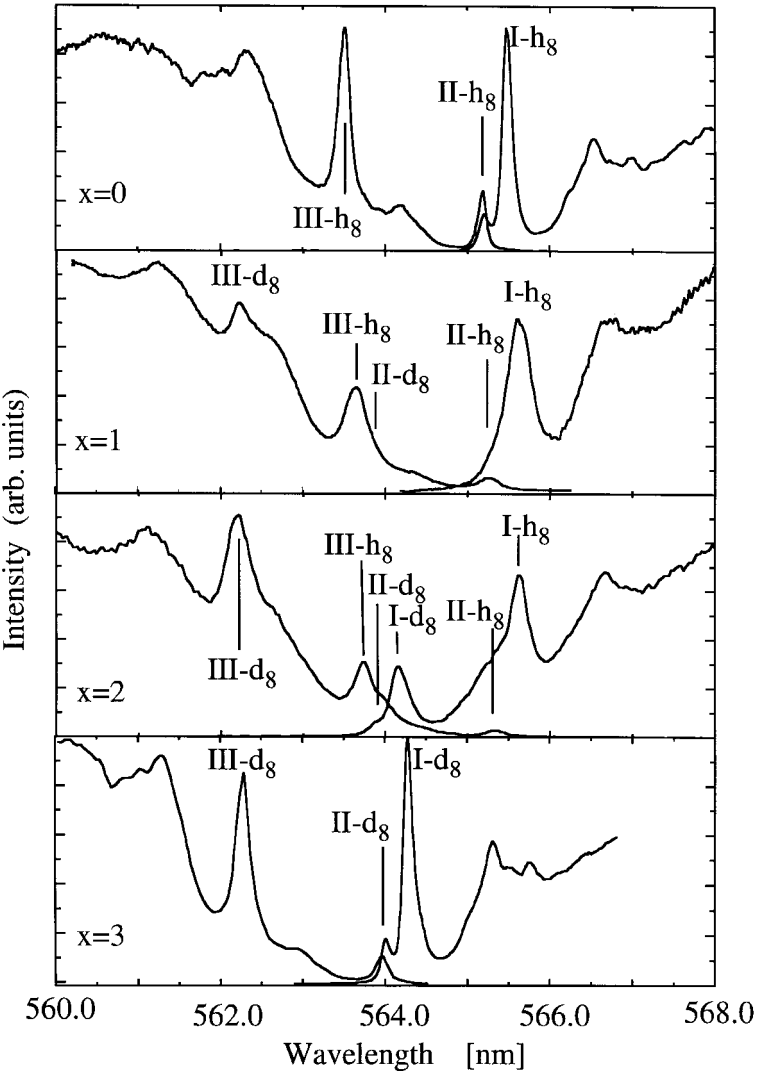

Figure 16. Non-selective excitation and luminescence spectra of the series $[Ru(bpy)_{3-x}(bpy\text{-}d_8)_x]^{2+}$ (x = 0–3) in $[Zn(bpy)_3](ClO_4)_2$ at 1·8 K. ^{3}MLCT transitions of the bpy-h_8 and bpy-d_8 ligands are denoted by {I, II, III}-h_8 and {I, II, III}-d_8 respectively.

vibrational frequencies are lower in energy than ground state frequencies, and the difference of the sum of zero point energies between the excited state and the ground state increases. Such a blue shift upon deuteration is observed for π–π* excitations of organic molecules. This shift to higher energy is approximately a linear function of the deuteration degree. For example, benzene, naphthalene and anthracene show shifts of 33, 15 and 6 cm^{-1} per hydrogen, respectively (Broude *et al.* 1985).

Consequently, deuteration effects provide a direct insight to the localization/delocalization question. The origins of $[Ru(bpy)_{3-x}(bpy\text{-}d_n)_x]^{2+}$ would gradually shift to higher energy from x = 0 to x = 3 if the lowest-excited ^{3}MLCT states were delocalized. In contrast, independent ^{3}MLCT transitions to the bpy and the bpy-d_n ligands are expected for localized ^{3}MLCT states.

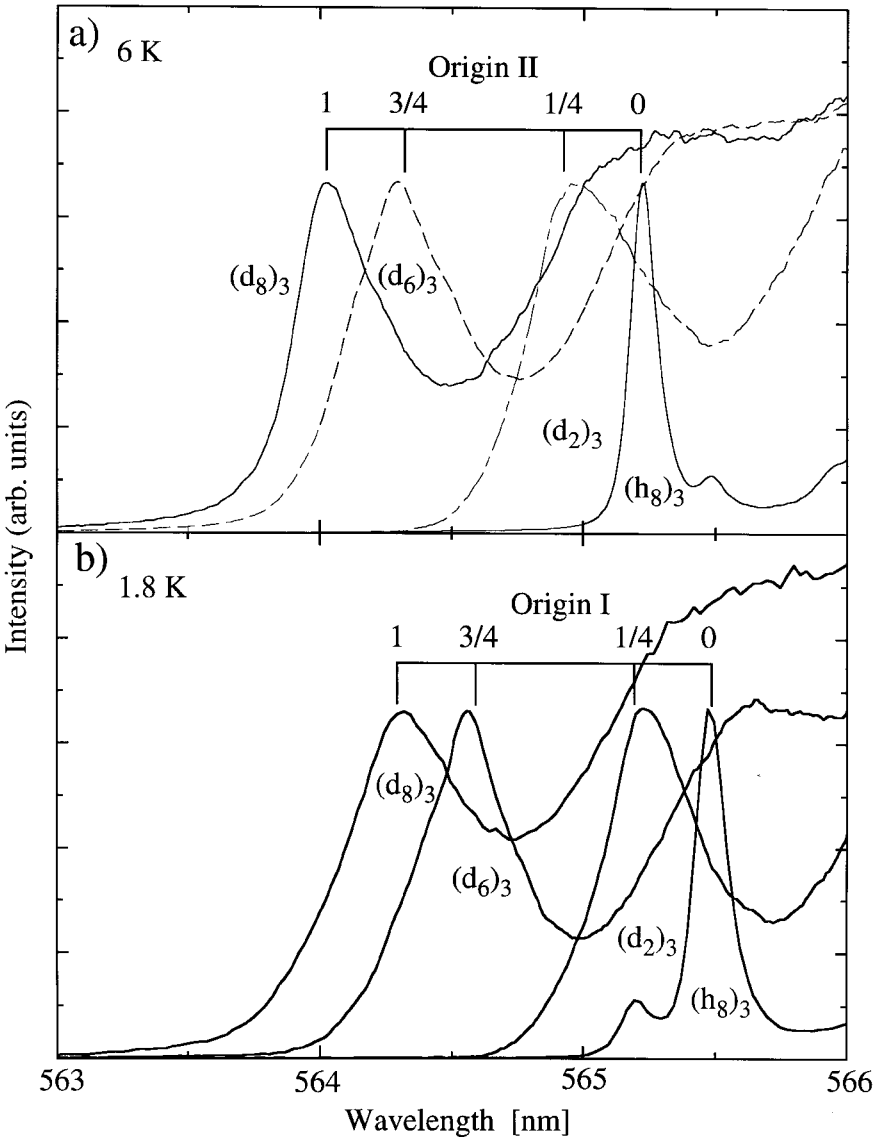

Figure 17. Luminescence spectra in the region of the electronic origins of $[Ru(bpy)_3]^{2+}$, $[Ru(bpy\text{-}3,3'\text{-}d_2)_3]^{2+}$, $[Ru(bpy\text{-}4,4',5,5',6,6'\text{-}d_6)_3]^{2+}$ and $[Ru(bpy\text{-}d_8)_3]^{2+}$ in $[Zn(bpy)_3](ClO_4)_2$.

The excitation and luminescence spectra of the $[Ru(bpy)_{3-x}(bpy\text{-}d_8)_x]^{2+}$ (x = 0 to 3) series doped into the $[Zn(bpy)_3](ClO_4)_2$ lattice, shown in figure 16, indicate that the lowest-excited states are localized (Riesen and Krausz 1993b). A doubling of electronic origins I, II and III occurs in the excitation spectra of the x = 1 and x = 2 systems. From their energies and relative intensities one can assign the two sets of origins to transitions involving the bpy-h_8 or the bpy-d_8 ligand(s). *Delocalization* would lead to a gradual shift of one set of origins to higher energy as a function of x. The low-temperature luminescence of the x = 2 system shows ^{3}MLCT emission from the bpy and the bpy-d_8 ligands. In this system one third of the complexes enters the C2/c lattice with both bpy-d_8 ligands in the crystallographically equivalent positions (see figure

11). The ^{3}MLCT transitions to the bpy-h_8 ligand in the crystallographically distinct position are significantly (more than 100 cm^{-1}) higher in energy (see section 4). Then ^{3}MLCT emission occurs from bpy-d_8 since the deuteration shift is only about 37 cm^{-1}. A linear shift and no doubling is observed (see figure 17) in the series $[Ru(bpy\text{-}d_n)_3]^{2+}$ (n = 0, 2, 6, 8) where all three bpy ligands have the same deuteration degree.

Our assignments of the electronic origins in the $[Ru(bpy)_{3-x}(bpy\text{-}d_8)_x]^{2+}$ systems with x = 1, 2 to independent ^{3}MLCT transitions of the bpy or the bpy-d_8 ligands are corroborated by the following observations:

(a) intensity ratios in absorption, and non-selective and narrowed excitation and luminescence (see figure 18),
(b) origins (I, II, III)-h_8 and (I, II, III)-d_8 in the x = 1 and x = 2 systems coincide with the origins of the x = 0 and x = 3 systems (see figure 16),
(c) intensity ratios between narrowed and broad features observed in excitation and luminescence line narrowing experiments (Riesen *et al.* (1994a, 1995a), see also section 5.3),
(d) variation of the coupling of vibrational sidelines (see section 5.8),
(e) longer lifetime observed for the ^{3}MLCT emission of bpy-d_8 in comparison with the ^{3}MLCT emission of bpy-h_8 in the x = 2 system (see section 5.9),
(f) a rise in ^{3}MLCT emission of bpy-d_8 in comparison with ^{3}MLCT emission of bpy-h_8 occurs in the x = 2 system with increasing temperature (see also bpy/bpy-6,6′-d_2 series below),
(g) pseudo-Stark splittings observed for the $[Ru(bpy)(bpy\text{-}d_8)_2]^{2+}$ system (see section 5.5)

In luminescence of the x = 2 system the ratio I-h_8:I-d_8 (= c:d in figure 18) is $\approx$ 1·8:1. Deviation from the ideal ratio of 2:1 (one third of the complexes enter the lattice with the bpy-d_8 ligands in the crystallographically equivalent positions) is due to the higher quantum efficiency of the ^{3}MLCT emission from the bpy-d_8 ligands (see section 5.9). In non-selective excitation and absorption spectra, intensity ratios of II-h_8:II-d_8 and III-h_8:III-d_8 of $\approx$ 1:2 are observed. This simply reflects the number of bpy and bpy-d_8 ligands in the crystallographically equivalent positions. The lower panel of figure 18 shows a narrowed excitation spectrum that has been obtained by monitoring the luminescence at λ_{obs} indicated in the upper panel. If the two sets of transitions observed arose from two distinct crystallographic sites, an intensity ratio of $\approx$ 2·4:1 (= a:b in figure 18) would be expected for III-h_8:III-d_8 in the narrowed excitation spectrum. However, a ratio of $\approx$ 2:3 is observed. Emission involving the bpy ligand occurs when it is in one of the crystallographically equivalent positions. All the complexes which contribute to ^{3}MLCT emission of bpy have a bpy-d_8 ligand in the crystallographically equivalent ligand position. Some ^{3}MLCT emission from the bpy-d_8 ligands is observed at λ_{obs} due to the phonon sideband of I-d_8 (fraction denoted as b in figure 18). This leads to a deviation from the ideal ratio of 1:1 of III-h_8:III-d_8 in the narrowed excitation spectrum.

Our initial assignments were *directly* tested by a wide range of studies of deuteration effects. Deuteration/protonation of the $[Ru(bpy)(bpy\text{-}d_8)_2]^{2+}$ complex can only occur on the bpy-h_8/bpy-d_8 ligands respectively (Riesen *et al.* 1995b). Selective deuteration/protonation of the 3,3′ position of the bpy/bpy-d_8 ligands occurs in alkaline solutions (Constable and Seddon 1982, Strommen *et al.* 1990). Transitions which have been assigned in the x = 2 system to ^{3}MLCT origins involving the bpy-h_8 ligand are predicted to shift to higher energy upon deuteration. Correspondingly, transitions

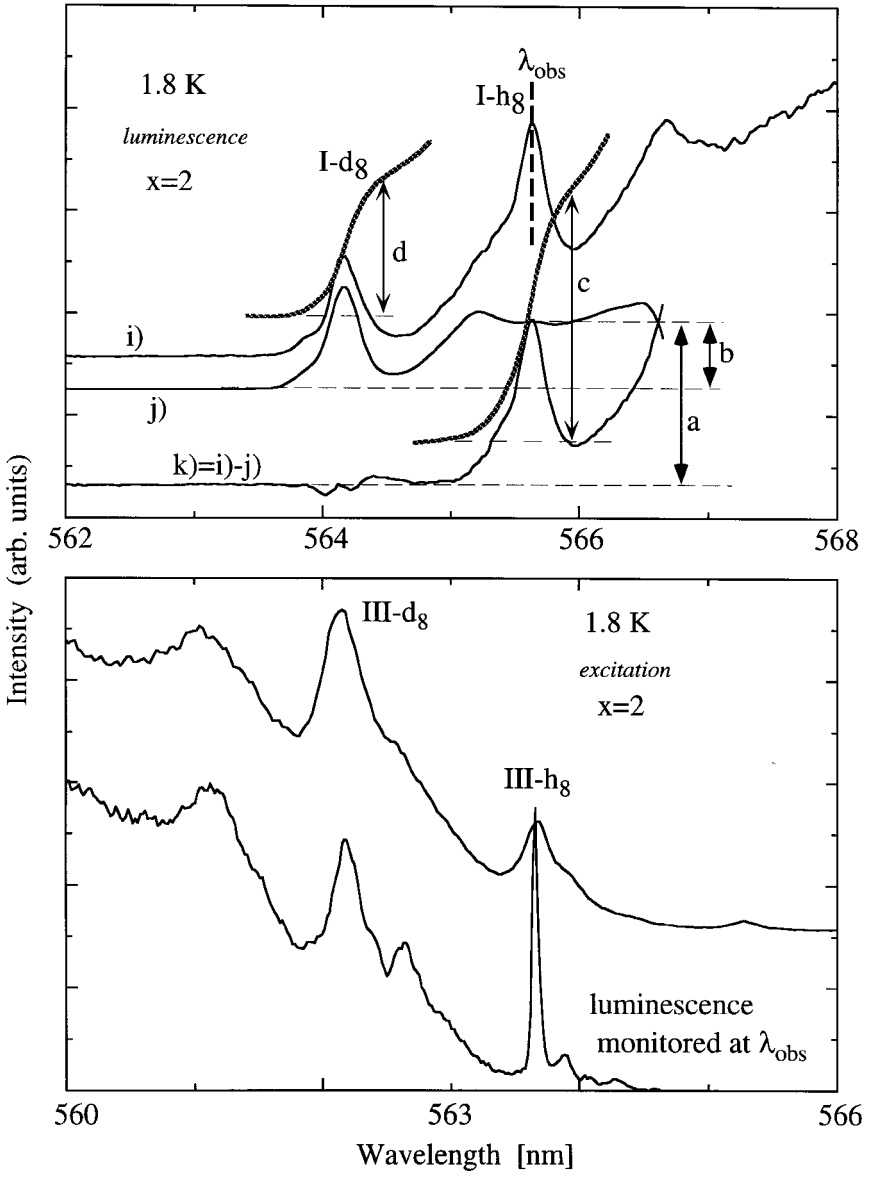

Figure 18. Intensity ratios observed in luminescence and excitation of $[Ru(bpy)(bpy\text{-}d_8)_2]^{2+}$ in $[Zn(bpy)_3](ClO_4)_2$ at $\approx$ 1·8 K. In the upper panel trace (i) is the non-selectively excited luminescence and trace (j) is the spectrum of the perprotonated complex which has been shifted to coincide with the I-d_8 origin. The lower panel compares narrowed and non-narrowed excitation spectra in the region of the origins III-h_8 and III-d_8. λ_{obs} for the narrowed spectrum is indicated in the upper panel.

assigned to the bpy-d_8 ligand will shift to lower energy upon protonation of the $[Ru(bpy)(bpy\text{-}d_8)_2]^{2+}$ complex. The luminescence spectra in the region of the electronic origins of the $[Ru(bpy)(bpy\text{-}d_6)_2]^{2+}$ and $[Ru(bpy\text{-}d_2)(bpy\text{-}d_8)_2]^{2+}$ complexes doped in $[Zn(bpy)_3](ClO_4)_2$ are shown in figure 19. The ^{3}MLCT origins involving the bpy-d_6 or the bpy-d_2 ligands shift to lower or higher energy, respectively, in comparison with the transitions involving the bpy-d_8 or the bpy-h_8 ligand in the $[Ru(bpy)(bpy\text{-}d_8)_2]^{2+}$

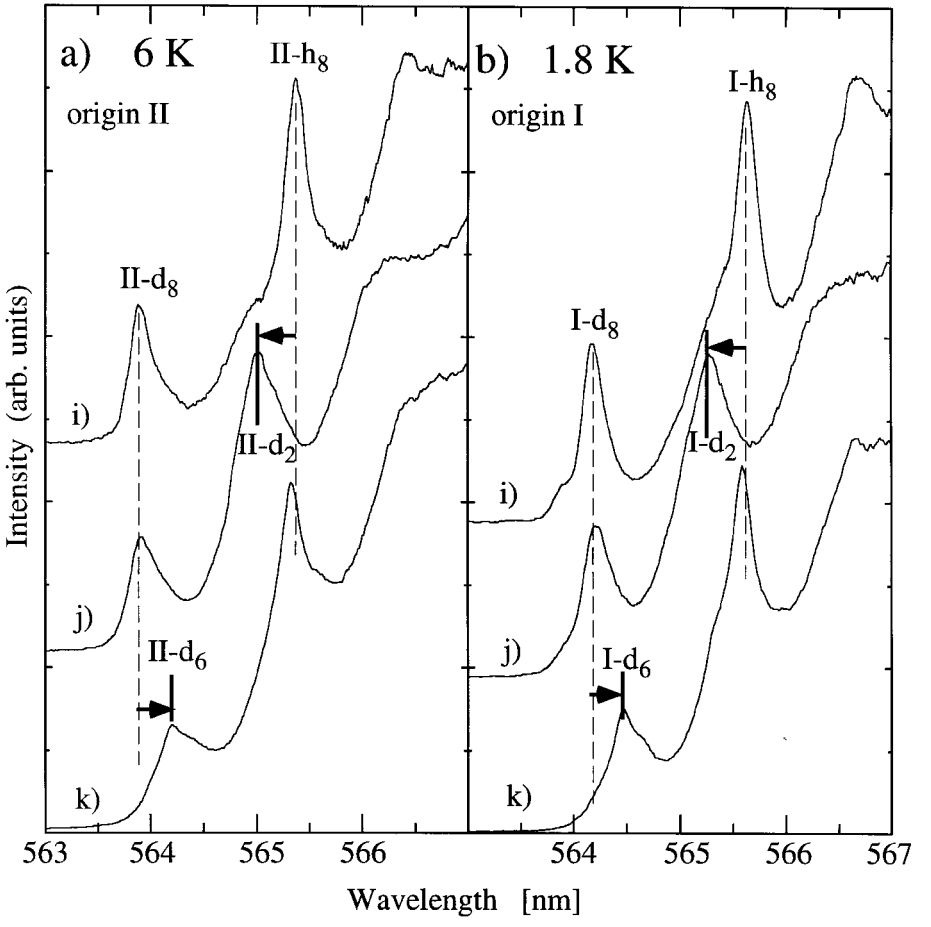

Figure 19. Luminescence spectra in $[Zn(bpy)_3](ClO_4)_2$ of $[Ru(bpy)(bpy\text{-}4,4',5,5',6,6'\text{-}d_6)_2]^{2+}$ (k), $[Ru(bpy\text{-}3,3'\text{-}d_2)(bpy\text{-}d_8)_2]^{2+}$ (j) and $[Ru(bpy)(bpy\text{-}d_8)_2]^{2+}$ (i).

system. These origins coincide with those of $[Ru(bpy\text{-}d_6)_3]^{2+}$ and $[Ru(bpy\text{-}d_2)_3]^{2+}$ (figure 17). Furthermore, the origins of the bpy-h_8 and bpy-d_8 ligands in the $[Ru(bpy)(bpy\text{-}d_6)_2]^{2+}$ and $[Ru(bpy\text{-}d_2)(bpy\text{-}d_8)_2]^{2+}$ complexes coincide with the corresponding origins in $[Ru(bpy)(bpy\text{-}d_8)_2]^{2+}$ (Riesen *et al.* 1995b).

Deuteration or protonation in strongly alkaline solutions does not terminate at full exchange of the 3,3′positions, but other positions are exchanged at somewhat slower rates. In the results of figure 20, $[Ru(bpy)(bpy\text{-}d_8)_2]^{2+}$ was exposed to a strongly alkaline solution of D_2O and the deuterium exchange was stopped after the time intervals Δt_1 and Δt_2 (with $\Delta t_2 > \Delta t_1$). A gradual exchange of hydrogens by deuterium is observed and the ^{3}MLCT origin of the affected bpy ligand shifts gradually to higher energy as a function of the number of exchanged hydrogens. As predicted, the ^{3}MLCT origin of the unaltered bpy-d_8 remains virtually at the same energy. Corresponding behaviour is observed upon protonation in strongly alkaline H_2O solutions.

A minimal perturbation of the bpy ligand can be achieved by deuteration of the 6,6′ positions (McClanahan and Kincaid 1984, Riesen *et al.* 1996c). These positions are adjacent to the ligating nitrogen atoms and are well isolated from the host environment. Hence variations in guest–host interactions are minimized for the series

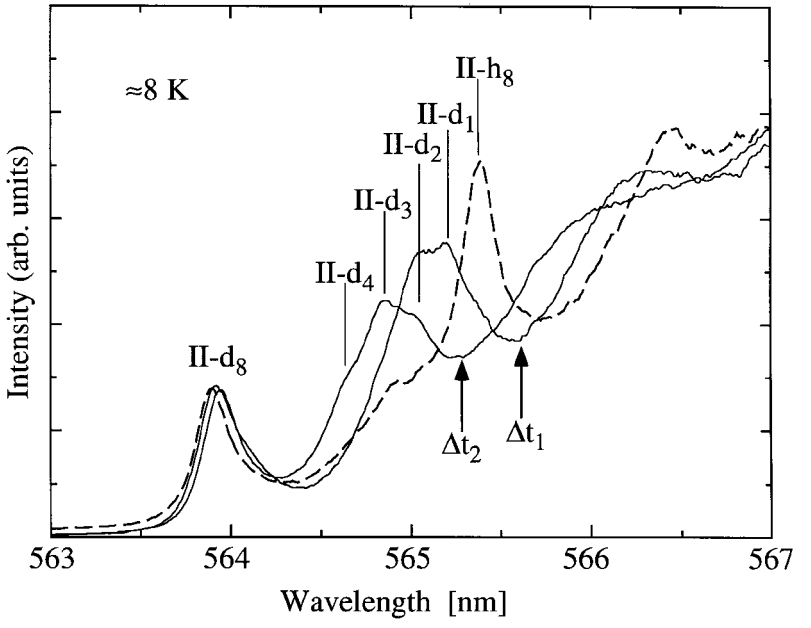

Figure 20. Luminescence spectra of $[Ru(bpy)(bpy\text{-}d_n)_2]^{2+}/[Zn(bpy)_3](ClO_4)_2$ systems. The parent $[Ru(bpy)(bpy\text{-}d_8)_2]^{2+}$ complex whose spectrum is shown as a dashed line has been exposed at progressive times Δt_1 and Δt_2 to a strongly alkaline deuterated medium (see text).

$[Ru(bpy)_{3-x}(bpy\text{-}6,6'\text{-}d_2)_x]^{2+}$ (x = 0–3) in $[Zn(bpy)_3](ClO_4)_2$. The $[Ru(bpy)_{3-x}(bpy\text{-}6,6'\text{-}d_2)_x]^{2+}$ (x = 1, 2) complexes offer the advantage, in comparison to the bpy-d_8/bpy series, that the energy difference between the two sets of origins (I-h_8, II-h_8, III-h_8) and (I-d_2, II-d_2, III-d_2) is low ($\approx$ 10 cm^{-1}). Thus significant variations of intensity ratios of the ^{3}MLCT emission of bpy/bpy-6,6′-d_2 occur in the x = 1 and x = 2 systems between 1·8 K and 20 K. The bpy-6,6′-d_2 ^{3}MLCT emission rises as a function of temperature due to backtransfer of excitation energy in both systems. The high temperature limit for the intensity ratio of bpy-6,6′-d_2/bpy emission is 2:1 for x = 2 and 1:2 for x = 1.

In figure 21 non-selective excitation spectra of the $[Ru(bpy)_{3-x}(bpy\text{-}6,6'\text{-}d_2)_x]^{2+}$ series in $[Zn(bpy)_3](ClO_4)_2$ are shown in the region of the lowest-energy ^{3}MLCT origins. The x = 3 system is shifted by $\approx$ 9 cm^{-1} to higher energy in comparison with the x = 0 system. As predicted, this is 1/4 of the shift observed upon perdeuteration of the complex. Independent ^{3}MLCT transitions to the bpy or bpy-6,6′-d_2 ligands are observed for the x = 1 and x = 2 systems. The intensity ratios III-d_2/III-h_8, II-d_2/II-h_8 of 1:2 and 2:1 for the x = 1 and x = 2 systems reflect the statistics of figure 11. Figure 22 presents the luminescence spectra (x = 0–3) at various temperatures. The spectra are dominated by luminescence from origin I at 1·8 K and origin II at temperatures greater than 3 K. At 1·8 K the x = 1 system shows ^{3}MLCT luminescence predominantly from bpy. In contrast the x = 2 system shows additionally ^{3}MLCT luminescence from bpy-6,6′-d_2 and the observed ratio of bpy-6,6′-d_2 to bpy luminescence is 1:2 as predicted. The temperature dependence of the intensity ratios is in agreement with a calculation based on a Boltzmann distribution.

Selective spectroscopy clearly demonstrates the independence of the two sets of transitions. For example, when origin III-h_8 in the x = 2 system is used to excite the

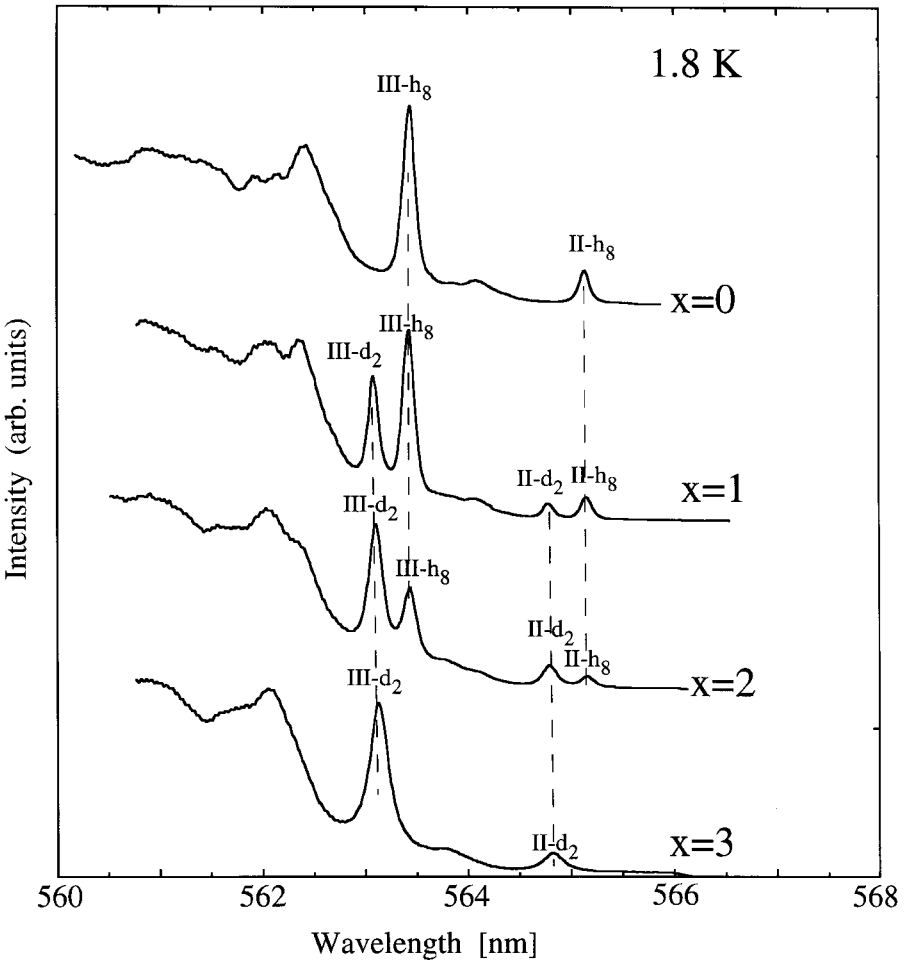

Figure 21. Non-selective excitation spectra of $[Ru(bpy)_{3-x}(bpy\text{-}6,6'\text{-}d_2)_x]^{2+}$ (x = 0–3) in $[Zn(bpy)_3](ClO_4)_2$ in the region of the lowest-energy ^{3}MLCT origins. Concentrations of dopants are less than 0·1%. Origins are assigned to ^{3}MLCT transitions of bpy-d_2 and bpy-h_8.

luminescence, only ^{3}MLCT emission from bpy occurs. When ^{3}MLCT luminescence from bpy-6,6′-d_2 is excited via III-d_2 excitation, 2/3 of the complexes transfer ^{3}MLCT energy localized on bpy-6,6′-d_2 to the bpy in the crystallographically equivalent ligand position and non-narrowed ^{3}MLCT emission from bpy is observed.

As mentioned in section 3.1, the $[Ru(bpy)_3](PF_6)_2$ crystal remains trigonal at low temperatures but the unit cell triples leading to three sites for the $[Ru(bpy)_3]^{2+}$ cation with C3 symmetry. *Intermolecular* excitation energy transfer is much faster than the luminescence lifetime at temperatures of less than 10 K and consequently luminescence occurs predominantly from the lowest-energy site.

Low temperature luminescence spectra of the series $[Ru(bpy)_{3-x}(bpy\text{-}d_8)_x](PF_6)_2$ (x = 0–3) are shown in figure 23. They manifest the localized nature of the lowest-excited states (Riesen *et al.* 1988). In the x = 1 and x = 2 systems intramolecular energy transfer between the three ligands (in addition to the *intermolecular* energy transfer) ensures that ^{3}MLCT emission occurs predominantly from the bpy-h_8

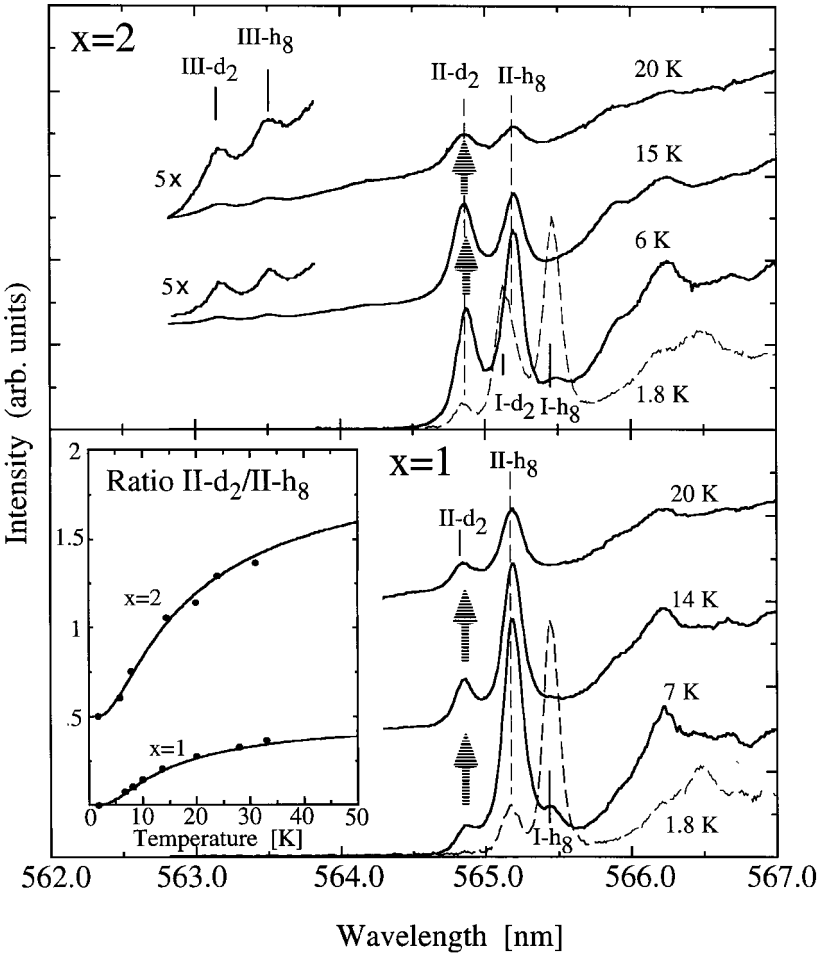

Figure 22. Temperature dependence of the luminescence of $[Ru(bpy)(bpy\text{-}6,6'\text{-}d_2)_2]^{2+}$ (x = 2) and $[Ru(bpy)_2(bpy\text{-}6,6'\text{-}d_2)]^{2+}$ (x = 1) in $[Zn(bpy)_3](ClO_4)_2$ in the region of the electronic origins. The inset shows the intensity ratio of the transitions II-d_2 and II-h_8 as a function of temperature. The solid lines are calculations based on a Boltzmann distribution.

ligand(s) of the lowest-energy site. Figure 24 compares the excitation spectrum of the x = 2 system with those of the x = 0 and x = 3 systems. In these systems the deuteration shift is somewhat larger than in the perchlorate salts, so that the origins II-d_8 and III-h_8 are close in energy. This in turn complicates the analysis. The difference spectrum denoted as δ in figure 24 confirms our earlier assignments of transitions to bpy-h_8 and bpy-d_8 ligands in the x = 2 system. Note that in our original work (Riesen *et al.* 1988) we did not identify origin III. Also the narrowing effects reported in this early work were most likely due to the narrowing via origin III-h_8 since the energies of the bpy-h_8 and bpy-d_8 ligands are poorly correlated due to nanoheterogeneity. Excitation into II-d_8 will not lead to substantial narrowing of I-h_8 or II-h_8.

Independent ^{3}MLCT transitions to bpy and bpy-6,6′-d_2 are not obscured by coincidences in the $[Ru(bpy)_{3-x}(bpy\text{-}6,6'\text{-}d_2)_x](PF_6)_2$ (x = 1, 2) crystals. In figure 25 non-selective excitation and luminescence spectra of $[Ru(bpy)(bpy\text{-}6,6'\text{-}d_2)_2](PF_6)_2$ are compared with the spectra of $[Ru(bpy)_3](PF_6)_2$ and $[Ru(bpy\text{-}6,6'\text{-}d_2)_3](PF_6)_2$ in the

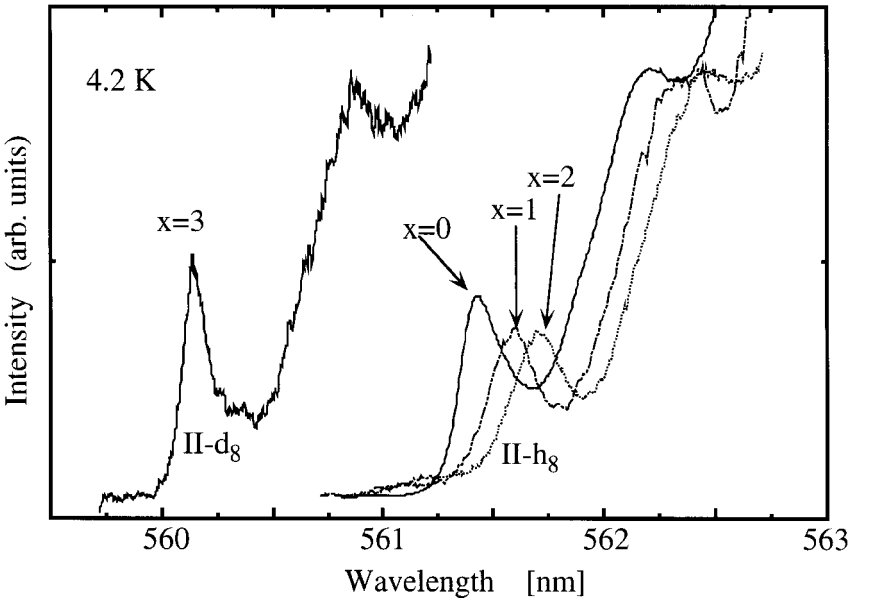

Figure 23. Luminescence spectra of the series $[Ru(bpy)_{3-x}(bpy\text{-}d_8)_x](PF_6)_2$ (x = 0–3) at 4·2 K in the region of the electronic origins.

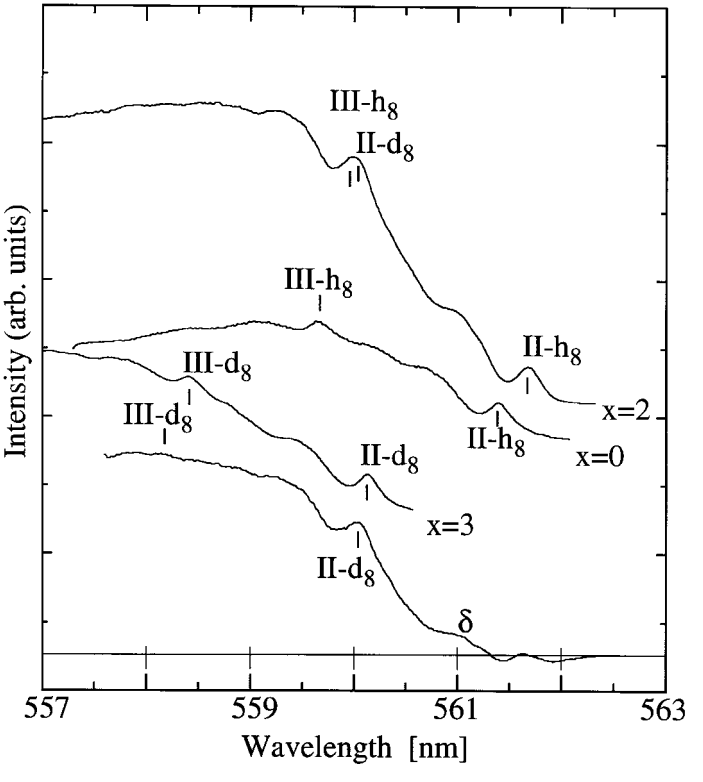

Figure 24. Excitation spectra of $[Ru(bpy)_{3-x}(bpy\text{-}d_8)_x](PF_6)_2$ with $x = 0, 2, 3$ at ≈ 2 K. Intensities are normalized with respect to the lowest-energy origin, i.e. II-h_8 for x = 0, 2 and II-d_8 for x = 3. The origin II-h_8 of the x = 0 spectrum is aligned with II-h_8 of the x = 2 spectrum to obtain the difference spectrum $\delta = (x = 2) - (x = 0)$.

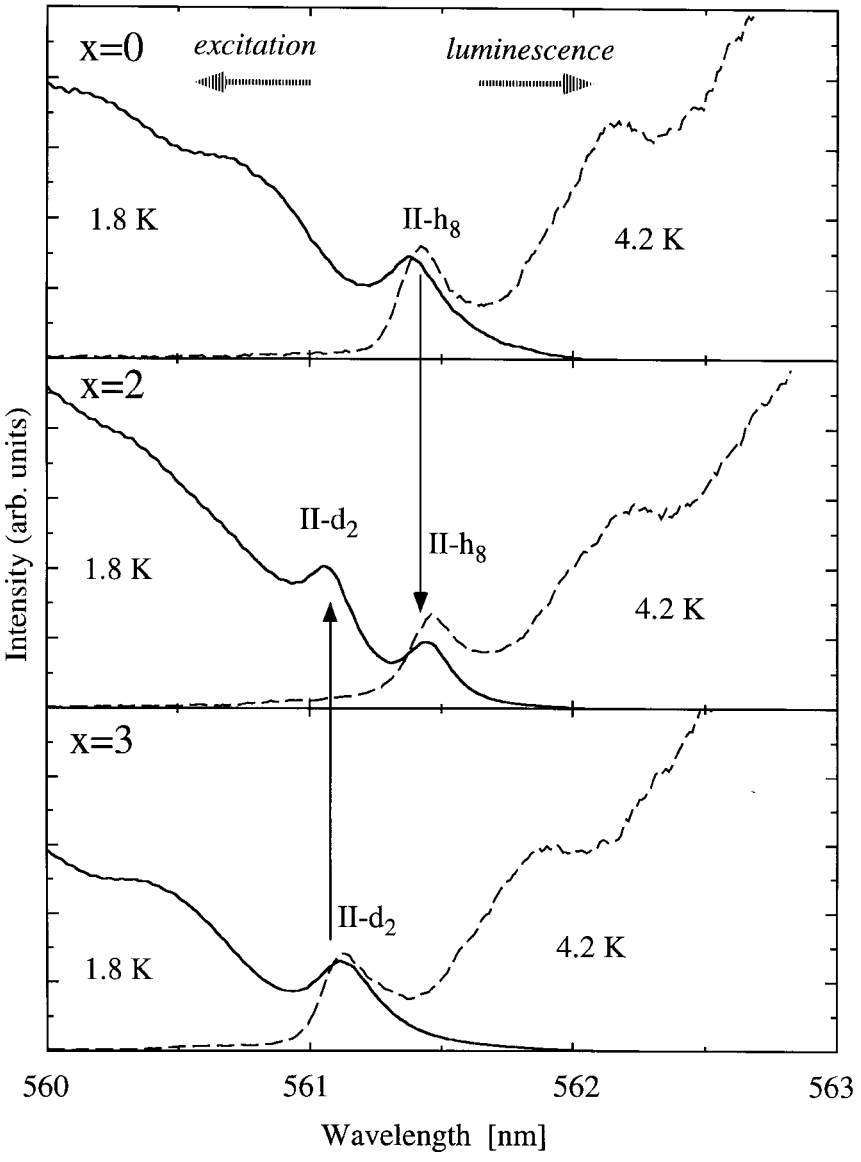

Figure 25. Non-selective excitation and luminescence spectra of $[Ru(bpy)_{3-x}(bpy\text{-}6,6'\text{-}d_2)_x](PF_6)_2$ ($x = 0, 2, 3$) in the region of the lowest-energy electronic origins.

region of the lowest-energy origins. The spectrum of the $x = 3$ system is blue shifted by $\approx 10{\cdot}5$ cm^{-1} in comparison with the $x = 0$ system. As predicted, this is $\approx 1/4$ of the 41 cm^{-1} shift observed for perdeuteration. Independent ^{3}MLCT origins of bpy-h_8 and bpy-6,6′-d_2 are observed for the $x = 2$ and $x = 1$ systems. The ratio of II-d_2 : II-h_8 is $\approx 2:1$ in excitation of the $x = 2$ system and $\approx 1:2$ in the $x = 1$ system. Again, ^{3}MLCT emission occurs predominantly from bpy-h_8 of the lowest-energy site at lowest temperature in the $x = 2$ and $x = 1$ systems. At higher temperatures both the $x = 1$ and $x = 2$ systems show a rise in ^{3}MLCT luminescence from the bpy-6,6′-d_2 ligand because of intramolecular backtransfer of excitation energy. This is analogous to the behaviour of the dilute perchlorate system discussed above.

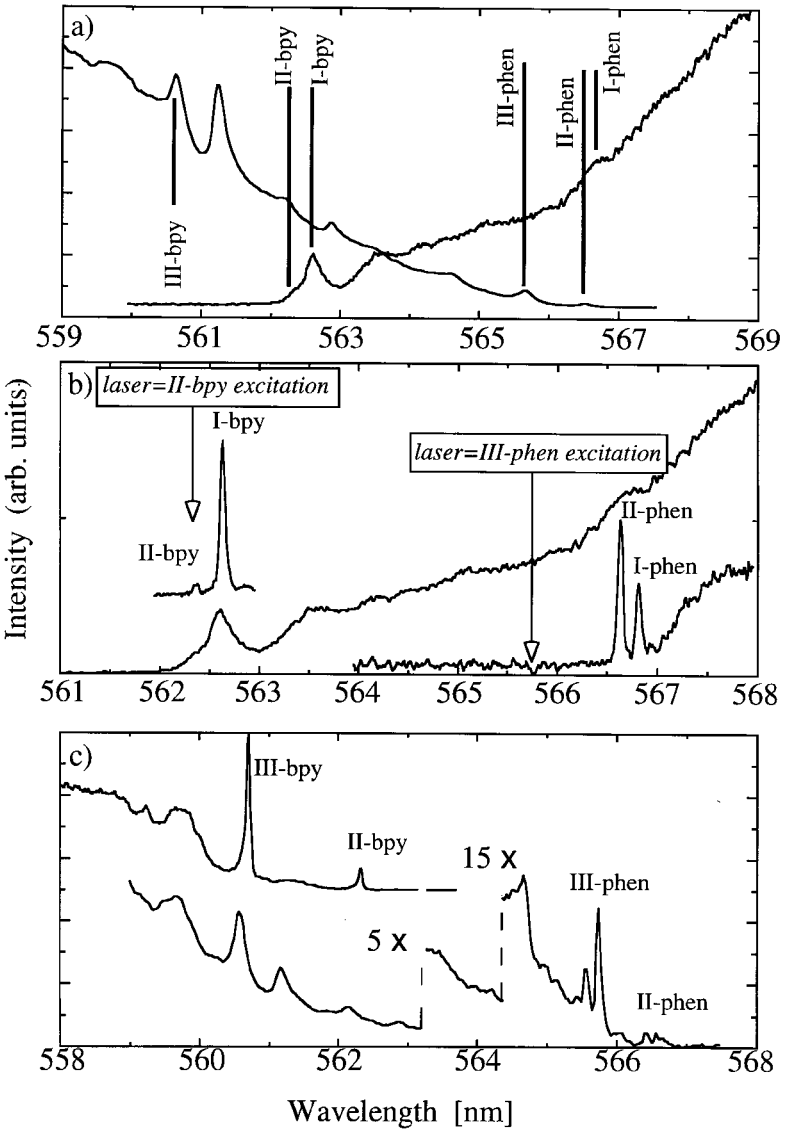

Figure 26. Luminescence and excitation spectra of $[Ru(bpy)_2(phen)]^{2+}$ in $[Zn(bpy)_3](ClO_4)_2$ at $\approx$ 2 K. (*a*) Non-selective excitation and luminescence spectra. (*b*) Narrowed luminescence spectra for bpy and phen in comparison with the non-selectively excited luminescence. (*c*) Narrowed excitation spectra for the bpy and phen transitions.

The dominant deuteration shift is determined by the degree of deuteration of the ligand on which the ^{3}MLCT excitation is localized. This arises because bpy anion frequencies are on average significantly lower in energy than corresponding bpy frequencies. However, the degree of deuteration of the spectator ligands affects the energy of the ^{3}MLCT transition to a much lesser extent (Riesen *et al.* 1996c). Vibrational frequencies in $[Ru(bpy)_3]^{3+}$ are on average slightly higher in comparison with the 2+ oxidation state. Thus deuteration of the spectator ligands leads to a slight red shift of localized ^{3}MLCT origins.

Table 1. Energy spacings (in cm^{-1}) of the lowest-excited ^{3}MLCT states observed in the series $[Ru(bpy)_{3-x}(phen)_x]^{2+}$ (x = 0 to 3) doped in racemic $[Zn(bpy)_3](ClO_4)_2$ (estimated error $\pm 0{\cdot}2$ cm^{-1} unless stated otherwise).

Complex	ΔE(I–II)$_{bpy}$	ΔE(I–III)$_{bpy}$	ΔE(I–II)$_{phen}$	ΔE(I–III)$_{phen}$
x = 0	8·7	62·1	–	–
x = 1	8·5	61·0($\pm$0·5)	5·7	32·7
x = 2	[a]	[a]	6·0	33·5
x = 3	–	–	6·0($\pm$0·5)	34·0($\pm$1)

[a] Not identified.

An illustration of this effect is provided by the bpz localized ^{3}MLCT origins in $[Ru(bpy)_2(bpz)]^{2+}/[Zn(bpy)_3](ClO_4)_2$ which shift slightly (≈ 3 cm^{-1}) to the red upon deuteration of the bpy ligands (see figure 15). Likewise ^{3}MLCT transitions in $[Ru(bpy)_{3-x}(bpy\text{-}6,6'\text{-}d_2)_x]^{2+}/[Zn(bpy)_3](ClO_4)_2$ to the bpy ligand shift to the red from $x = 0$ to $x = 2$ and the ^{3}MLCT transitions to the bpy-6,6′-d_2 ligand show a corresponding shift from $x = 1$ to $x = 3$ (see figures 21 and 22). Corresponding red shifts of the localized transitions upon deuteration of the spectator ligands are also observed in the bpy/bpy-d_8 series (see figures 16 and 23).

5.2. *Mixed chelate systems*

In this section we consider ruthenium(II) diimine complexes in which the symmetry is broken by chemical inequivalence of the ligands rather than by deuteration. The series $[Ru(bpy)_{3-x}(phen)_x]^{2+}$ (x = 0 to 3) in $[Zn(bpy)_3](ClO_4)_2$ (Riesen *et al.* 1994c) is interesting since the ^{3}MLCT origin I of the phen ligand lies only 125 cm^{-1} lower in energy than the corresponding excitation involving the bpy ligand. The independent ^{3}MLCT origins involving the phen or the bpy ligand are easily identified from characteristic energy spacings.

The luminescence of the $x = 1$ system consists of two overlapping spectra; firstly, ^{3}MLCT emission from phen for the complexes which enter the lattice with phen in one of the crystallographically equivalent positions of the $[Zn(bpy)_3](ClO_4)_2$ host (see figure 11); secondly, ^{3}MLCT emission from bpy for the complexes which have the phen ligand in the crystallographically distinct position. The energies of the ^{3}MLCT transitions to the phen ligand in this position are again significantly higher in energy.

In figure 26 excitation and luminescence spectra in the region of the electronic origins are shown for the $[Ru(bpy)_2(phen)]^{2+}/[Zn(bpy)_3](ClO_4)_2$ system. The non-selective luminescence and excitation spectra show two sets of independent electronic origins (figure 26(*a*)) involving the bpy/phen ligands. Selective luminescence and excitation line narrowing is achieved for both sets of origins as is illustrated in figures 26(*b*) and (*c*). In the case of the narrowed excitation spectrum of the transitions involving the phen ligand, a doubling is observed. This arises because the inhomogeneous broadening is greater than the I–II separation and thus the selectivity is affected. The narrowed excitation spectrum consists of two contributions; namely, subsets of species whose I-phen or II-phen transitions are monitored at the detected wavelength. Fast intramolecular excitation energy transfer ensures that in the $[Ru(bpy)(phen)_2]^{2+}/[Zn(bpy)_3](ClO_4)_2$ system ^{3}MLCT emission occurs predominantly from the phen ligands.

In table 1 we summarize the energy splittings for the series. The lowest-excited

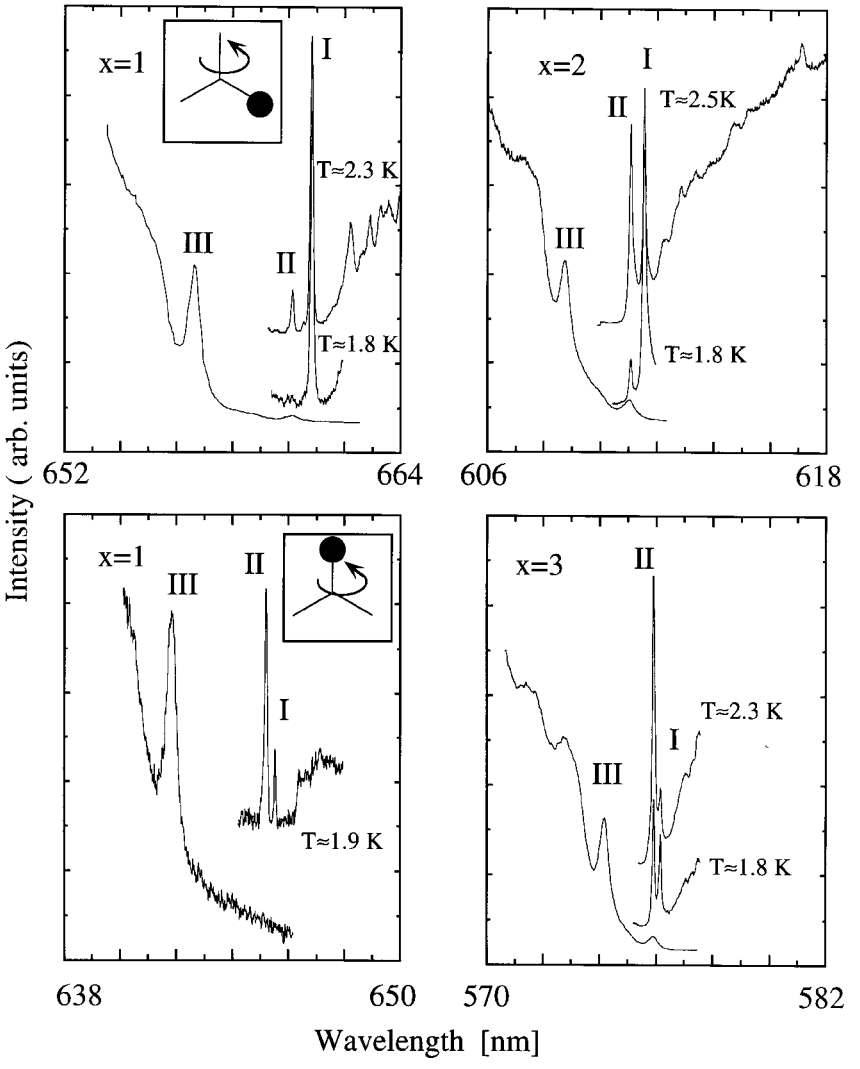

Figure 27. Excitation and luminescence spectra in the region of the lowest-energy origins in the series $[Ru(bpy)_{3-x}(bprid)_x]^{2+}$ (x = 1 to 3) in $[Zn(bpy)_3](ClO_4)_2$. The luminescence spectra were excited at the maxima of origins III. The orientation of the bprid ligand for the x = 1 spectra is indicated.

^{3}MLCT states involving the phen ligand have substantially smaller energy spacings compared to those involving the bpy ligand. The energy spacings and relative intensities of the ^{3}MLCT transitions of either phen or bpy stay virtually constant within the series. For example, the spacings between the origins I-bpy, II-bpy and III-bpy and their relative intensities in the $[Ru(bpy)_2(phen)]^{2+}/[Zn(bpy)_3](ClO_4)_2$ complex are practically identical to those of the $[Ru(bpy)_3]^{2+}/[Zn(bpy)_3](ClO_4)_2$ system. Substantial variations of energy spacings and intensities would occur if the excitation exchange interaction were comparable to or larger than the inhomogeneous line width. These results provide an upper limit for the effective excitation exchange interaction β between the metal–ligand subunits of 0·5 cm^{-1}.

Another useful mixed chelate series is $[Ru(bpy)_{3-x}(bprid)_x]^{2+}$ (x = 1–3) (see section

4). The ^{3}MLCT transitions to the bprid ligand are far lower in energy ($\approx$ 3700 cm^{-1}) than those to the bpy ligand. Figure 27 shows non-selective excitation and narrowed luminescence spectra in the region of the lowest-energy ^{3}MLCT origins of this series in the $[Zn(bpy)_3](ClO_4)_2$ host (Riesen *et al.* 1995a). In each case the luminescence spectrum was excited at the peak maximum of the inhomogeneously broadened origin III.

The general pattern of the I, II and III origins remains intact through the entire series. Again, variations of this pattern would result if the excitation exchange interaction was larger than or comparable to the inhomogeneous width of the electronic origins.

It has been suggested (Riesen *et al.* 1995a) that the lower intensities of the electronic origins I and II of the bprid ligand on the crystal *b* axis are related to the higher symmetry of the ligand in this position. The ligand has twofold symmetry in this position. The origin features are also weak in the C_3-3 $[Ru(bpy)_3](PF_6)_2$ lattice, where each ligand has twofold symmetry.

5.3. *Luminescence and excitation line narrowing experiments*

As we have outlined in section 2 line narrowing experiments enable the observation of distinct features associated with ^{3}MLCT transitions to nominally equivalent ligands. In this section we show that such experiments, on a number of systems, lead to entirely systematic observations having consistent interpretations.

In figure 28 excitation line narrowing experiments are shown for the origin III of the series $[Ru(bpy)_{3-x}(bprid)_x]^{2+}$ (x = 1–3) in the $[Zn(bpy)_3](ClO_4)_2$ host. These experiments were performed by detecting origin I luminescence at the red edge of the inhomogeneous distribution. Levels I, II and III are well correlated within a single metal–ligand subunit. Nanoheterogeneity leads to a poor correlation amongst the metal–ligand subunits (see section 2). A spectral consequence is that upon observation of ^{3}MLCT luminescence at the red edge of the inhomogeneous distribution of origin I, two features are observed in excitation line narrowing of origin III. The narrowed feature is due to the bprid ligand whose ^{3}MLCT luminescence is directly excited. The corresponding ^{3}MLCT excitations of the bprid ligand in the crystallographically equivalent position are spread over the inhomogeneous distribution, leading to a non-narrowed feature. As expected, the x = 1 system (having a single bprid ligand) shows *only* a narrowed feature for all observation wavelengths, for both positions of the bprid ligand. This is because corresponding excitations of the bpy ligands are $\approx$ 3000 cm^{-1} higher in energy.

In contrast, the x = 2 and x = 3 systems show a narrowed *and* a broad feature. When the luminescence is detected at the red edge of the inhomogeneous distribution of the origin I at low temperatures, the intensity ratio of the narrowed to broad feature approaches 2 : 1 and 1 : 1 for the x = 2 and x = 3 systems, respectively. This reflects the occupancy of the crystallographically equivalent ligand position by bprid (50% and 100% for the x = 2 and x = 3 systems respectively). The line narrowing experiments provide an upper limit for the effective excitation exchange interaction between Ru-bprid subunits of 0·5 cm^{-1}.

As is the case for the bprid/bpy series, narrowing experiments establish that the excitation exchange interaction β between metal–ligand subunits is also small in the series $[Ru(bpy)_{3-x}(bpy\text{-}d_8)_x]^{2+}$ (x = 0–3) doped in $[Zn(bpy)_3](ClO_4)_2$. Figure 29 presents some excitation line narrowing experiments of the origin III of this series.

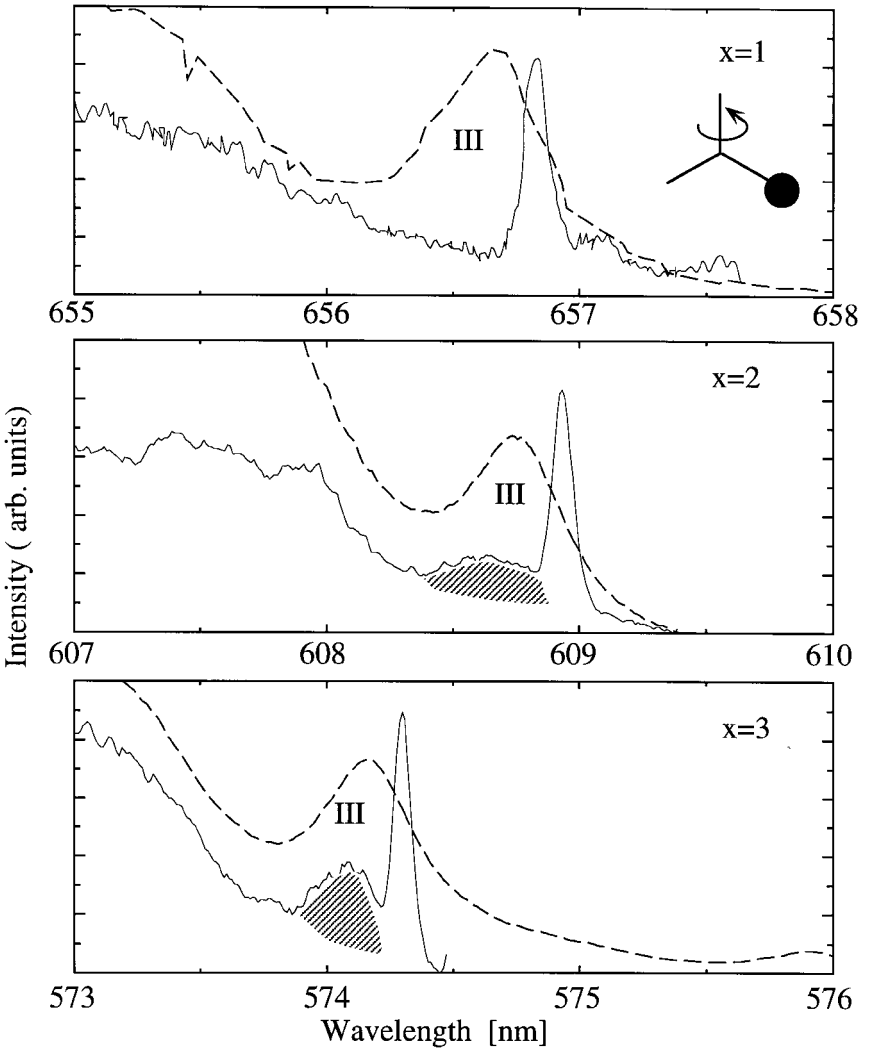

Figure 28. Excitation line narrowing of the ^{3}MLCT origin III of bprid in the series $[Ru(bpy)_{3-x}(bprid)_x]^{2+}$ (x = 1 to 3) in $[Zn(bpy)_3](ClO_4)_2$ at $\approx$ 2 K.

Again, no broad feature can be detected in these experiments for origin III-h_8 in the x = 2 system, since the crystallographically equivalent ligand position is occupied by bpy-d_8, with transitions $\approx$ 37 cm^{-1} higher in energy. The observed intensity ratios between the narrowed and the broad feature reflect the occupancy of the crystallographically equivalent ligand position by an equivalent ligand (bpy or bpy-d_8). In figure 30 excitation line narrowing experiments in the x = 2 system of origin II-d_8 and III-d_8 are shown for two wavelengths of observation (λ_m) together with simulated spectra (Riesen and Krausz 1996a). The agreement between experiment and calculation is quantitative and provides an upper limit of 0·5 cm^{-1} for β.

Luminescence line narrowing experiments provide complementary results. In figure 31 we show some experiments performed on the $[Ru(bpy)(bpy\text{-}d_8)_2]^{2+}/[Zn(bpy)_3](ClO_4)_2$ system (Riesen and Krausz 1993b). Corresponding to the excitation line narrowing experiments, the I-h_8/II-h_8 origins of the x = 2 system show

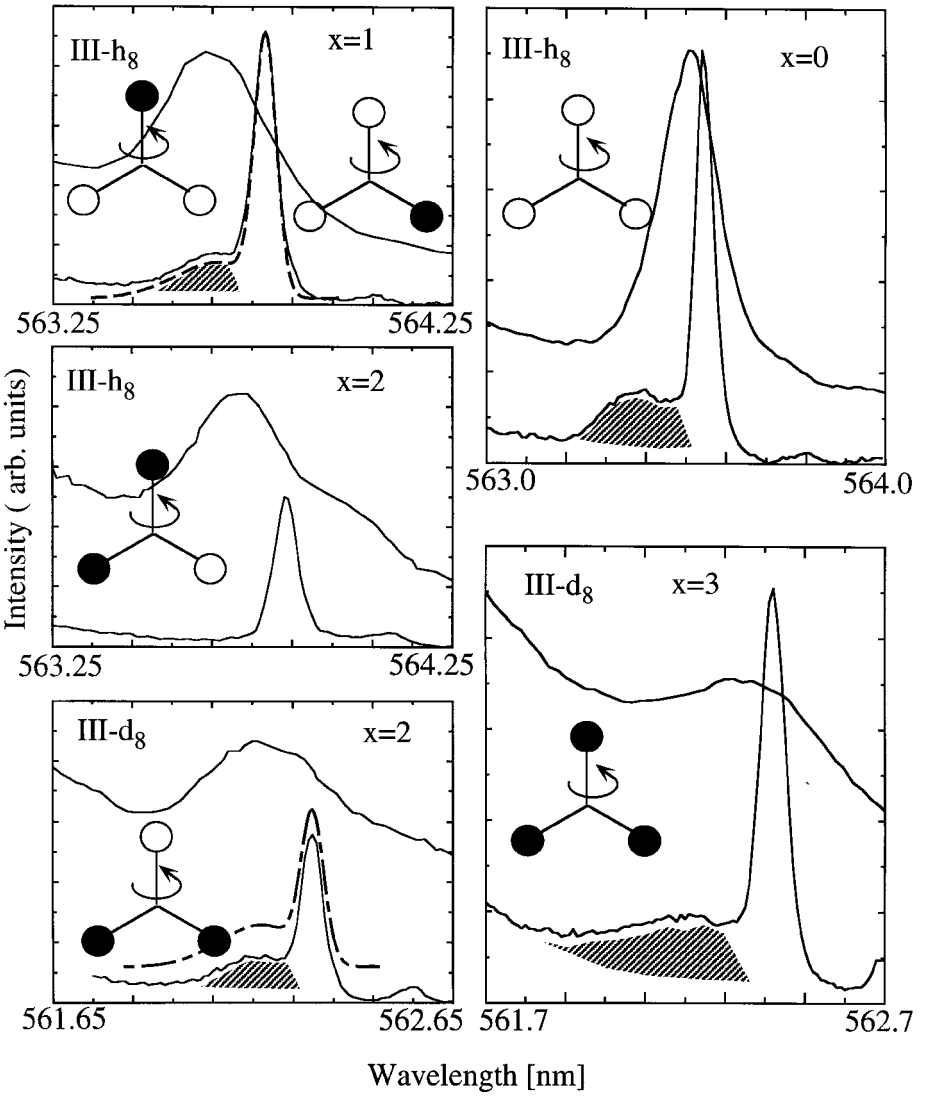

Figure 29. Excitation line narrowing of the origins III-h_8/III-d_8 of the series $[Ru(bpy)_{3-x}(bpy\text{-}d_8)_x]^{2+}$ (x = 0 to 3) in $[Zn(bpy)_3](ClO_4)_2$ at ≈ 1·8 K. The luminescence was monitored at the red edge of the corresponding origin I. The shading indicates the broad feature due to the ligand in the crystallographically equivalent position. The dashed lines show simulations for the x = 1, 2 systems. The non-selective excitation spectra are also shown.

only narrowed features, *independent* of the excitation wavelength. This is because there is but *one* bpy-h_8 ligand and the crystallographically equivalent position is occupied by bpy-d_8.

The I-d_8/II-d_8 origins show a broad feature when excited at the blue edge of the origin III-d_8 (shaded in figure 31). This feature is due to ^{3}MLCT emission of a like ligand (bpy-d_8) in the crystallographically equivalent ligand position which is activated via intramolecular ^{3}MLCT excitation energy transfer from the *directly* excited ligand.

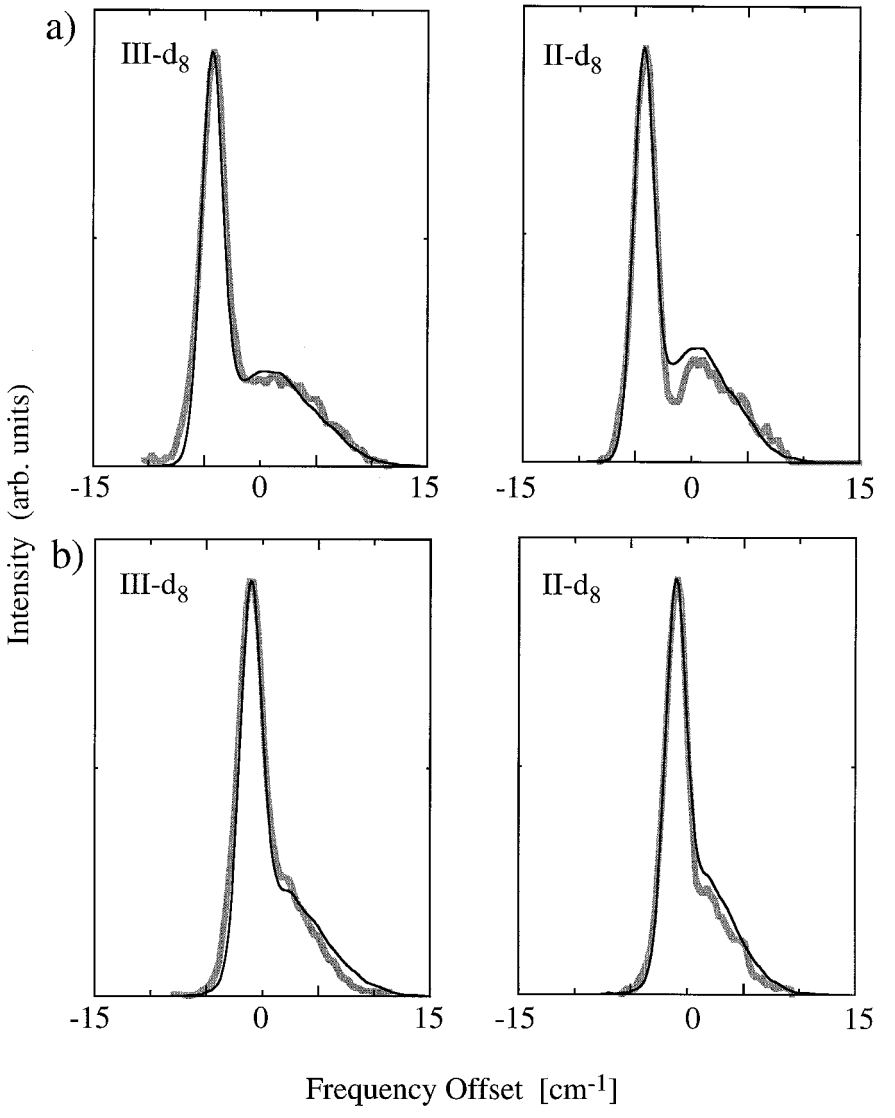

Figure 30. Simulations of narrowed excitation spectra of origins III-d_8 and II-d_8 in the $[Ru(bpy)(bpy\text{-}d_8)_2]^{2+}/[Zn(bpy)_3](ClO_4)_2$ system in comparison with experimental data (thick line). Data shown in (*a*) and (*b*) were monitored in I-d_8 at 564·28 nm and 564·18 nm, respectively. Parameters used: (*a*) $\Delta = -4{\cdot}4\ cm^{-1}$, $\Gamma_m = 1{\cdot}2\ cm^{-1}$, $T = 1{\cdot}8$ K, $\Gamma_{laser} = 1{\cdot}1\ cm^{-1}$, $\Gamma_\varepsilon = 4{\cdot}5\ cm^{-1}$ (III-d_8) and $3{\cdot}5\ cm^{-1}$ (II-d_8); (*b*) as in (*a*) but with $\Delta = -0{\cdot}95\ cm^{-1}$. Spectra are shifted with respect to the centre frequencies of the origins II-d_8 and III-d_8. $\Delta = \varepsilon_0 - 1/\lambda_m$ (ε_0 is the centre frequency of I-d_8).

In excitation line narrowing experiments of origin III-bpy and II-bpy in $[Ru(bpy)_2(phen)]^{2+}/[Zn(bpy)_3](ClO_4)_2$, the two bpy ligands are observed as a narrowed and a broad feature with a ratio of 1 : 1 when the I-bpy origin is monitored at the red edge, as expected. This is shown for the III-bpy transition in figure 32. In contrast, the III-phen and II-phen transitions show no broad feature since there is only one phen ligand.

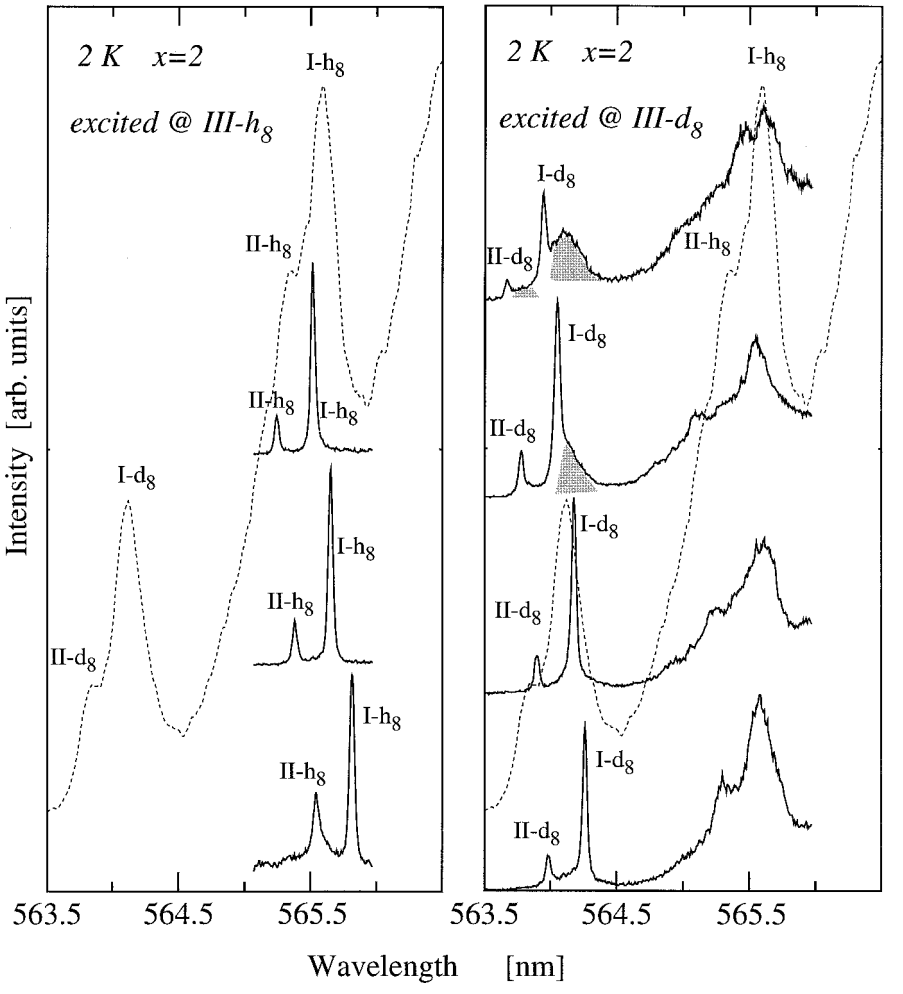

Figure 31. Luminescence line narrowing experiments in $[Ru(bpy)(bpy\text{-}d_8)_2]^{2+}/[Zn(bpy)_3](ClO_4)_2$. Excitation wavelengths were chosen within the inhomogeneously broadened origins III-h_8 and III-d_8. The non-selectively excited spectrum is shown as a dashed line.

5.4. *Direct measurements of intramolecular energy transfer rates*

Phenomena discussed in the previous section point to the possibility of direct measurements of intramolecular ^{3}MLCT excitation energy transfer rates by time resolved luminescence line narrowing experiments. In these experiments, the selectively excited luminescence is recorded at various delay times after pulsed laser excitation. Rates of intramolecular ^{3}MLCT excitation transfer can be deduced from the time dependence of the intensities of the narrowed and the broad features.

In the $[Ru(bpy)_3]^{2+}/[Zn(bpy)_3](ClO_4)_2$ and related deuterated systems, intramolecular excitation energy transfer can be observed in level II at 1·8 K because the intra metal–ligand subunit relaxation from level II to I is relatively slow ($k \approx 5 \times 10^6$ s^{-1}) at this temperature (Riesen and Krausz 1994a). The upper panels of figure 33 present time resolved luminescence line narrowing experiments for the ^{3}MLCT luminescence of the bpy-d_8 ligand in the $[Ru(bpy)(bpy\text{-}d_8)_2]^{2+}/$

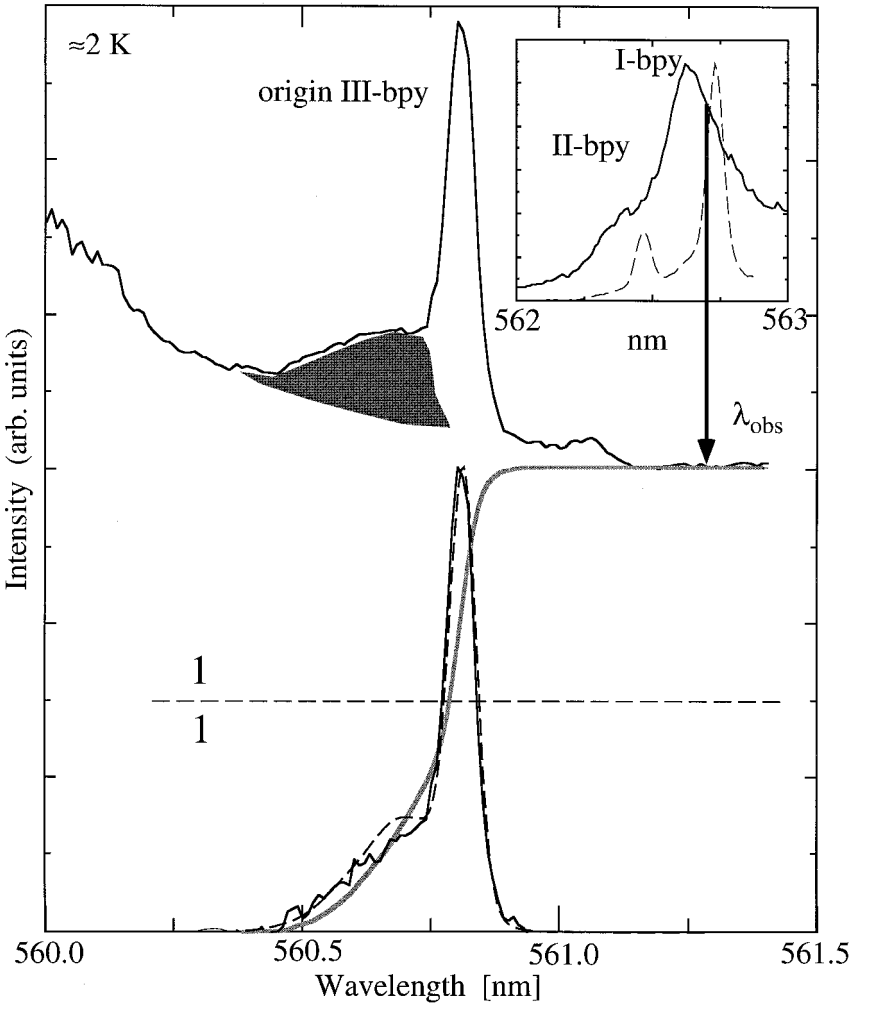

Figure 32. Excitation line narrowing in origin III-bpy of $[Ru(bpy)_2(phen)]^{2+}/[Zn(bpy)_3](ClO_4)_2$. The inset compares a narrowed with a non-selectively excited luminescence spectrum in the region of the lowest-energy origins I-bpy and II-bpy. The arrow indicates the monitoring wavelength for the narrowed excitation spectrum. A rising background has been subtracted in the bottom trace. The integral of the intensity is shown.

$[Zn(bpy)_3](ClO_4)_2$ system at 1·8 K (Riesen *et al.* 1994a). The luminescence was excited with a pulsed laser at the high energy side of the inhomogeneously broadened transition III-d_8. The luminescence was then averaged with a gatewidth of 10 ns or 100 ns.

The broad feature in the II-d_8 origin region is due to the bpy-d_8 ligand in the crystallographically equivalent position. Its ^{3}MLCT luminescence is activated by intramolecular energy transfer from the directly excited ligand. The narrowed II-d_8 feature of the directly excited metal–ligand subunit shows a relatively rapid decay in the first 20 ns due to this transfer process. The broad feature of II-d_8 shows a complementary rise.

After ≈ 100 ns decay kinetics of the narrowed and the broad feature approach the

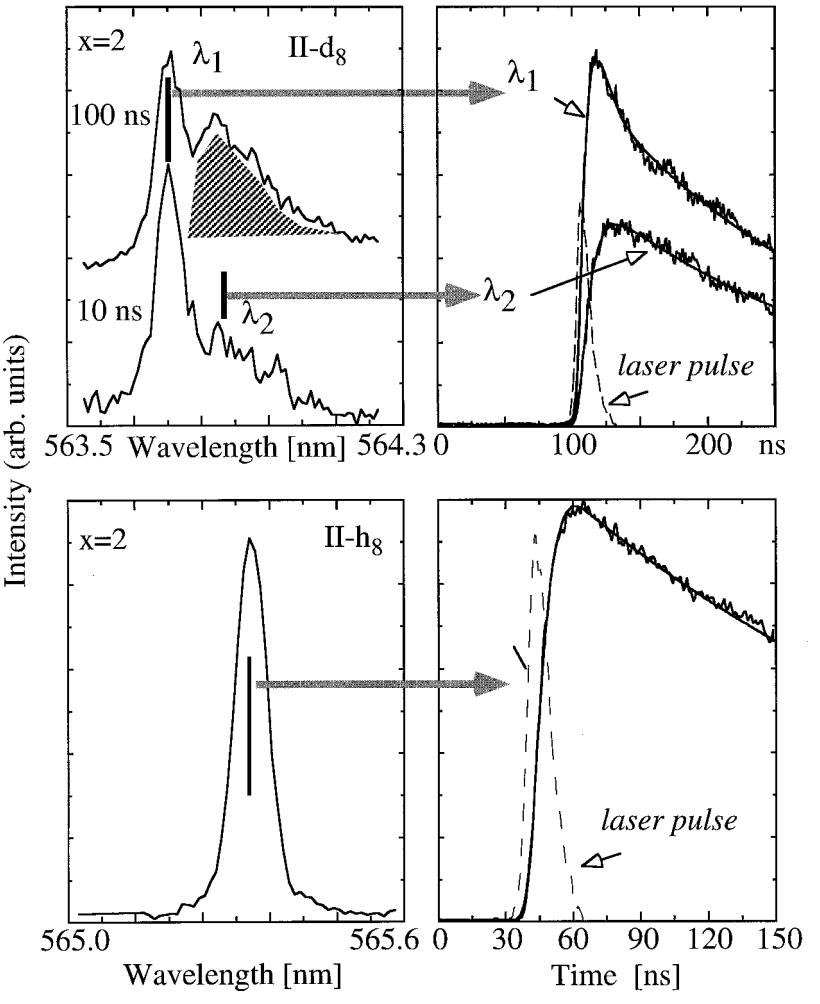

Figure 33. Time resolved luminescence line narrowing experiments of the origins II-d_8 and II-h_8 of $[Ru(bpy)(bpy\text{-}d_8)_2]^{2+}/[Zn(bpy)_3](ClO_4)_2$ at nominal 1·8 K. The luminescence was monitored for 10 ns or 100 ns for II-d_8. Decay curves were measured at the indicated wavelengths λ. The profile of the laser pulse is also shown.

rate given by the II–I relaxation rate. Equations (17) and (18) describe the kinetics of intramolecular ^{3}MLCT energy transfer between two nominally equivalent subunits (Riesen *et al.* 1994a).

$$n_A(t) = \int_0^t \rho(t-\tau)\{c_1 \exp[-k\tau] + c_2 \exp[-(k+k_{et}+k_{bt})\tau]\}\,d\tau. \quad (17)$$

$$n_B(t) = \int_0^t \rho(t-\tau)\{c_3 \exp[-k\tau] - c_4 \exp[-(k+k_{et}+k_{bt})\tau]\}\,d\tau. \quad (18)$$

k_{et} and k_{bt} denote the transfer and backtransfer in level II, respectively, k is the II–I relaxation rate and $\rho(t)$ is the experimentally determined shape of the laser pulse. n_A and n_B denote the population of ^{3}MLCT level II localized on the ligand A or B.

Excellent agreement with the experiment is obtained with the fitting parameters $k = 4{\cdot}8 \times 10^6\ s^{-1}$ and $(k_{et} + k_{bt}) = 1{\cdot}3 \times 10^8\ s^{-1}$.

In the $x = 2$ system, ^{3}MLCT luminescence of the bpy-d_8 ligand occurs when both crystallographically equivalent positions are occupied by bpy-d_8. ^{3}MLCT luminescence of the bpy ligand occurs when it occupies one of the crystallographically equivalent positions. Time resolved luminescence line narrowing experiments on the ^{3}MLCT excitation of the bpy ligand thus provide an internal blank experiment. The lower panels in figure 33 show such experiments. The decay curve is solely determined by the II–I relaxation rate (Riesen *et al.* 1994a) since no intramolecular ^{3}MLCT excitation energy transfer can occur in II-h_8.

Comparable results were obtained for the perprotonated and perdeuterated complexes in the same host. Within the experimental accuracy the transfer rate in level II is the same between crystallographically equivalent bpy-h_8 or bpy-d_8 ligands.

The relatively slow rate between equivalent ligands in level II is in part due to the low excitation exchange interaction, which is substantially smaller than the inhomogeneous width. Furthermore, the ^{3}MLCT transitions of the two crystallographically equivalent ligands are poorly correlated, which leads to an average energy gap of a few wavenumbers. Taking a Gaussian lineshape of width Γ, the average energy difference between nominally equivalent subunits becomes $\Gamma/(2(2\pi \ln(2))^{1/2})$. For example, if Γ is 5 cm^{-1} the average gap is 1·2 cm^{-1}. To conserve energy in the ^{3}MLCT energy transfer process, a matching phonon must be emitted or absorbed. The density of phonon states vanishes at low energies. Hence the transfer process is slowed. In a Debye approximation for the density of phonon states, one predicts the phonon-assisted energy transfer rate to increase with the cube of the gap.

From measurements of a small delay ($\approx$ 500 ps) of the ^{3}MLCT emission of bpy-h_8 in the $[Ru(bpy)(bpy\text{-}6,6'\text{-}d_2)_2]^{2+}/[Zn(bpy)_3](ClO_4)_2$ system, we have estimated (Riesen *et al.* 1996c) a value of $2{\cdot}1 \pm 0{\cdot}8 \times 10^9\ s^{-1}$ for the intramolecular ^{3}MLCT excitation transfer rate from bpy-6,6′-d_2 to bpy where the energy gap is 10 cm^{-1}. Corresponding experiments indicate that the transfer rate from bpy-d_8 to bpy, where the energy gap is 40 cm^{-1}, is substantially faster. A correlation of the rate with the energy gap is thus evident.

As outlined in section 2 (figure 4) the intramolecular energy transfer also manifests itself by small Stokes shifts and variations in the linewidth of the origins in excitation/absorption and luminescence (Riesen and Krausz 1996a). This arises since the ^{3}MLCT excitation energy can flow, at lowest temperature, to the crystallographically equivalent ligand if its ^{3}MLCT level is at lower energy. These processes are a function of the inhomogeneous width and the temperature. Some spectra in figures 16, 21 and 22 indeed show these subtle effects. For example, the origin II-d_8 in the $[Ru(bpy\text{-}d_8)_3]^{2+}/[Zn(bpy)_3](ClO_4)_2$ system of figure 16 shows a larger Stokes shift than origin II-h_8 of the $[Ru(bpy)_3]^{2+}/[Zn(bpy)_3](ClO_4)_2$ system. These shifts correlate with the varying inhomogeneous widths. Figure 34(*a*) shows that the gap between the I-d_8 origin in luminescence and the II-d_8 origin in excitation is 9·7 cm^{-1}. However, luminescence line narrowing experiments establish (Riesen and Krausz 1993b) a value of 8·7 cm^{-1} for this splitting. This discrepancy of $\approx$ 1 cm^{-1} can quantitatively be accounted for by the treatment presented in section 2.2 (see figure 5).

The $[Ru(bpy)(bpy\text{-}6,6'\text{-}d_2)_2]^{2+}/[Zn(bpy)_3](ClO_4)_2$ and the $[Ru(bpy)(bpy\text{-}d_8)_2]^{2+}/[Zn(bpy)_3](ClO_4)_2$ systems are particularly useful since the ^{3}MLCT origins of the single bpy ligand provide an internal blank experiment. No shift for the origins involving this ligand can occur. The gap between ^{3}MLCT origins of the bpy and the

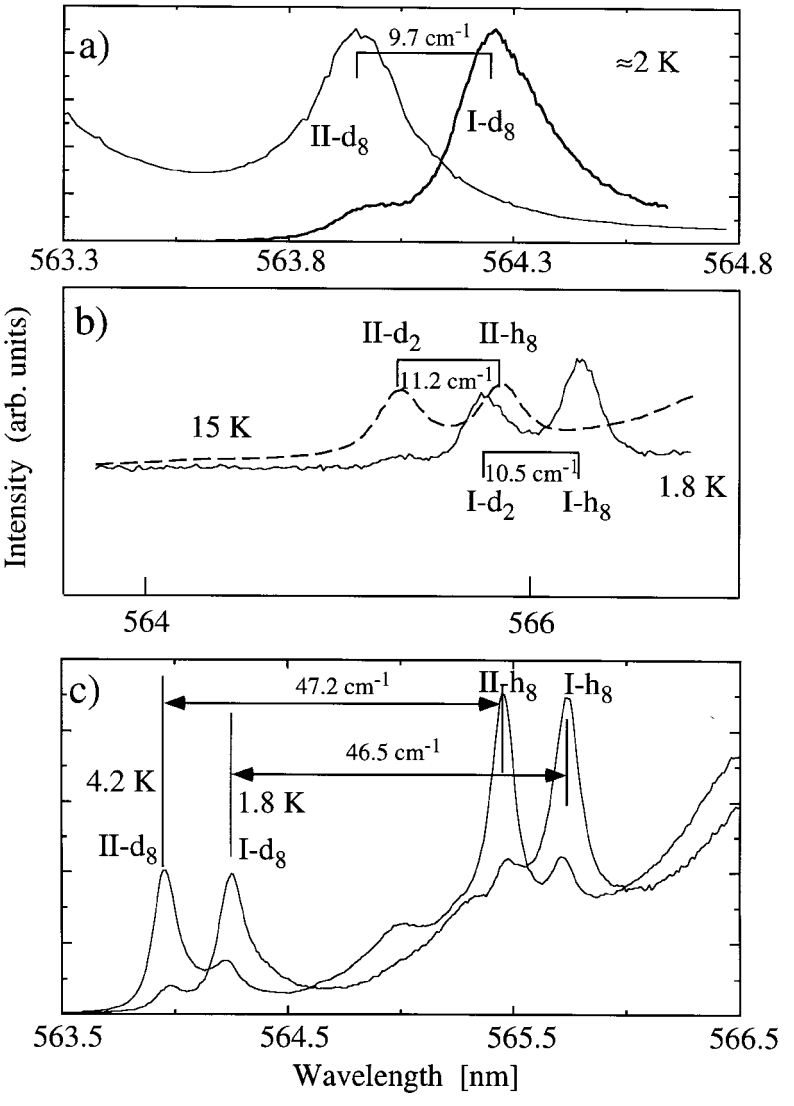

Figure 34. Stokes shift as seen in the comparison of: (*a*) luminescence and excitation spectra of the origin region of $[Ru(bpy\text{-}d_8)_3]^{2+}/[Zn(bpy)_3](ClO_4)_2$; (*b*) luminescence spectra of $[Ru(bpy)(bpy\text{-}6,6'\text{-}d_2)_2]^{2+}/[Zn(bpy)_3](ClO_4)_2$ in the region of the origins; (*c*) as in (*b*) but for $[Ru(bpy)(bpy\text{-}d_8)_2]^{2+}/[Zn(bpy)_3](ClO_4)_2$.

bpy-d_8 or bpy-6,6′-d_2 ligands increases between 1·8 K to 4·2 K when measured in luminescence. This is illustrated in panels (*b*) and (*c*) of figure 34. These effects are again quantitatively accounted for.

5.5. *Stark effects in* $[Ru(bpy)_3]^{2+}$ *and* $[Ru(bpy)(bpy\text{-}d_8)_2]^{2+}$

Stark experiments are a natural probe in the study of charge transfer transitions (Solomon *et al.* 1975, Høg *et al.* 1976, Oh and Boxer 1989, Oh *et al.* 1991). The most informative single crystal Stark data are obtained for the C2/c perchlorate crystals upon the application of an electric field perpendicular to the crystal *c* and *b* axes, that is $\mathbf{E} \| a$. Figure 35 schematically depicts a Stark experiment for a dilute $[Ru(bpy)_3]^{2+}/$

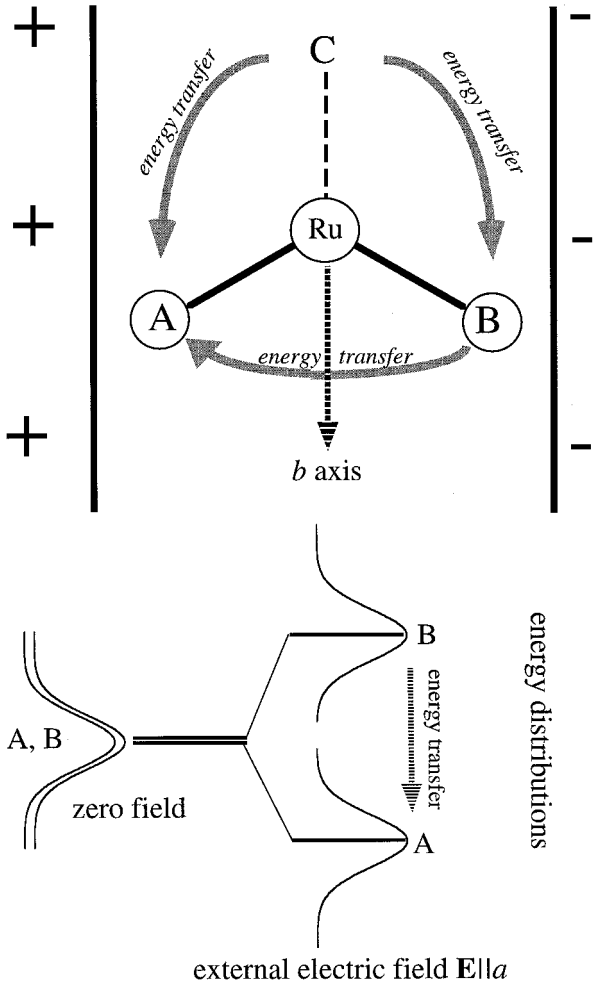

Figure 35. Schematic representation of the Stark effect with an electric field perpendicular to the crystal axes *b* and *c* in $[Ru(bpy)_3]^{2+}/[Zn(bpy)_3](ClO_4)_2$.

$[Zn(bpy)_3](ClO_4)_2$ crystal (Riesen *et al.* 1994b). The crystallographically equivalent ligands, labelled A and B in figure 35, become inequivalent in the external electric field. The ^{3}MLCT transitions to ligands A and B shift to lower/higher energy, respectively, for the direction of the electric field shown. A pseudo-Stark splitting of the electronic origins results. Fast intramolecular ^{3}MLCT excitation energy transfer between ligands A and B leads to thermalization well within the lifetime of the luminescence.

Figure 36 depicts the pseudo-Stark splitting of origin II and III of $[Ru(bpy)_3]^{2+}/[Zn(bpy)_3](ClO_4)_2$ in the non-selective excitation spectrum at 1·8 K (Riesen *et al.* 1994b). Origin I is obscured by the tail of origin II. Below 2 K most luminescence occurs from level I. Thus the pseudo-Stark splitting of origin I can be quantified in the luminescence spectra, as shown in figure 37 (*a*). ^{3}MLCT luminescence occurs predominantly from ligand A (see figure 36) which becomes lower in energy in the applied electric field. The pseudo-Stark splitting is the same for all three transitions, to within the experimental accuracy. This indicates that all three levels have the same

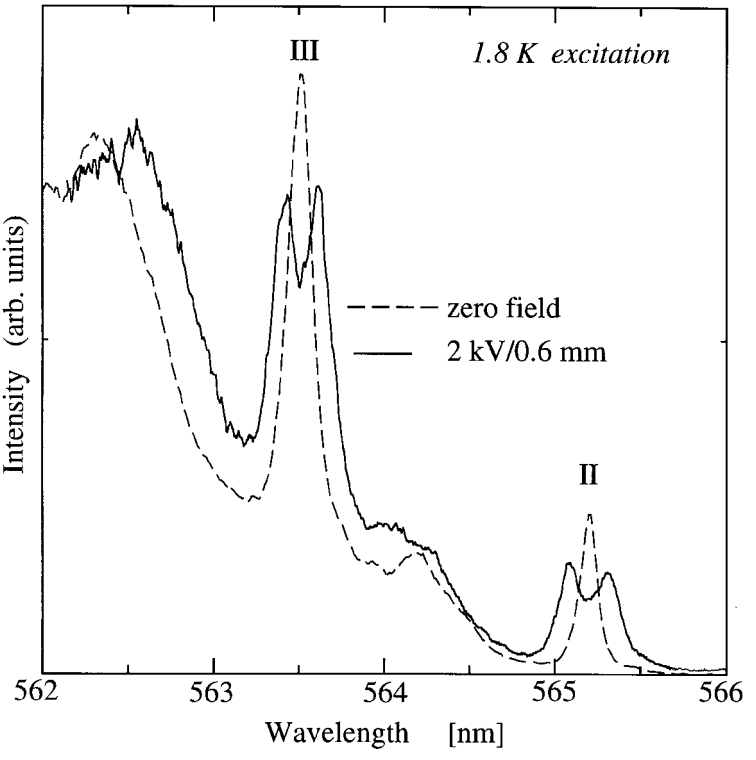

Figure 36. Pseudo-Stark splitting of origins II and III of $[Ru(bpy)_3]^{2+}$ in $[Zn(bpy)_3](ClO_4)_2$ as observed in excitation at 1·8 K.

orbital parentage. The large Stark effect corresponds to an excited state dipole moment of 1·2 eÅ which firmly establishes the charge transfer character of the lowest-excited states.

Non-resonantly narrowed luminescence spectra are shown in figure 37(*b*). They confirm that the observed Stark effect is a pseudo-splitting. When exciting into III-B, that is to say the ^{3}MLCT origin III of ligand B in the field $\mathbf{E} \| a$, the origins II-B and I-B are narrowed but the spectrum is dominated by non-narrowed ^{3}MLCT emission of ligand A at ≈ 2 K. The energies of the two crystallographically equivalent ligands are poorly correlated as is discussed above. Thus after excitation into III-B some narrowed ^{3}MLCT luminescence of ligand B is observed but at 2·1 K most of the ^{3}MLCT excitation energy is transferred to the lower-lying ligand A. The width of the feature activated by intramolecular energy transfer is close to the width of the inhomogeneous distribution because of the lack of correlation. If the observed structure were due to a Stark splitting of a degenerate level on a single chromophoric unit, narrowing would occur in all features.

When the luminescence is excited into III-A, the spectrum is dominated by the *narrowed* transitions I-A and II-A. However, at the high energy side of both transitions, a broad background of the non-narrowed ^{3}MLCT luminescence of B is also evident (shaded). This background is weak at 2·1 K because the ^{3}MLCT level of ligand B lies at higher energy. Assuming a Gaussian lineshape for the inhomogeneous distribution, the intensity ratio $I(B)/I(A)$ for the non-resonantly narrowed luminescence spectra shown in figure 37 is given by equation (19). The ratio is dependent

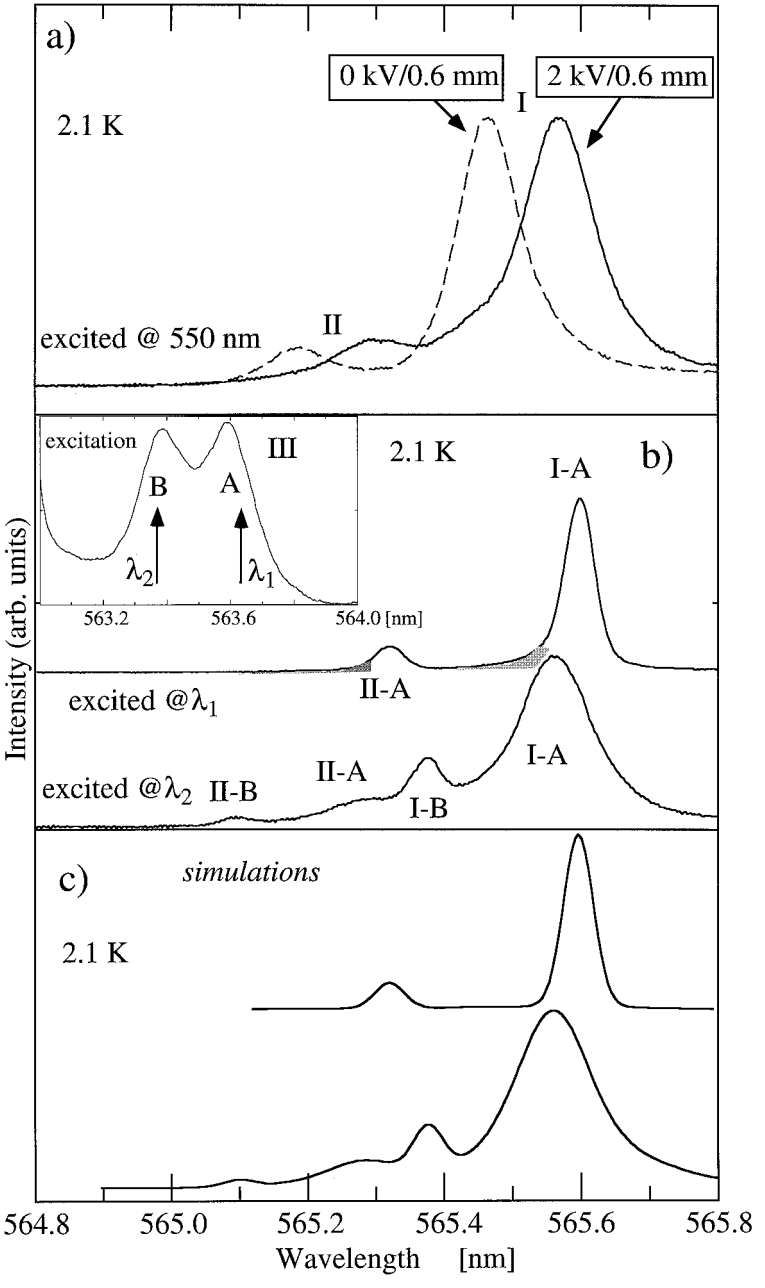

Figure 37. Stark effect in luminescence of $[Ru(bpy)_3]^{2+}/[Zn(bpy)_3](ClO_4)_2$. (*a*) Non-selectively excited luminescence spectrum in the region of origins I and II in zero and applied electric field $\mathbf{E} \| a$. (*b*) Luminescence line narrowing experiments using the pseudo-Stark split components of origin III. Excitation wavelengths λ_1 and λ_2 are indicated. (*c*) Simulated spectra corresponding to those in (*b*).

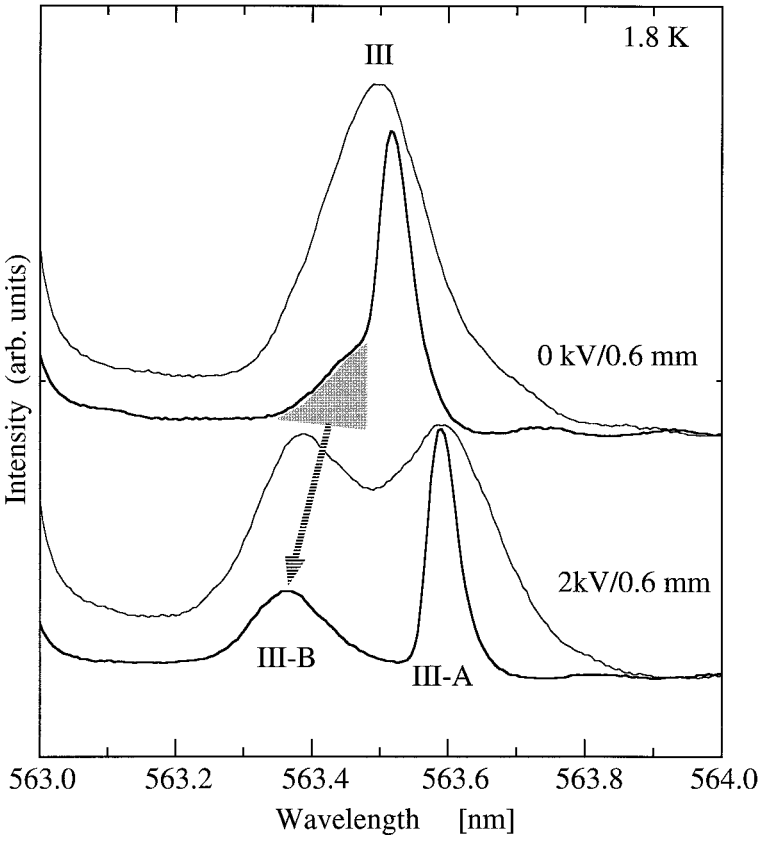

Figure 38. Narrowed excitation spectra of origin III of $[Ru(bpy)_3]^{2+}/[Zn(bpy)_3](ClO_4)_2$ in zero field and applied electric field $\mathbf{E} \| a$. Non-selective spectra are shown as thin lines.

on the excitation wavelength because the ^{3}MLCT energies of the ligands A and B are poorly correlated.

$$\frac{I(\mathrm{B})}{I(\mathrm{A})} = \frac{\displaystyle\int_{-\infty}^{\infty} \frac{\exp\left[\frac{-\Delta E}{kT}\right]}{1+\exp\left[\frac{-\Delta E}{kT}\right]} \exp\left[4\ln(2)\left(\frac{\Delta E-\Delta E_0}{\Gamma}\right)^2\right] \mathrm{d}\Delta E}{\displaystyle\int_{-\infty}^{\infty} \frac{1}{1+\exp\left[\frac{-\Delta E}{kT}\right]} \exp\left[4\ln(2)\left(\frac{\Delta E-\Delta E_0}{\Gamma}\right)^2\right] \mathrm{d}\Delta E}. \tag{19}$$

In equation (19) Γ is the inhomogeneous line width. ΔE_0 is the energy difference between the narrowed feature and the maximum of the inhomogeneous distribution of the ^{3}MLCT energy of the crystallographically related ligand. The latter is taken from non-selective spectra.

In figure 37 (*c*) we show simulations of the narrowed spectra assuming a Boltzmann distribution with a temperature of 2·1 K. The sum of two Gaussians, as obtained from a least squares fit of the zero field spectrum, was used to describe the inhomogeneous distribution of each origin. The agreement between experimental and simulated Stark spectra is excellent.

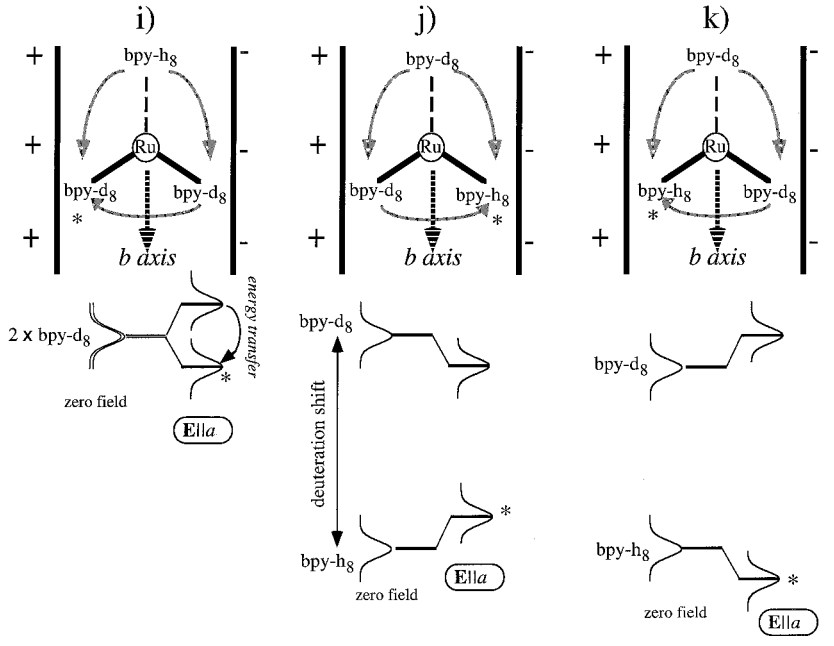

Figure 39. Schematic of Stark effects in $[Ru(bpy)(bpy\text{-}d_8)_2]^{2+}/[Zn(bpy)_3](ClO_4)_2$ with an electric field $\mathbf{E} \| a$. Asterisks denote the ligand from which ^{3}MLCT emission can occur at lowest temperature and in moderate electric fields. The direction of the *b* axis is indicated. Curved arrows show the directions of intramolecular ^{3}MLCT excitation energy transfer.

The independence of the ^{3}MLCT transitions to the two ligands A and B manifests itself in the excitation line narrowing experiments illustrated in figure 38 (Riesen *et al.* 1994b). While the lower component III-A due to the ligand A shows a significant narrowing, the higher component III-B remains broad. This is because the emission was selectively monitored in origin I-A. The independence of the two components is also corroborated by the observation that the energy separation between the narrowed and the broad feature in the selective excitation spectra is dependent on the wavelength at which the luminescence is detected. The peak maximum of the broad III-B component is less dependent on the monitoring wavelength within I-A than that of the narrowed III-A feature. The intensity ratio of the narrowed III-A to the broad III-B origin is 1:1, in accord with expectations.

We have extended the studies of the Stark effects to $[Ru(bpy)(bpy\text{-}d_8)_2]^{2+}$ doped in $[Zn(bpy)_3](ClO_4)_2$ (Riesen and Krausz 1996b). These experiments confirm, in an elegant fashion, assignments of origins to independent ^{3}MLCT excitations of the bpy-h_8 and the bpy-d_8 ligands. They also demonstrate that the observed effect is indeed a pseudo-Stark splitting. Figure 39 outlines the Stark effects in this system. One third of the complexes enter the lattice with both bpy-d_8 ligands in the crystallographically equivalent positions. We denote this as configuration (i) in figure 39. In this configuration ^{3}MLCT luminescence occurs from the bpy-d_8 ligands since the bpy-h_8 ligand in the distinct position is significantly higher in energy. For an electric field $\mathbf{E} \| a$ the two byp-d_8 ligands become inequivalent. Intramolecular excitation energy transfer ensures that this pseudo-Stark splitting is thermalized in luminescence.

Two thirds of the complexes enter the lattice with one bpy-d_8 ligand in the distinct position. We denote these as configurations (j) and (k) in figure 39. The two

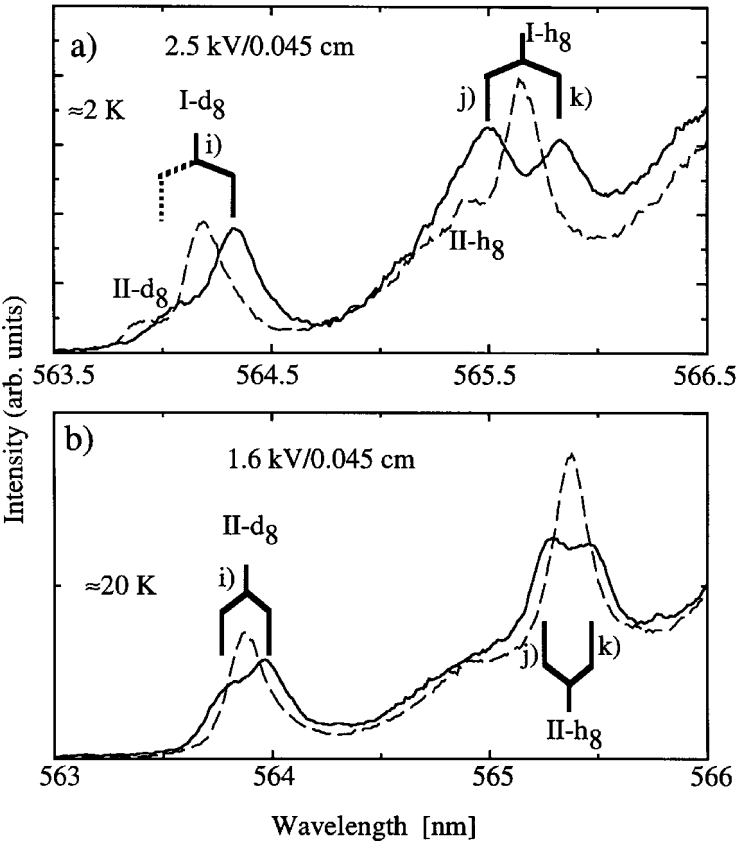

Figure 40. Luminescence spectra of $[Ru(bpy)(bpy\text{-}d_8)_2]^{2+}/[Zn(bpy)_3](ClO_4)_2$ in the region of the electronic origins I-(h_8, d_8), II-(h_8, d_8) for an electric field $\mathbf{E} \| a$. The dashed lines show the spectra in zero field.

configurations (j) and (k) are equivalent in zero field but become inequivalent in the electric field. For the direction of the field indicated in figure 39 the ^{3}MLCT transitions of the bpy-h_8 ligand in the crystallographically equivalent position shift to higher energy for configuration (j) and to lower energy for configuration (k). The pseudo-Stark splitting is not thermalized, since the cations in configurations (j) and (k) are well separated, inhibiting *inter*molecular energy transfer.

Figure 40 shows 2 K and 20 K luminescence spectra of the electronic origins in an electric field. As predicted, the pseudo-splittings of I-h_8 and II-h_8 are not thermalized because the components at higher and lower energy are associated with configurations (j) and (k), respectively. In contrast, the relative intensities of the two components of I-d_8 and II-d_8 are governed by a Boltzmann distribution, since they arise from the same configuration (i). At elevated temperatures the ^{3}MLCT emission may occur from the ligand which is higher in energy in the electric field. Calculated intensity ratios for the two split components of I-d_8 or II-d_8 are in quantitative agreement with the experiment.

The components of I-h_8 and II-h_8 arising from the configurations (j) and (k) can be selectively excited by using the corresponding components of III-h_8 (Riesen and Krausz 1996b). Narrowed luminescence spectra of I-d_8, II-d_8 display corresponding behaviour to the $[Ru(bpy)_3]^{2+}/[Zn(bpy)_3](ClO_4)_2$ system (see figure 37). Figure 41 shows narrowed excitation spectra for the origins III-d_8 and III-h_8 of the

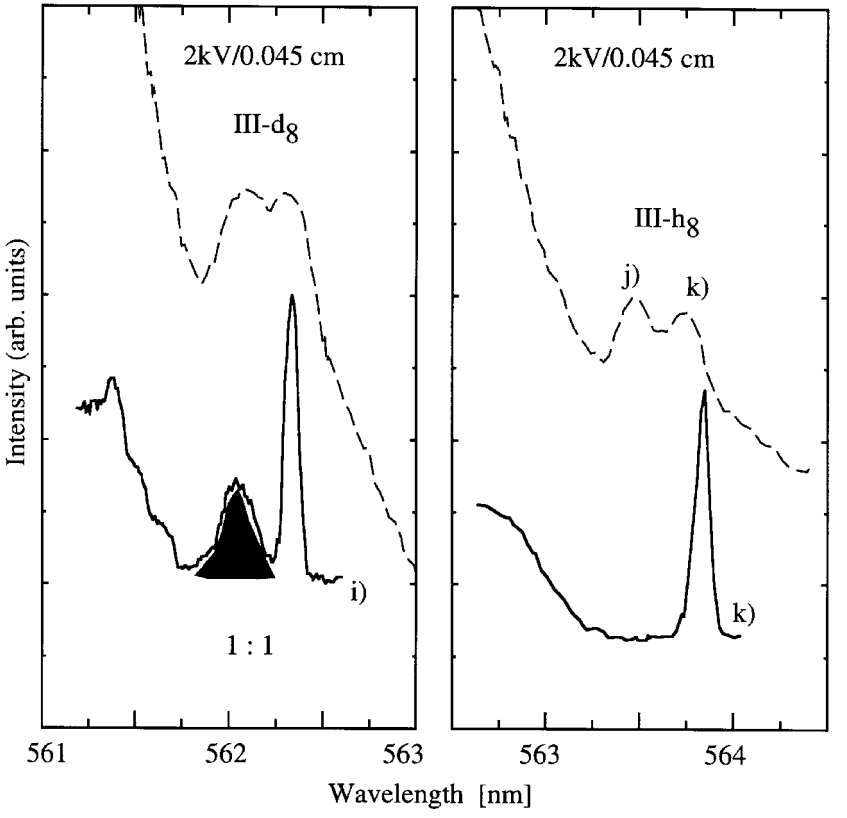

Figure 41. Narrowed excitation spectra of origins III-h_8, III-d_8 of $[Ru(bpy)(bpy\text{-}d_8)_2]^{2+}/[Zn(bpy)_3](ClO_4)_2$ in $\mathbf{E} \| a$ at 2 K. The non-selective spectrum monitored at 570 nm is shown as a dashed line. The narrowed excitation spectra were monitored in I-h_8 and I-d_8.

$[Ru(bpy)(bpy\text{-}d_8)_2]^{2+}/[Zn(bpy)_3](ClO_4)_2$ system. When the component (k) of I-h_8 is monitored in luminescence with a narrow bandwidth the lower-energy component of III-h_8 is narrowed. Complementarily, the higher component of III-h_8 is narrowed upon monitoring of the component (j) of I-h_8. In contrast, when I-d_8 is monitored, two features with a ratio of the integrated intensities of 1 : 1 are observed for origin III-d_8. The lower-energy feature is narrowed whereas the higher-energy feature shows a width comparable to the inhomogeneous width. The selective spectrum for III-d_8 monitored in I-d_8 arises from the configuration (i) since this is the only configuration which leads to ^{3}MLCT emission from the bpy-d_8 ligand at 2 K. The narrowed feature is due to the bpy-d_8 ligand whose ^{3}MLCT transition is at lower energy in the electric field. The broader feature is due to the bpy-d_8 ligand whose ^{3}MLCT transition is at higher energy in the electric field and thus is deactivated by intramolecular excitation energy transfer to the Ru-bpy-d_8 subunit monitored in luminescence at lower energy. Again nanoheterogeneity leads to the broad feature showing a width comparable to the inhomogeneous broadening.

5.6. *High resolution experiments on* $[Ru(bpy)_3]^{2+}$

Line widths observed in narrowing experiments reviewed in previous sections were limited by the direct relaxation rate of the level III and/or the instrumental resolution

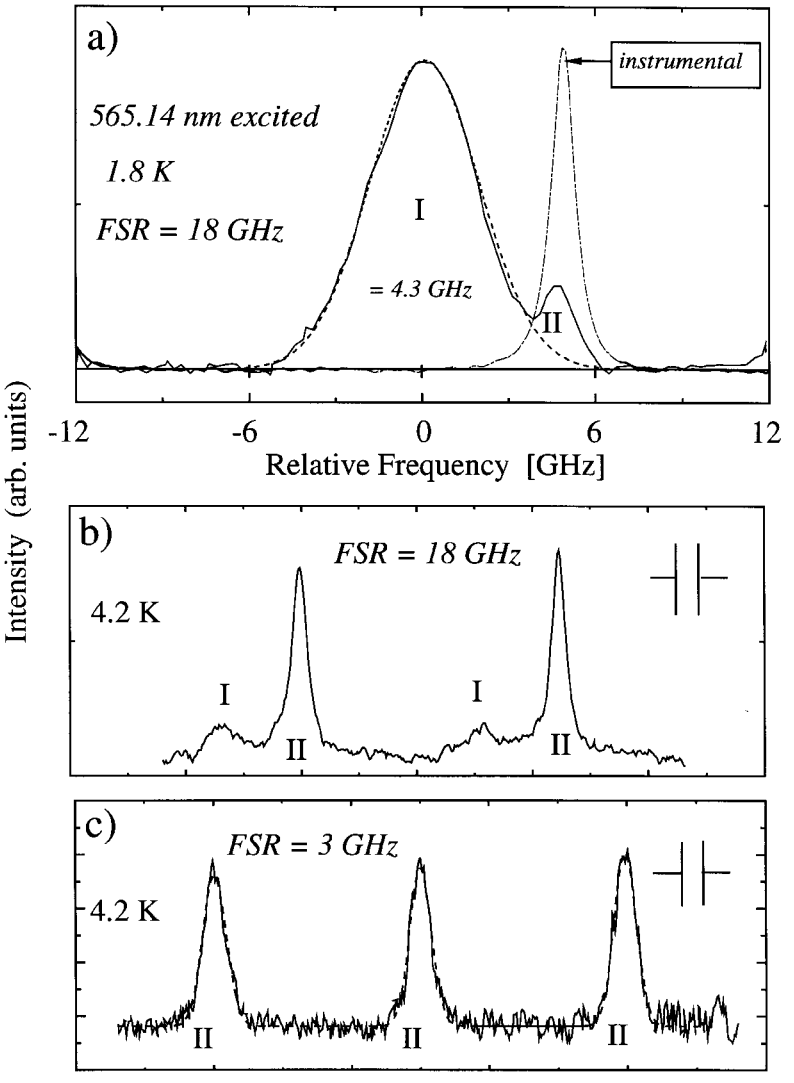

Figure 42. Resonant luminescence line narrowing in origin II of $[Ru(bpy)_3]^{2+}/[Zn(bpy)_3](ClO_4)_2$. The instrumental lineshape is indicated in the panel (*a*). The instrumental line width is given in (*b*) and (*c*). The free spectral range (FSR) of the Fabry–Pérot interferometer is indicated for all three traces.

of 1 cm^{-1} = 30 GHz. We have performed high resolution resonant luminescence line narrowing experiments by exciting into origin II and analysing the luminescence with a scanning plane-parallel Fabry–Pérot interferometer. Some of the data is illustrated in figure 42. An upper limit of $\approx 25 \pm 5$ MHz can be deduced for the homogeneous line width of origin II at 4·2 K. These experiments also show that the energies of level I and level II on a single metal–ligand subunit are well correlated, with a variation of only $\approx 1\%$ (Riesen and Krausz 1993c).

The large pseudo-Stark splittings, reported in the previous section, together with the small homogeneous line width of origin II facilitate Stark-swept transient hole-burning experiments. Such an experiment is schematically portrayed in figure 43 (Muramato *et al.* 1977, Shoemaker 1979). In a conventional transient hole-burning

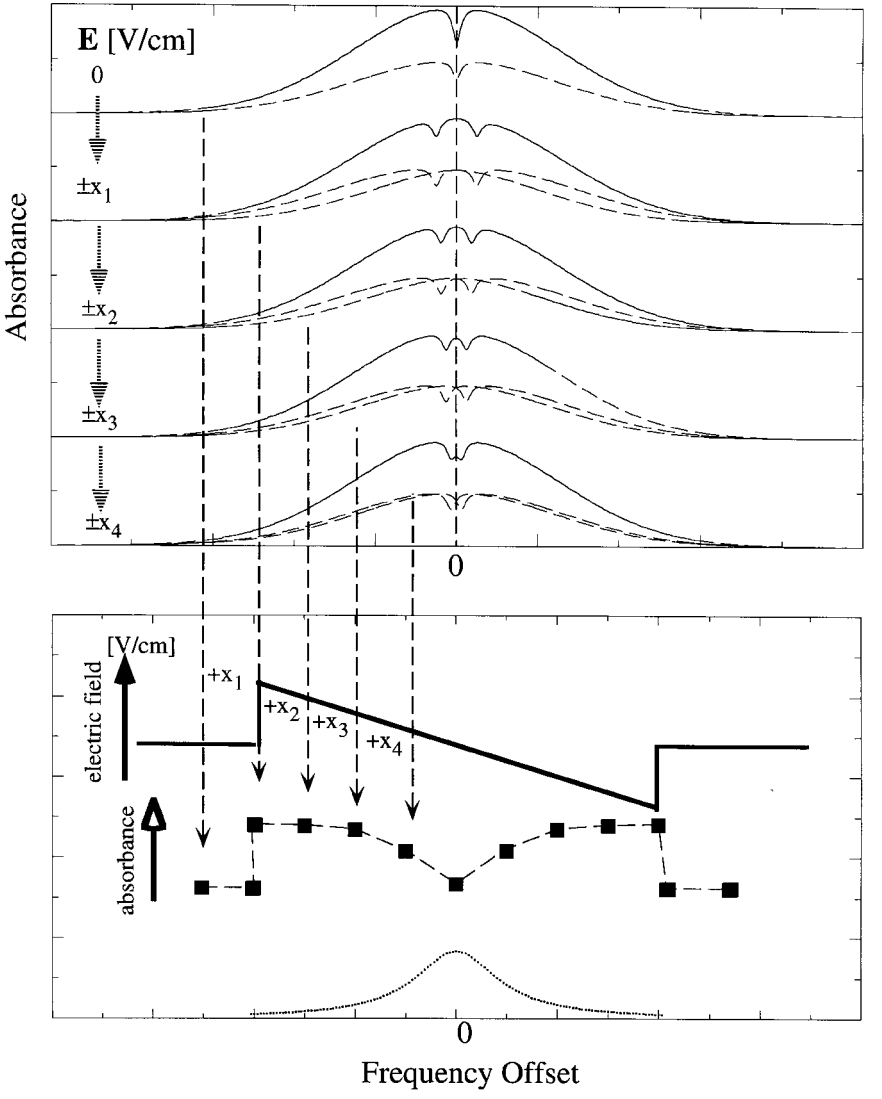

Figure 43. Schematic representation of Stark-swept transient hole-burning. After burning in zero field the spectral hole is read out by an applied electric field x. The transmission at the laser wavelength changes with x.

experiment the laser is scanned across the spectral hole within the lifetime of the metastable state. In the Stark-swept hole-burning experiment the 'sample frequency' is swept via the application of a small external field and the laser is kept at constant frequency.

In the experiment performed on $[Ru(bpy)_3]^{2+}$ doped in $[Zn(bpy)_3](ClO_4)_2$ a single-frequency dye laser is held at constant wavelength within the inhomogeneous width of origin II. The sample is kept in zero field for a burn period of ≈ 300 μs. At adequate laser powers a ground state depletion occurs for the chromophores which have the origin II in resonance with the laser frequency. To read out the hole an electric field $\mathbf{E} \| a$ of $+2$ V/0·6 mm is then applied and swept to -2 V/0·6 mm in ≈ 45 μs (Riesen and Krausz 1993c). This readout of the spectral hole is illustrated in figure 44. The

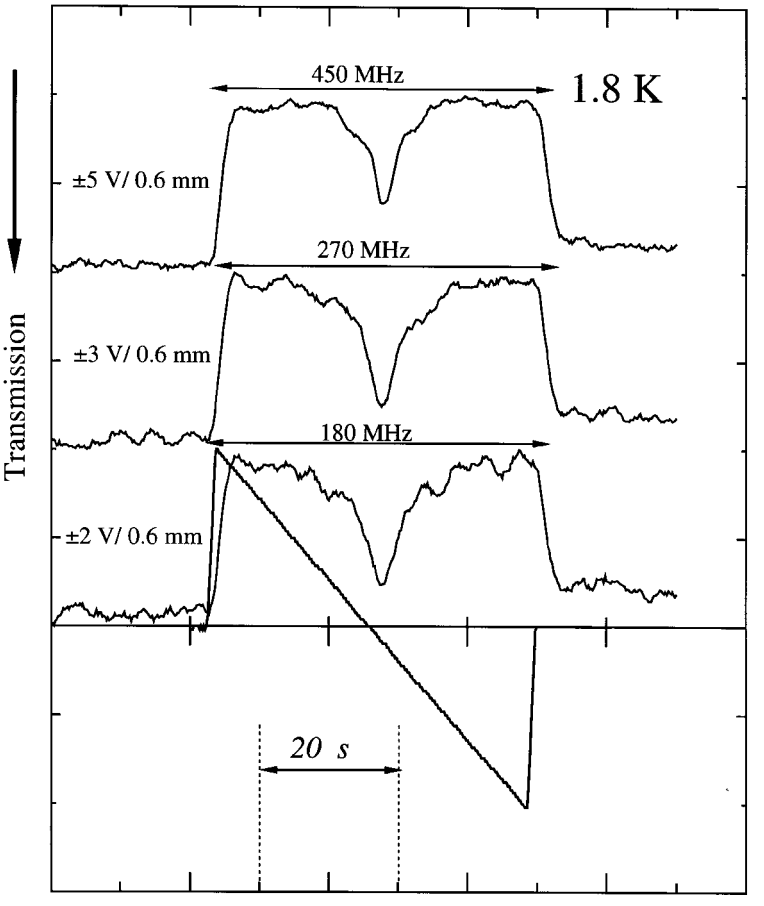

Figure 44. Transient Stark-swept spectral hole-burning in origin II of $[Ru(bpy)_3]^{2+}/[Zn(bpy)_3](ClO_4)_2$. The timescale and the amplitude of the applied voltage ramp (electric field) are indicated.

observed hole-width of ≈ 30 MHz at 1·8 K provides an upper limit of the homogeneous line width of ≈ 15 MHz ($= 0{\cdot}0005$ cm^{-1}). The rate of the direct relaxation process to level I is $\approx 5 \times 10^6$ s^{-1} and is too slow to be responsible for the observed line width. Relaxation times T_1 are related to homogeneous line widths by equation (20).

$$\Gamma = \frac{1}{2\pi T_1}. \tag{20}$$

The upper limit for the homogeneous line width provided by this experiment indicates that the average excitation energy transfer within the excited state II cannot be faster than $\approx 1 \times 10^8$ s^{-1}. This value is in remarkable agreement with the directly measured transfer rate in time resolved luminescence line narrowing experiments (see section 5.4).

A range of luminescence line narrowing and hole-burning experiments confirm the non-degenerate nature of the lowest-excited states. The absence of side lines and side holes in the narrowed luminescence spectra and transient hole-burning experiments in the range of 300 MHz to 15 GHz is in conflict with the interpretation of a number of optically detected magnetic resonance (ODMR) experiments (Yamauchi *et al.* 1986,

Table 2. Reported ODMR resonances of some ^{3}MLCT systems.

System	Frequencies (GHz)	Reference
Crystalline $[Ru(bpy)_3](BF_4)_2$	0·64, 1·80, 2·51, 3·36, 4·11	Yamauchi *et al.* (1986)
$[Ru(bpy)_3](BF_4)_2$ in methanol	0·62, 1·73, 2·56, 3·49, 4·06	Yamauchi *et al.* (1986)
$[IrCl_2(phen)_2]Cl$ in 4:1 ethanol/methanol	0·59, 1·76, 2·43, 2·85, 3·26	Yamauchi *et al.* (1986)
Crystalline $[Ru(bpy)_3](PF_6)_2$	1·89, 2·81, 3·26, 4·16, 4·35	Yersin *et al.* (1989)
Crystalline $[Ru(bpy)_3](ClO_4)_2$	3·41, 4·34, 4·75	Yersin *et al.* (1989)

Yersin *et al.* 1989). Weak signals in the 1 to 5 GHz range were interpreted as due to electronic fine structure. Some ODMR results are summarized in table 2.

Yamauchi *et al.* (1986) attributed the observed resonances to transitions between the levels of a triplet state with small zero field splittings (ZFSs). This is analogous to the situation in a $^3\pi$–π^* state or a ligand-centred triplet state. Such a triplet state with $S = 1$ and $g = 2{\cdot}0$ has a well defined Zeeman pattern in optical spectroscopy. The splitting becomes linear as soon as the Zeeman energy is significantly larger than the ZFSs (Glynn *et al.* 1969). For ZFSs of the order of magnitude of a few GHz, this is easily achieved. Characteristic spin triplet patterns are *not* observed (see section 5.7) for the lowest-excited states in $[Ru(bpy)_3]^{2+}$, clearly excluding this explanation.

Yersin *et al.* (1989) assigned the observed frequencies to the transition between the components of a weakly split E state at a number of distinct sites. This model is inconsistent with the observation of comparable frequencies in the lower symmetry *bis*-diimine complex $[IrCl_2(phen)_2]Cl$ (Yamauchi *et al.* 1986) and the crystal structures of the investigated materials. Furthermore, if the proposed E level splitting was so strongly dependent on local environments, a *continuous* range of splittings would result for amorphous hosts. The experiments discussed in previous sections exclude the possibility of small ZFSs. The apparent ODMR resonances may be due to heating phenomena, since very high microwave powers were used in these experiments.

5.7. *Zeeman effects in* $[Ru(bpy)_3]^{2+}$

For localized ^{3}MLCT states the Zeeman effect on each metal–ligand subunit can be treated independently. We choose the Z coordinate parallel to the threefold and quasi-threefold axis of $[Ru(bpy)_3]^{2+}$ in $[Ru(bpy)_3](PF_6)_2$ and $[Zn(bpy)_3](ClO_4)_2$, respectively. The Y axis is chosen parallel to the metal–ligand direction. Equation (21) describes the Zeeman interaction energy between any two of the levels I, II and III.

$$H_{a\_b} = \mu_B \mathbf{B} \cdot \langle a | \mathbf{L} + 2\mathbf{S} | b \rangle. \tag{21}$$

μ_B is the Bohr magneton, $\mathbf{B} = (B^X, B^Y, B^Z)$ is the magnetic field, and $\mathbf{L}$ and $\mathbf{S}$ are dimensionless electronic orbital and spin momenta respectively.

The interaction between the three levels on one metal–ligand subunit in an external magnetic field is then described by the matrix (22).

$$\begin{bmatrix} 0 & H_{\text{I–II}} & H_{\text{I–III}} \\ H_{\text{I–II}} & \Delta E_{\text{I–II}} & H_{\text{II–III}} \\ H_{\text{I–III}} & H_{\text{II–III}} & \Delta E_{\text{I–III}} \end{bmatrix}. \tag{22}$$

The elements H_{a-b} are conveniently described in terms of *effective* g-values in the directions X, Y and Z.

$$\langle a|\mathbf{L}+2\mathbf{S}|b\rangle = \mathbf{g}_{a-b} = (g_{a-b}{}^{X}, g_{a-b}{}^{Y}, g_{a-b}{}^{Z}). \tag{23}$$

The energy spacings $\Delta E_{\mathrm{I-II}}$ and $\Delta E_{\mathrm{I-III}}$ in the diagonal of equation (22) are determined from the spectra in zero field.

With a magnetic field parallel to the crystal c axis crystallographically identical ligands remain equivalent for both the $[Ru(bpy)_3]^{2+}/[Zn(bpy)_3](ClO_4)_2$ and the $[Ru(bpy)_3](PF_6)_2$ systems. If the magnetic field is applied in the metal–ligand plane perpendicular to the (quasi-)threefold axis, the two like ligands in the perchlorate crystal and the three ligands in the hexafluorophosphate crystal become, in general, inequivalent. The Zeeman effect on levels I, II and III for each subunit is calculated by diagonalizing matrix (22). For a general direction of **B**, the energies I, II and III of each subunit are affected differently. We assume thermal equilibrium amongst all levels of the metal–ligand subunits. For each subunit the eigenvectors $|\mathrm{I}'\rangle$, $|\mathrm{II}'\rangle$, and $|\mathrm{III}'\rangle$ of matrix (22) are linear combinations of the zero field wavefunctions $|\mathrm{I}\rangle$, $|\mathrm{II}\rangle$, and $|\mathrm{III}\rangle$. The relative intensities of the transitions between the ground state and the perturbed I′, II′, and III′ levels are readily calculated by using the experimentally determined intensities in zero field (Riesen *et al.* 1994b).

Narrowed luminescence spectra in a magnetic field $\mathbf{B}\perp c$ of 5 T are shown in figure 45 for the C2/c $[Ru(bpy)_3]^{2+}/[Zn(bpy)_3](ClO_4)_2$ system. In these spectra the luminescence lines I and II were non-resonantly narrowed by exciting into origin III. The main effect observed in figure 45 is due to a dominant I–II Zeeman interaction, since the I–II energy spacing is relatively small. Peak positions, intensities and the lineshapes show a significant dependence on the angle α between the direction of the magnetic field and the crystal b axis. No angular dependence would be observed for delocalized states of a trigonal chromophore. Each direction in the metal–ligand plane would give rise to the same Zeeman pattern.

The spectra in figure 45 can then be modelled by using the effective g-values of g_X(I–II) = 2·3 and g_Y(I–III) = 2·5 and energy splittings, line widths and intensity ratios determined in zero field. The crystal used in this work was twinned but with a large single crystal section which was ≈ 3 times as big as the smaller section. The calculated spectra of the two twins were added (Riesen *et al.* 1994b, Riesen and Krausz 1994b). Peak positions and intensities are quantitatively reproduced by a single set of parameters for all angles α. The temperature dependence of the MCPL spectra of the emitting levels I and II of $[Ru(bpy)_3](PF_6)_2$ also demonstrate their non-degenerate nature (Riesen and Krausz 1988). Correspondingly, no splitting is observed in Zeeman experiments with magnetic fields parallel to the crystal c axis (Krausz 1987, Riesen and Krausz 1994b). Polarized luminescence spectra with fields perpendicular to the crystal c axis were used as evidence for delocalization (Braun *et al.* 1990).

We have subsequently shown (Riesen and Krausz 1994b) that details of the Zeeman spectra can only be rationalized by the localized model. The effective g values that were used for the perchlorate system are also adequate for the hexafluorophosphate crystal. Experimentally determined energy spacings of $\Delta E_{\mathrm{I-II}} = 6{\cdot}9\ \mathrm{cm}^{-1}$ and $\Delta E_{\mathrm{I-III}} = 61\ \mathrm{cm}^{-1}$ were used in the calculation. The inhomogeneously broadened lines were described by Gaussians of $2{\cdot}5\ \mathrm{cm}^{-1}$ width. Intensity ratios of II:I = 70:1 and III:I = 400:1 were used. Contributions from each metal–ligand subunit were then added. For the special direction of the magnetic field

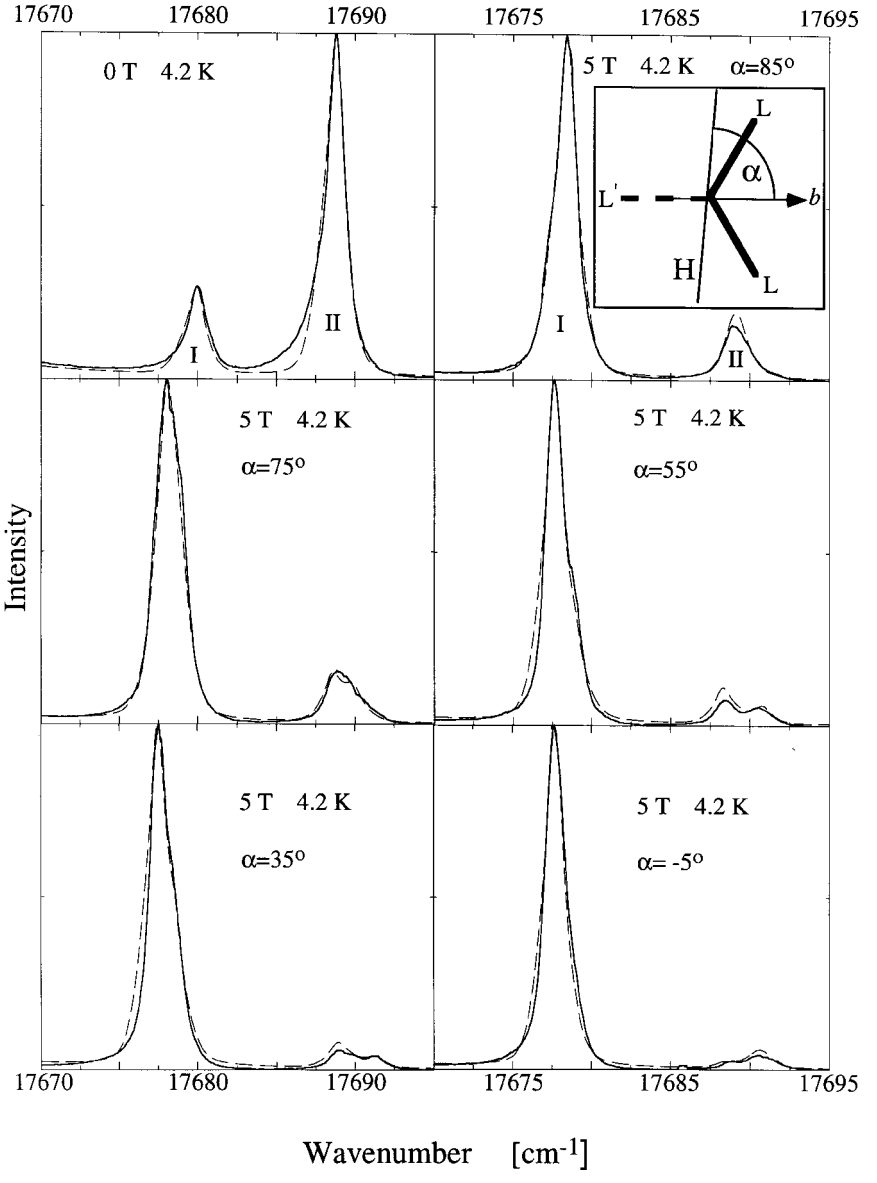

Figure 45. Non-resonant luminescence line narrowing of origins I and II in $[Ru(bpy)_3]^{2+}/[Zn(bpy)_3](ClO_4)_2$ in an external magnetic field of 5 T with $\mathbf{B} \perp c$. The spectra were non-resonantly excited via origin III. The angle α between the crystal b axis and the magnetic field is indicated. The calculated spectra are shown as dashed lines (see text).

shown in figure 46 two subunits remain equivalent. These subunits show a relatively large Zeeman effect. The other metal–ligand subunit lies parallel to the direction of the magnetic field leading to a vanishing I–II Zeeman interaction. Features at the higher and lower side of origins II and I, respectively, involve the magnetically equivalent ligands. Features seen close to those in zero field are associated with the metal–ligand subunit lying parallel to the magnetic field. The simulated spectra for the two polarizations are shown as dashed lines in figure 46 and show remarkable agreement with the observed spectra.

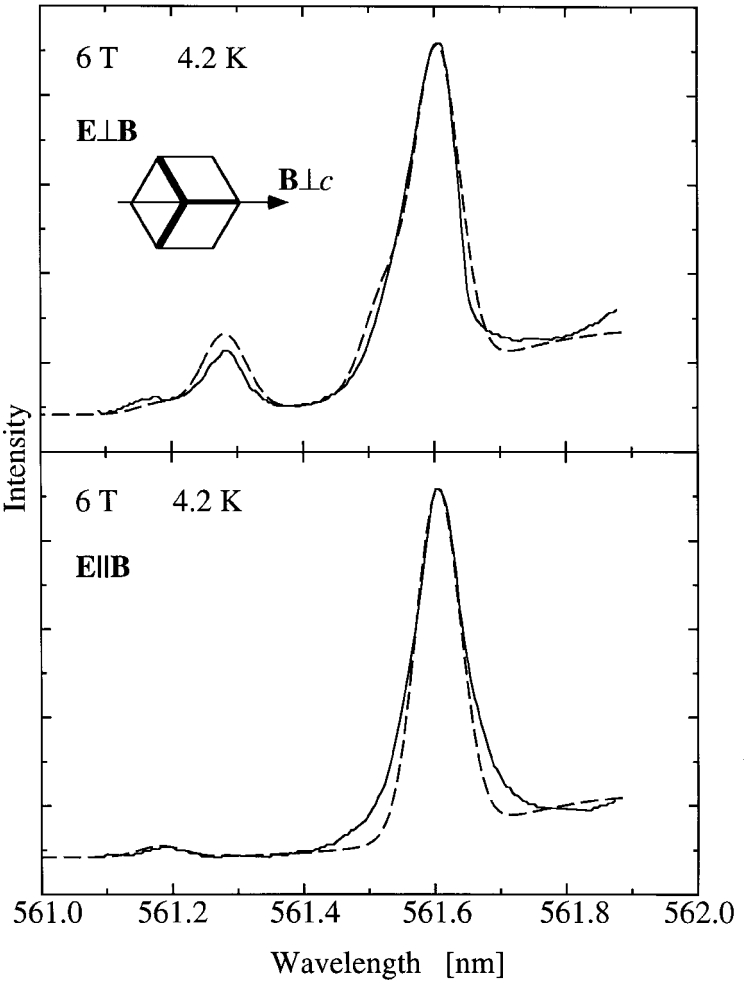

Figure 46. Luminescence spectra of $[Ru(bpy)_3](PF_6)_2$ in the region of the electronic origins I and II in 6 T with $\mathbf{B} \perp c$ and 4·2 K. The experimental data, shown as solid lines, were taken from Braun *et al.* (1990). Dashed lines were calculated as discussed in the text.

5.8. *Vibrational sidelines in localized ^{3}MLCT emission*

The displacement of potential energy surfaces in excited states is characteristic of the nature of the excitation. Huang–Rhys parameters S_v are used to quantify displacements of potentials along normal coordinates v.

For chromophores in the solid state one also has to consider the coupling to modes of the host environment. The extent to which a chromophore couples to the modes of the environment has been used as an indicator of delocalization/localization of electronic excitation. For example, the relative intensity of naphthalene-d_8 modes (host modes) in the luminescence spectra of partially deuterated naphthalene-d_x doped in naphthalene-d_8 was used to estimate the delocalization of the d_x triplet exciton into the d_8 host (Ochs *et al.* 1974).

The ^{3}LC emission of mixed chelate metal–diimine systems, such as [Rh(2-thienylpyridine)$_x$(2-phenylpyridine)$_{2-x}$(bpy)]$^+$ (x = 1, 2), is dominated by vibrational sidelines associated with the ligand on which the ^{3}LC transition is localized (Colombo

et al. 1991, Frei *et al.* 1992, Glasbeek and Giesbergen 1996). The ^{3}MLCT emission process is distinctly different. The presence/absence, in the luminescence spectrum, of vibrational sidelines associated with a particular ligand cannot be used, *a priori*, as evidence for localization or delocalization of the ^{3}MLCT excitation.

The Huang–Rhys parameters S_v for the observed high frequency bpy modes in $[Ru(bpy)_3]^{2+}$ do not exceed $\approx 0{\cdot}1$. These values of S are only an order of magnitude smaller in the $^2E \rightarrow {}^4A_2$ luminescence of $[Cr(bpy)_3]^{3+}$. This d–d transition is metal-centred and thus shielded from the environment. Furthermore, this transition can be described as a pure spin–flip of the d-configuration and is thus minimally coupled to the environment, since it is crystal field independent in a first order approximation. For example, the S value for the 1322 cm^{-1} bpy mode is $\approx 0{\cdot}06$ in $[Ru(bpy)_3]^{2+}$, $\approx 0{\cdot}04$ in $[Os(bpy)_3]^{2+}$, $\approx 0{\cdot}02$ in $[Ru(bpy)_2(bpz)]^{2+}$ and $\approx 0{\cdot}003$ in $[Cr(bpy)_3]^{3+}$.

^{3}MLCT transitions are *two centre* transitions. Ligands not directly involved in the ^{3}MLCT transition do see the metal change oxidation state in the charge transfer process. The interaction with the bpy ligand is quite different for ruthenium(II) and ruthenium(III). This is reflected in the lowering of bpy frequencies in the $[Ru(bpy)_3]^{2+}$ complex in comparison with the 3+ oxidation state. Thus vibrational sidelines associated with spectator ligands will appear in luminescence spectra. Their Huang–Rhys parameter can be expected to be larger than in the $^2E \rightarrow {}^4A_2$ emission mentioned above, where no charge redistribution occurs on the central metal atom.

We note that bpy modes can be observed in the localized ^{3}MLCT emission of the $[Ru(bpy)_2(bpz)]^{2+}$ and the $[Ru(bpy)_2(bprid)]^{2+}$ complexes (see also section 5.2). This is exemplified in figure 47 where the vibrational sidelines in the region of high-energy frequencies in the luminescence of $[Ru(bpy)_2(bpz)]^{2+}$ are compared with the sidelines of the $[Ru(bpy)_3]^{2+}$ and $[Os(bpy)_3]^{2+}$ complexes. We stress here that the relative intensities of vibrational sidelines vary significantly between the osmium and the ruthenium tris-bpy complexes. Although the lowest-excited ^{3}MLCT states are localized on the bpz ligand in the $[Ru(bpy)_2(bpz)]^{2+}$ complex, we observe sidelines attributable to bpy vibrations over the 50–2000 cm^{-1} frequency range. The bpy modes were unambiguously identified by a comparison of sidelines with those of the corresponding deuterated complex $[Ru(bpy\text{-}d_8)_2(bpz)]^{2+}$.

Figure 48 shows the sidelines in the luminescence spectra of the $[Ru(bpy)_{3-x}(bpy\text{-}d_8)_x]^{2+}$ (x = 0 to 3) series in $[Zn(bpy)_3](ClO_4)_2$ in the 1000–1600 cm^{-1} region (Riesen *et al.* 1995a). The ^{3}MLCT emission of bpy-d_8 shows a stronger coupling to bpy-d_8 modes than the ^{3}MLCT emission of bpy. Vibrational sidelines couple more strongly if they involve the ligand from which the ^{3}MLCT emission occurs. The 1495 cm^{-1} bpy mode is not apparent in the ^{3}MLCT emission of bpy-d_8 and bpy-d_2 in $[Ru(bpy)(bpy\text{-}d_8)_2]^{2+}$ and $[Ru(bpy)(bpy\text{-}6,6'\text{-}d_2)_2]^{2+}$ in $[Zn(bpy)_3](ClO_4)_2$. For these emissions to occur, the bpy ligand is in the distinct position and thus has C_2 symmetry. The 1495 cm^{-1} mode is also absent in the hexafluorophosphate salt in which all ligands have C2 symmetry. It is possible that this mode occurs only for the ligands which have lower symmetry.

5.9. *Lifetime measurements*

In sufficiently dilute systems, intermolecular energy transfer does not occur within the lifetime of the excited state. However, intramolecular ^{3}MLCT excitation energy transfer is fast ($\geqslant 1 \times 10^8$ s^{-1}). Thus the luminescence of each isolated chromophore decays as a single exponential. The luminescence below 10 K in the $[Ru(bpy)_2(bpy\text{-}d_8)]^{2+}/[Zn(bpy)_3](ClO_4)_2$ system occurs predominantly from the bpy ligands and the energy transfer rate from the bpy-d_8 to the bpy ligand is more than 10^5 times faster

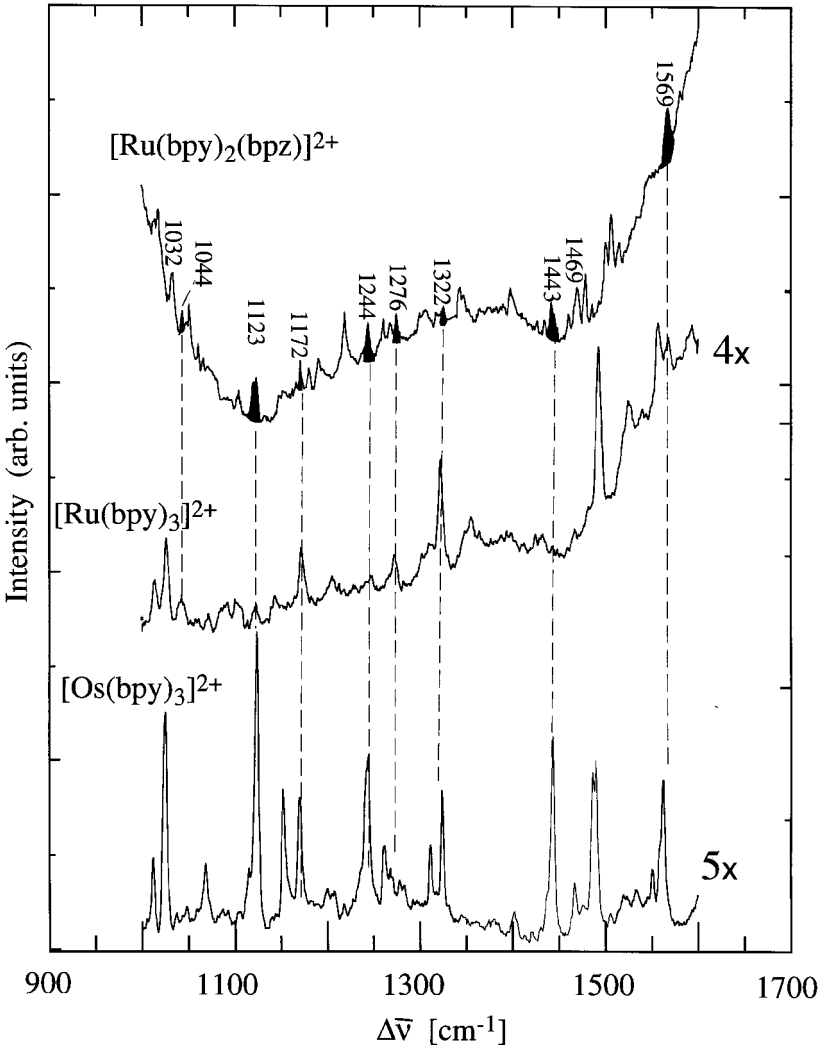

Figure 47. Vibrational sidelines in the luminescence of $[Ru(bpy)_2(bpz)]^{2+}$, $[Ru(bpy)_3]^{2+}$ and $[Os(bpy)_3]^{2+}$ in $[Zn(bpy)_3](ClO_4)_2$ in the region of high-frequency modes. Sidelines attributed to bpy are shaded in the top trace. Spectra were normalized with respect to the electronic origin. The intensities in the lower two traces are multiplied as indicated.

than the luminescence decay. Complex decay kinetics (non-single exponentials) would occur if the intramolecular transfer rate was comparable to or slower than the decay rate of the excited state.

Table 3 summarizes some lifetime data for $[Ru(bpy)_2(bpz)]^{2+}$, $[Ru(bpy\text{-}d_8)_2(bpz)]^{2+}$ and $[Ru(bpy)_{3-x}(bpy\text{-}d_8)_x]^{2+}$ (x = 0–3) in $[Zn(bpy)_3](ClO_4)_2$. The substantial increase of the lifetime observed for the bpz localized ^{3}MLCT emission in the $[Ru(bpy)_2(bpz)]^{2+}/[Zn(bpy)_3](ClO_4)_2$ system upon deuteration of the bpy ligands indicates that the high frequency spectator ligand modes are contributing significantly to the non-radiative deactivation process (Riesen *et al.* 1996a).

Correspondingly, the lifetime of the bpy localized ^{3}MLCT emission in both the $[Ru(bpy)_2(bpy\text{-}d_8)]^{2+}$ and the $[Ru(bpy)(bpy\text{-}d_8)_2]^{2+}$ complexes show an increase

Table 3. Luminescence lifetimes of $[Ru(bpy)_2(bpz)]^{2+}$, $[Ru(bpy\text{-}d_8)_2(bpz)]^{2+}$ and the series $[Ru(bpy)_{3-x}(bpy\text{-}d_8)_x]^{2+}$ in $[Zn(bpy)_3](ClO_4)_2$ (x = 0–3) at 1·8 K.

	Equivalent position		Distinct position	
$[Ru(bpy)_2(bpz)]^{2+}$	128 μs		142 μs	
$[Ru(bpy\text{-}d_8)_2(bpz)]^{2+}$	158 μs		186 μs	
$[Ru(bpy)_{3-x}(bpy\text{-}d_8)_x]^{2+}$	x = 0	x = 1	x = 2[a]	x = 3
	232 μs	248 μs	285 μs (I-d_8) 265 μs (I-h_8)	326 μs

[a] The lifetime was measured at the wavelengths of both origins I-d_8 and I-h_8 as noted.

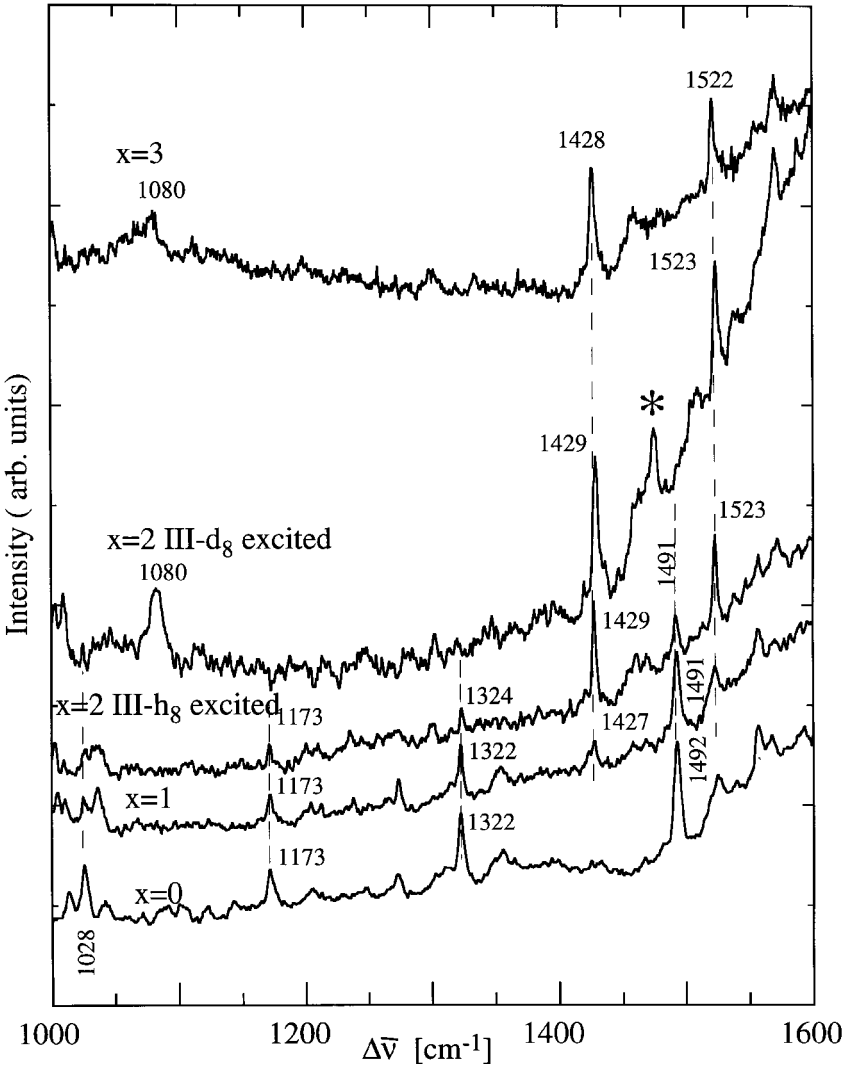

Figure 48. High frequency vibrational sidelines in the luminescence of the series $[Ru(bpy)_{3-x}(bpy\text{-}d_8)_x]^{2+}/[Zn(bpy)_3](ClO_4)_2$. The * in the III-$d_8$ excited x = 2 spectrum denotes a sideline which is based upon I-h_8.

compared to the perprotonated complex. The vibrational coupling of the ligand which is *directly* involved in the ^{3}MLCT emission can be expected to be higher than that of the spectator ligands. This differentiation is indeed observed. In the $[Ru(bpy)(bpy\text{-}d_8)_2]^{2+}$ system, the ^{3}MLCT emission of the bpy-d_8 ligand has a longer lifetime than the ^{3}MLCT emission of the bpy ligand.

The vibrational coupling in the non-radiative processes is related to the coupling of sidelines in the luminescence.

6. Intramolecular ^{3}MLCT excitons in $[Os(bpy)_3]^{2+}$

The ^{3}MLCT transitions are more intense in osmium(II) diimine complexes than in the ruthenium analogues. This is a consequence of the substantially higher spin–orbit coupling in the osmium(II) systems, which strongly admixes singlet character into the triplet state. As a consequence larger excitation exchange interactions are encountered in the lowest-excited states of these complexes. The spectroscopy of osmium(II) diimine complexes in crystals can be well described by the intramolecular exciton formalism outlined in section 2.

6.1. $[Os(bpy)_3]^{2+}$ *in* $[Ru(bpy)_3](PF_6)_2$

The $[Os(bpy)_{3-x}(bpy\text{-}d_8)_x]^{2+}$ series (x = 0 to 3) doped in $[Ru(bpy)_3](PF_6)_2$ is particularly interesting since the value of the excitation exchange interaction β is of the same order of magnitude as the inhomogeneous width of the electronic origins (Riesen *et al.* 1995c). The deuteration shift Δ is substantially larger (≈ 30 cm^{-1}) than β ($-2{\cdot}3$ cm^{-1}). As a consequence, the lowest-energy ^{3}MLCT exciton level is localized on the protonated ligand(s) in the $x = 1$ and $x = 2$ systems. The schematic shown in figure 1 describes this series, but the sign of β has to be reversed.

The crystal structure of $[Ru(bpy)_3](PF_6)_2$ has three trigonal sites for the cation (see section 3.1). Figure 49 displays excitation and luminescence spectra of the lowest-energy site, labelled $\mathscr{V}$, for the series $[Os(bpy)_{3-x}(bpy\text{-}d_8)_x]^{2+}$ (x = 0 to 3) in this host for the region of the lowest-energy origin I. Origin I is split in the $x = 0$, $x = 3$ and $x = 1$ systems. The positions of the lowest-energy components of the $x = 1$ and $x = 2$ systems are close to those observed for the $x = 0$ system whereas the pattern of the $x = 3$ system is similar to that of the $x = 0$ system, but shifted by ≈ 32 cm^{-1} to higher energy. The lowest-excited states in the $x = 1$ and $x = 2$ systems are localized on the protonated ligand(s). If the excitation exchange interaction was larger than the deuteration shift, the spectral pattern would remain unchanged in the series $x = 0$ to $x = 3$ with a gradual shift to higher energy of the lowest-energy origins.

In the $x = 0$ and $x = 3$ systems the second feature of origin I is ≈ 7 cm^{-1} higher in energy. The oscillator strength of this transition is far higher than that of the lowest-energy component. In the $x = 1$ system the second feature lies 5 cm^{-1} higher in energy and is about half as intense as the lowest-energy component, when observed in excitation. In luminescence and excitation spectra of the $x = 2$ system only one feature is observed in the region of origin I.

Intensities and energy spacings of these transitions are well accounted for by the exciton description given in equations (1)–(7) (see also figure 1). The two components of origin I in the $x = 0$ and $x = 3$ systems are transitions to the A and $E_\pm$ exciton levels. For site $\mathscr{V}$ the splitting between these two components is $\approx 3\beta = -7$ cm^{-1} ($\beta \approx -2{\cdot}3$ cm^{-1}). As in the ruthenium(II) systems, most of the ^{3}MLCT intensity is polarized in the metal–ligand plane. The transition to the lowest-energy component of origin I of the $x = 0$ or $x = 3$ system is far weaker than the component at higher

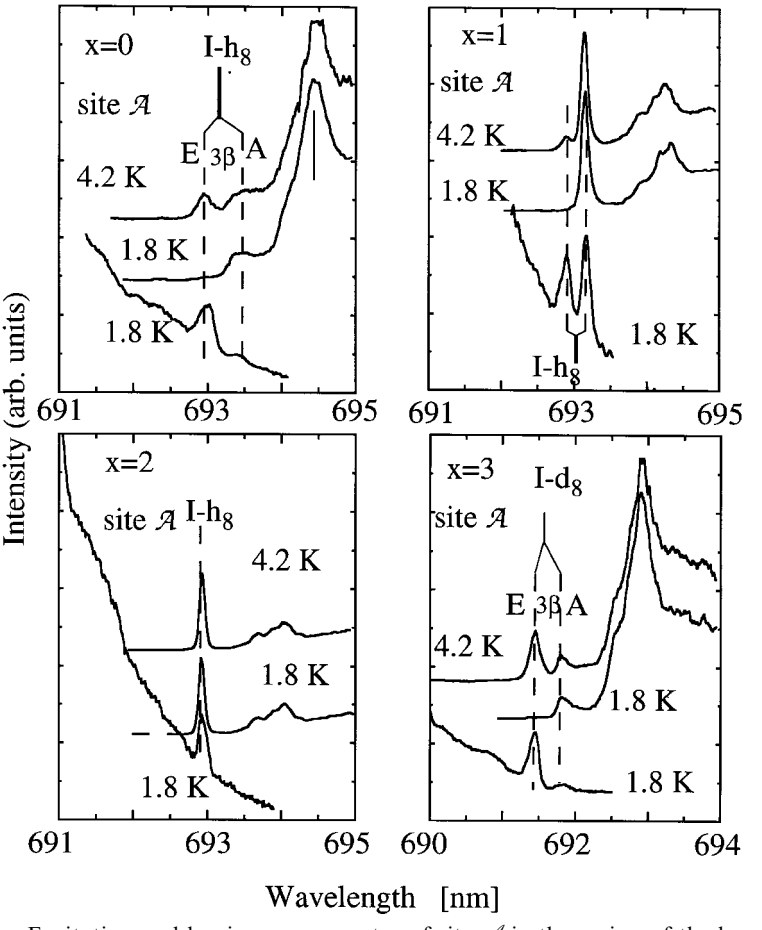

Figure 49. Excitation and luminescence spectra of site $\mathscr{A}$ in the region of the lowest-energy electronic origins of $[Os(bpy)_{3-x}(bpy\text{-}d_8)_x]^{2+}$ (x = 0–3) in $[Ru(bpy)_3](PF_6)_2$. The exciton splittings are indicated for the x = 0, 1 and 3 systems.

energy. This determines the ordering of the levels. The A level is lower than the E level, independently of the direction of the transition dipole within the metal–ligand plane. The residual intensity of the A level has been attributed to the nanoheterogeneity of the ligands, which for most cations breaks their threefold symmetry (Riesen *et al.* 1995c).

The splitting of origin I in the x = 1 system can be calculated by using equation (5). Inserting a value of $\beta = -2{\cdot}3\ cm^{-1}$ and a deuteration shift of 32 cm^{-1}, as determined experimentally for site $\mathscr{A}$ of the x = 0, x = 3 systems, a splitting of 4·9 cm^{-1} is calculated. This is in quantitative agreement with the experiment. From the eigenvectors of equation (5) an intensity ratio of 3:1 is predicted for the two components when the transition dipole moments are in the metal–ligand plane and perpendicular to the metal–ligand direction. If the transition dipole moment was polarized parallel the metal-to-ligand direction the corresponding intensity ratio would be reversed (1:3). The observed ratio of $\approx$ 2:1 corresponds to the transition dipole moments being predominantly perpendicular to the metal ligand direction. Nanoheterogeneity breaks the twofold symmetry of the exciton and thus will influence this ratio. Higher order perturbations will also affect the relative intensities. For

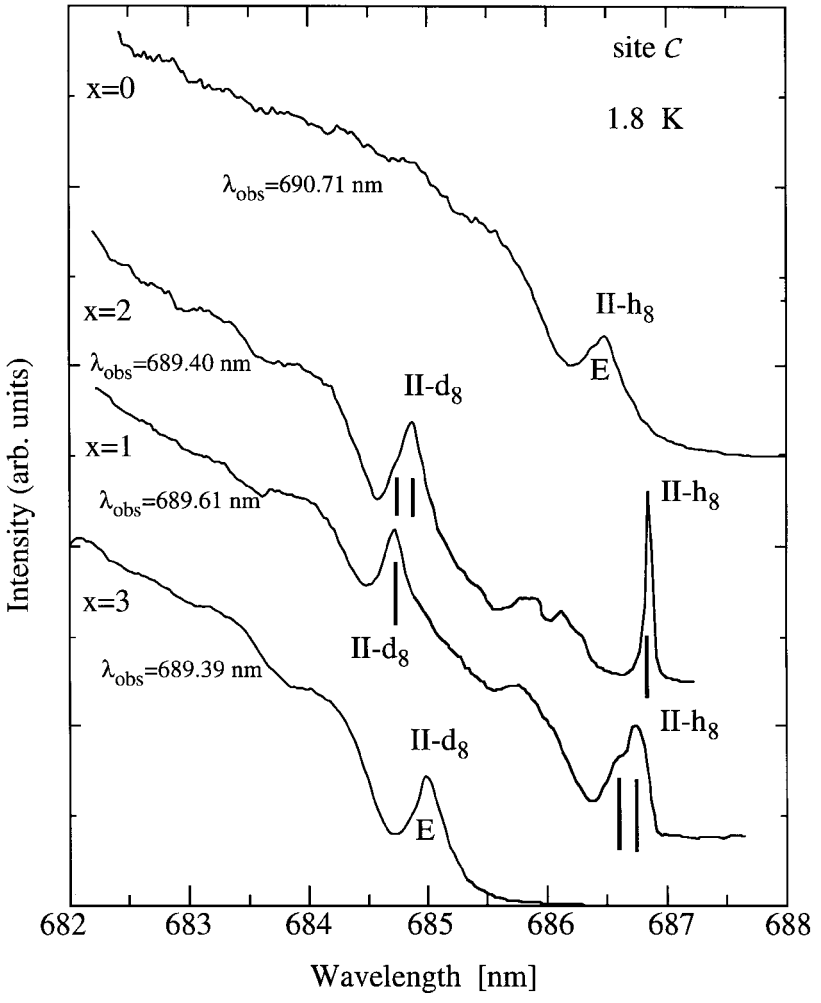

Figure 50. Excitation spectra of site $\mathscr{C}$ of $[Os(bpy)_{3-x}(bpy\text{-}d_8)_x]^{2+}$ (x = 0–3) in $[Ru(bpy)_3](PF_6)_2$ in the region of the origin II. Exciton splittings are indicated by bars for II-h_8 (x = 1) and II-d_8 (x = 2).

example, our model does not take into account the interaction of the lowest-energy exciton with higher lying levels.

The situation for the lowest-energy excitation of the x = 2 system becomes very simple (see figure 1). The excitation is localized on the protonated ligand and thus a single feature is observed in excitation and luminescence for the region of origin I. This localized feature shows strong narrowing in laser selective excitation and luminescence experiments. The behaviour of the intramolecular excitons in the x = 0, x = 3 and x = 1 systems in line narrowing experiments is characteristically different as is discussed below.

The negative sign for β excludes a simple dipole–dipole coupling mechanism (Riesen *et al.* 1995c). Exchange interactions associated with the overlap of electronic wavefunctions may provide a mechanism for the coupling of either sign as has been discussed for triplet excitons in aromatic crystals (Craig and Sommer 1973).

In figure 50 excitation spectra are shown for the highest-energy site $\mathscr{C}$ for the series

$x = 0$ to $x = 3$ in the region of origin II. The $x = 1$ and $x = 2$ systems show a superposition of independent origin features associated with the bpy (II-h_8) and bpy-d_8 (II-d_8) ligand(s). This again shows that the excitation exchange interaction β is substantially smaller than the deuteration shift. The ratio of integrated intensities of II-h_8:II-d_8 is $\approx 2:1$ in the $x = 1$ system and $\approx 1:2$ in the $x = 2$ system. These ratios reflect the number of protonated and deuterated ligands in the two systems. The ^{3}MLCT transitions II-h_8 and II-d_8 to the bpy-h_8 and bpy-d_8 ligand(s) are independent.

Origin II-h_8 in the $x = 1$ system shows a shoulder at ≈ 4 cm^{-1} higher in energy whereas the corresponding origin (II-h_8) in the $x = 2$ system consists of a single line. Excitation into this latter transition leads to substantial narrowing of origin I-h_8. Correspondingly, origin II-h_8 is substantially narrowed in non-resonant excitation line experiments, in which luminescence is selectively monitored within the inhomogeneously broadened origin I-h_8.

Origin II-d_8 shows a single feature for the $x = 1$ system and a shoulder at higher energy for the $x = 2$ system. The I-d_8 origin in the $x = 1$ and $x = 2$ systems is obscured by origin II-h_8, which is approximately 130 times more intense. However, origin I-d_8 can still be identified in carefully measured excitation spectra in these systems.

From a least-squares fit of two Gaussians to the line shape of transition II-h_8 in the $x = 1$ system of site $\mathscr{C}$ (see figure 50) we obtain an intensity ratio between the two components of $\approx 2:1$. The splitting is 4 cm^{-1} and thus β in level II is close to that in level I.

The lowest excited level in the $x = 2$ system is localized on the protonated ligand. When excited in the II-h_8 transition the excitation energy remains on the *same* metal–ligand subunit and thus strong narrowing is observed. Energies on the same metal–ligand subunit are well correlated. The $x = 0$ and $x = 3$ systems show little narrowing of the components of origin I when excited into the $E_\pm$ component of origin II. This is a consequence of the nanoheterogeneity which gives rise to static diagonal disorder in equation (5) (Riesen *et al.* 1995c).

In figure 51 some Stark experiments performed on the $x = 2$ and $x = 3$ systems are shown. In the $x = 2$ system the lowest-excited state is localized on the one protonated ligand. The protonated ligand can be in any of the three orientations relative to the external electric field. The origin I-h_8 of orientation (k) in figure 51 is unaffected by the electric field. In orientations (i) and (j) origin I-h_8 shifts to higher and lower energy, respectively. The non-selectively excited luminescence spectrum in the electric field is then a sum of these three independent spectra. The narrowed luminescence spectra shown in figure 51 were non-resonantly excited within the corresponding Stark structure of origin II-h_8. These spectra establish that I-h_8 and II-h_8 are well correlated. Furthermore, a single narrowed feature is observed for all excitation wavelengths within the Stark affected II-h_8 transition. Excitation into the high energy side of II-h_8 in the field predominantly excites orientation (i) and so forth. These results provide further evidence that the excitation is localized on the bpy-h_8 ligand in the lowest-excited state of this system.

The calculated spectrum for the $x = 2$ system was synthesized by adding three zero field spectra which were shifted by $\pm 4{\cdot}5$ cm^{-1} and 0 cm^{-1}, respectively. The $\pm 4{\cdot}5$ cm^{-1} shift corresponds to a Stark shift of $0{\cdot}052$ cm^{-1}/(kV cm^{-1}) or $0{\cdot}7$ eÅ (Riesen *et al.* 1995c).

The simulated spectrum for the $x = 3$ system in the external electric field was obtained by adding the Stark term δ_0 to the diagonal of equation (5). To account for the effects of nanoheterogeneity equation (5) was diagonalized for independent

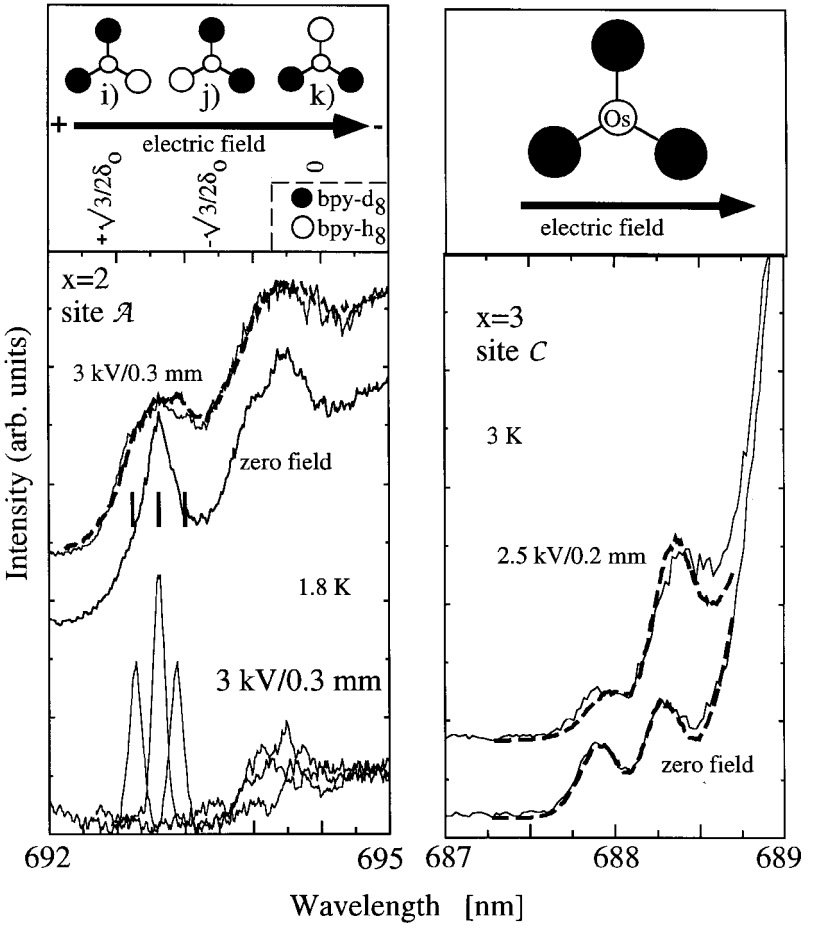

Figure 51. Stark effects in the lowest electronic origins of site $\mathcal{A}$ of $[Os(bpy)(bpy\text{-}d_8)_2]^{2+}$ and of site $\mathcal{C}$ of $[Os(bpy\text{-}d_8)_3]^{2+}$ in $[Ru(bpy)_3](PF_6)_2$ at low temperatures. The dashed lines are calculated (see text). Stark energies are given for the three orientations of the Os-bpy subunit in the $x = 2$ system. Spectra shown at the bottom of the left panel were non-resonantly narrowed via II-h_8 excitation.

energies ε_i described by an appropriate Gaussian distribution. The resulting spectra were accumulated and scaled with zero field parameters (Riesen *et al.* 1995c). Convergence is obtained after $\approx$ 20000 accumulations and reasonable agreement with the experiment is obtained. It follows from an analysis of the eigenvectors that the electric field partially localizes the intramolecular excitons in the $x = 0$ and $x = 3$ systems since the excitation exchange interaction is relatively small. The Stark parameter $\delta_0 = 0{\cdot}052\ cm^{-1}/(kV\ cm^{-1})$ is somewhat smaller than that $(0{\cdot}09 \pm 0{\cdot}01\ cm^{-1}/(kV\ cm^{-1}))$ observed for $[Ru(bpy)_3]^{2+}$ doped in $[Zn(bpy)_3](ClO_4)_2$.

6.2. $[Os(bpy)_3]^{2+}$ *in* $[Zn(bpy)_3](ClO_4)_2$ *and* $[Ru(bpy)_3](ClO_4)_2$

The spectroscopy of this series can be rationalized in terms of the one site C2/c crystal structure of the host. Again, charge transfer transitions to the distinct ligand are significantly higher in energy (see section 4). The $[Os(bpy)_{3-x}(bpy\text{-}d_8)_x]^{2+}$ complexes with $x = 1$ and $x = 2$ can enter the $[Zn(bpy)_3](ClO_4)_2$ or the $[Ru(bpy)_3](ClO_4)_2$ host in

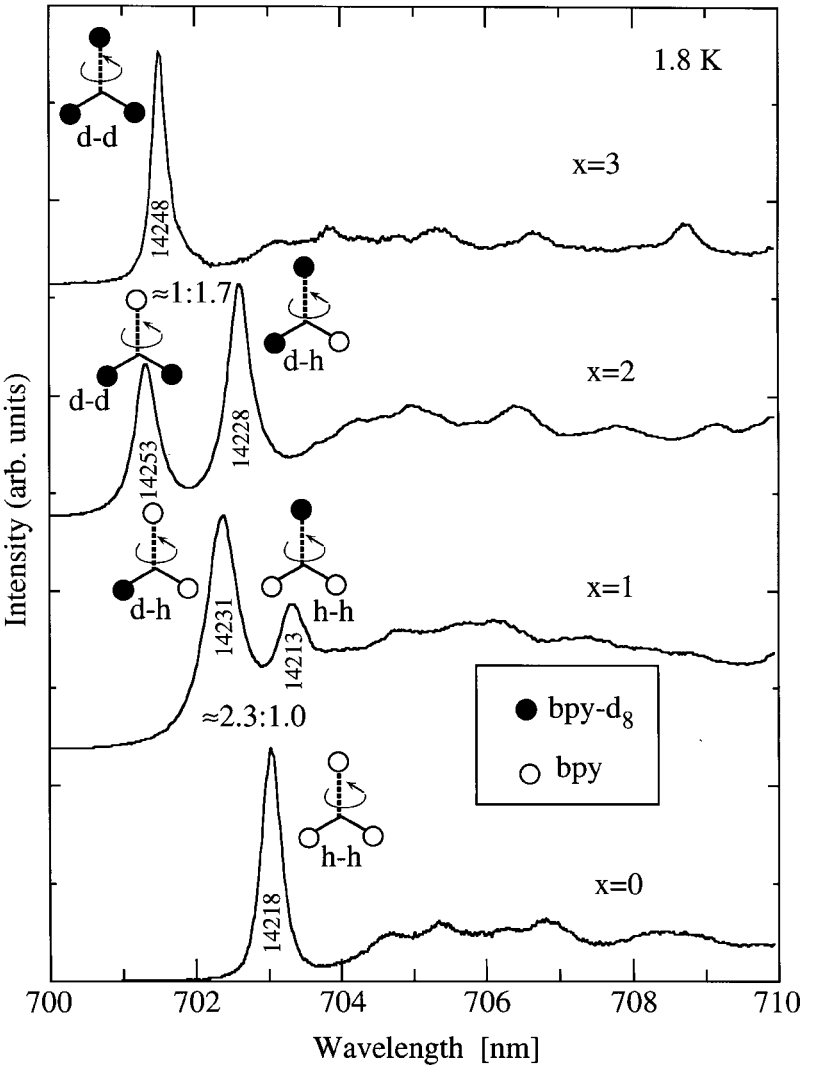

Figure 52. Luminescence spectra in the region of the electronic origins of the series $[Os(bpy)_{3-x}(bpy\text{-}d_8)_x]^{2+}$ (x = 0 to 3) in $[Zn(bpy)_3](ClO_4)_2$. The origins in the x = 1, 2 systems are assigned to the two possible orientations.

the two ways shown in figure 11. In an incomplete report Huber and Yersin (1993) incorrectly interpreted spectra in terms of a number of crystallographically distinct sites.

In figure 52 the non-selectively excited luminescence spectra of the series in the $[Zn(bpy)_3](ClO_4)_2$ host are shown in the region of the electronic origins at 1·8 K. The same pattern is also observed in the $[Ru(bpy)_3](ClO_4)_2$ host (Riesen *et al.* 1996b) in accord with an isomorphism of the crystal structures of the salts. The x = 3 and x = 0 spectra show one electronic origin with a deuteration shift of $\approx$ 30 cm^{-1}. The x = 1 and x = 2 systems show *two* electronic origins. These two origins arise from the two ways by which the x = 1 and x = 2 complexes can enter the lattice. The species which have no, one or two bpy-d_8 ligand(s) in the crystallographically equivalent positions are labelled as h-h, d-h and d-d respectively.

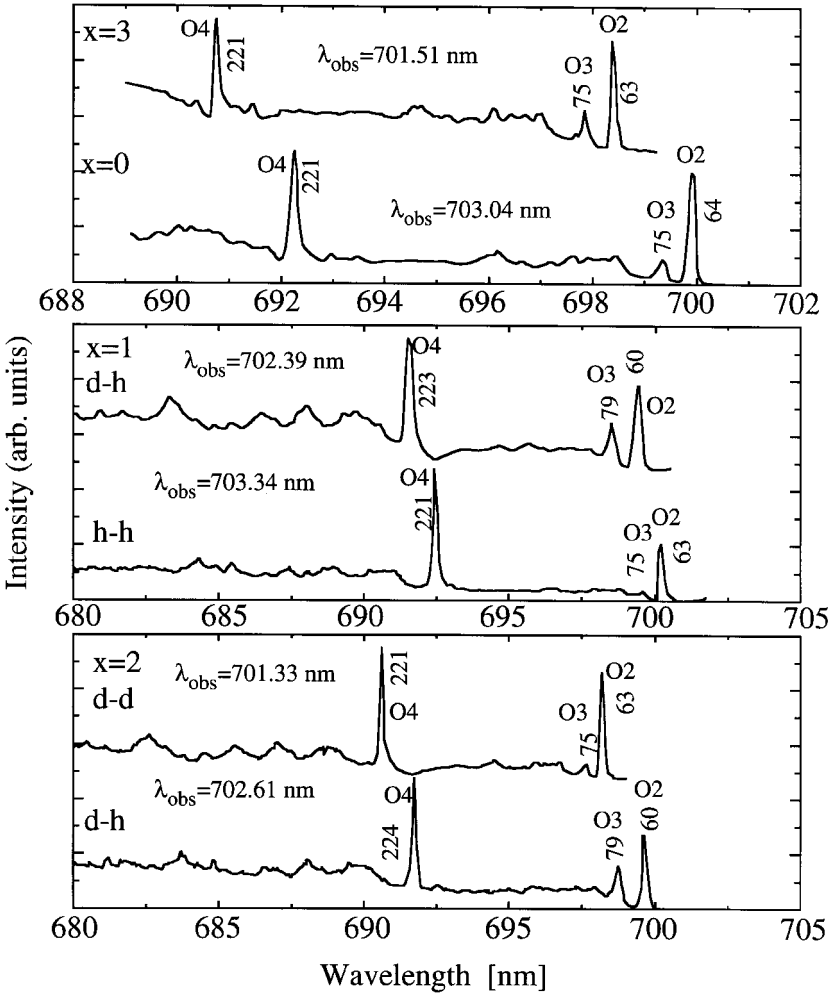

Figure 53. Narrowed excitation spectra of the series $[Os(bpy)_{3-x}(bpy\text{-}d_8)_x]^{2+}$ (x = 0 to 3) in $[Zn(bpy)_3](ClO_4)_2$ at 1·8 K. Electronic origins are denoted O2, O3 and O4. Shifts relative to O1 are indicated in cm^{-1}.

The d-h species has its lowest-energy origin about halfway between those of the h-h and d-d species (see section 2). Hence it follows that the excitation exchange interaction must be at least of the same order of magnitude as the deuteration shift. The observed intensity ratios of $\approx$ 1:2·5 for h-h:d-h in the x = 1 system and $\approx$ 1·3:2 for d-d:d-h in the x = 2 systems, relate to the probabilities of h-h, d-h, and d-d species in the lattice. Deviations from the ideal ratios of 1:2 and 2:1 are attributed to variations in quantum efficiencies arising from deuteration.

Selective excitation spectra obtained for the series $[Os(bpy)_{3-x}(bpy\text{-}d_8)_x]^{2+}$ (x = 0 to 3) doped in $[Zn(bpy)_3](ClO_4)_2$ are shown in figure 53. The spectral pattern in the $[Ru(bpy)_3](ClO_4)_2$ host is identical but with a small red shift of $\approx$ 60 cm^{-1}. Four origins can be identified in the luminescence and excitation spectra. They are labelled O1, O2, O3 and O4 (Riesen and Krausz 1995, Riesen *et al.* 1996b).

The spectroscopy of the series can be understood in terms of the exciton formalism outlined in section 2. The phenomenology in the hexafluorophosphate and the

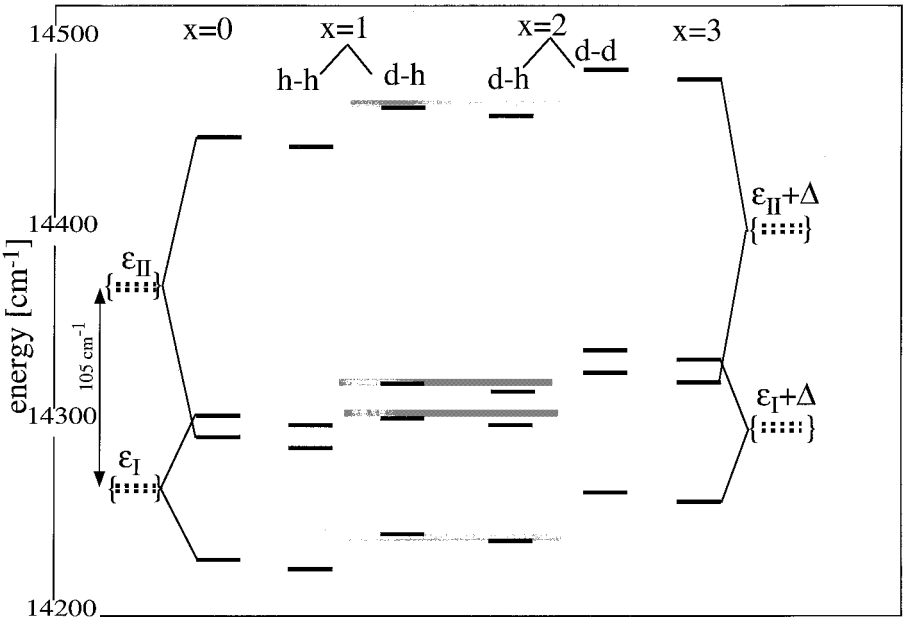

Figure 54. Summary of the electronic levels in the series $[Os(bpy)_{3-x}(bpy\text{-}d_8)_x]^{2+}$ in $[Zn(bpy)_3](ClO_4)_2$. The dashed levels ε_i are the baricentres of Davidov components. The shaded bars indicate calculated energies for the d-h configuration in the $x = 1$ and $x = 2$ systems. These calculations are based on parameters obtained from the $x = 0$ and $x = 3$ systems.

perchlorate lattices is very different. This is a consequence of the inequivalence of the ligands and the larger excitation exchange interaction in the perchlorate hosts. Polarized absorption spectra indicate that origins O2 and O4 are the Davidov components of the second electronic level, II (Riesen *et al.* 1996b). Polarizations and the intensity ratio of O2:O4 = 1:3 are in agreement with the model in section 2. The excitation exchange interaction $\beta \approx 79\ cm^{-1}$ and $\beta \approx 77\ cm^{-1}$ for level II in the $[Zn(bpy)_3](ClO_4)_2$ and the $[Ru(bpy)_3](ClO_4)_2$ hosts, respectively. Origins O3 and O1 are correspondingly assigned to the Davidov components of the lowest level, I. The excitation coupling is somewhat weaker in level I with $\beta \approx 37{\cdot}5\ cm^{-1}$ for both the perdeuterated and perprotonated complexes in the $[Zn(bpy)_3](ClO_4)_2$ and $[Ru(bpy)_3](ClO_4)_2$ hosts.

Assignments are supported by the prediction of splittings in the $x = 1$ and $x = 2$ systems. This is done by inserting the experimentally determined coupling constants and a deuteration shift of $32\ cm^{-1}$ into equation (10). A splitting of $81\ cm^{-1}$ is calculated for level I of the d-h species in the $x = 1$ and $x = 2$ systems. Predictions for level II in the d-h species are $161\ cm^{-1}$ and $157\ cm^{-1}$ in the $[Zn(bpy)_3](ClO_4)_2$ and the $[Ru(bpy)_3](ClO_4)_2$ lattices respectively. These values are in reasonable agreement with the experimentally observed spacings of $79\ cm^{-1}$ for level I in both lattices and of $163\ cm^{-1}$ and $159\ cm^{-1}$ in level II in the $[Zn(bpy)_3](ClO_4)_2$ and $[Ru(bpy)_3](ClO_4)_2$ hosts, respectively. The overall pattern is summarized in figure 54.

In a more rigorous approach, excitation exchange interactions between level I and level II have to be taken into account as well as the coupling to ^{3}MLCT excitations of the third ligand. Higher order perturbations may be responsible for the extra intensity of origin O3. The excitation exchange interaction is of the same order of magnitude as

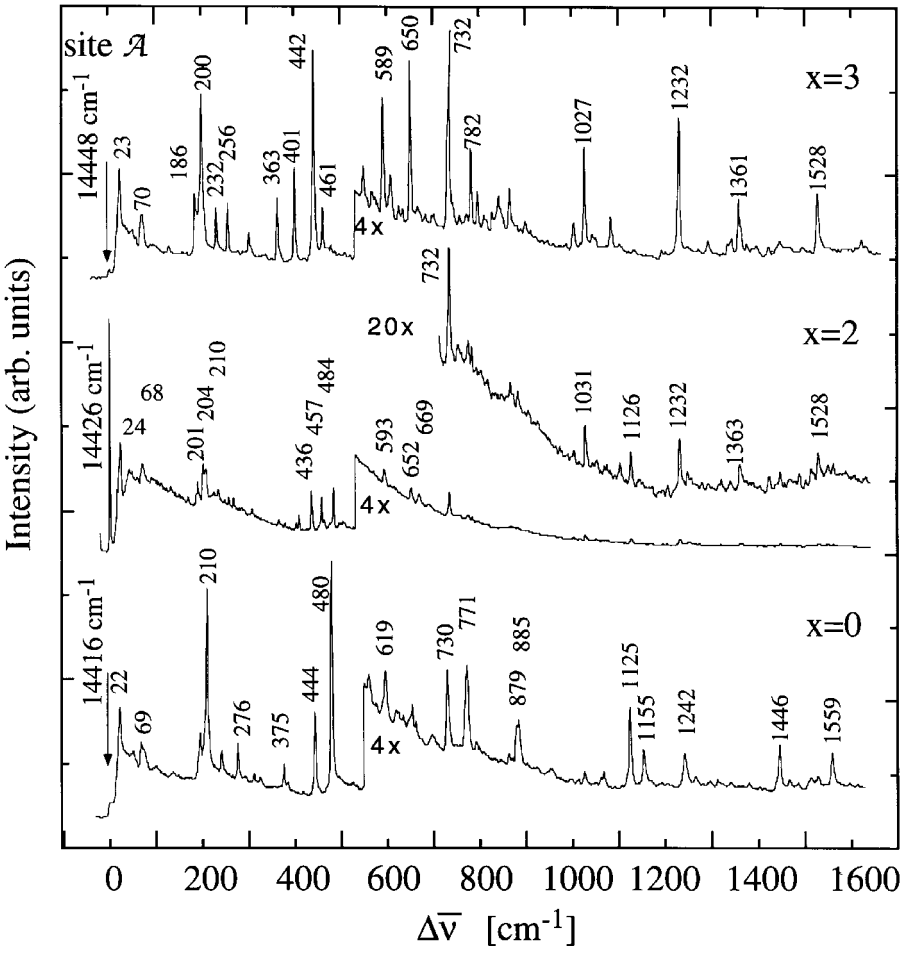

Figure 55. Comparison of the vibrational sidelines in selectively excited luminescence spectra of $[Os(bpy)(bpy\text{-}d_8)_2]^{2+}$, $[Os(bpy\text{-}d_8)_3]^{2+}$ and $[Os(bpy)_3]^{2+}$ in $[Ru(bpy)_3](PF_6)_2$ at 1·8 K.

the deuteration shift. The critical consequence is that origins of the d-h species are predicted to be about halfway between the origins of the h-h and d-d species. This is indeed observed.

6.3. *Vibrational sidelines in the luminescence*

In figure 55 the selectively excited luminescence spectrum of the lowest-energy site $\mathscr{X}$ of the $[Os(bpy)(bpy\text{-}d_8)_2]^{2+}/[Ru(bpy)_3](PF_6)_2$ system is compared with the spectra of perprotonated and perdeuterated complexes in the same host. Although the lowest-excited level in the $x = 2$ system is localized on the bpy-h_8 ligand, vibrational sidelines are observed which are due to modes of the bpy-d_8 ligand. However, the coupling of the deuterated and the protonated modes is not proportional to the number of protonated and deuterated ligands. The bpy-d_8 spectator ligands are less coupled. For instance the ≈ 480 cm^{-1} mode associated with the bpy-h_8 ligand subunit is the strongest sideline feature in the $x = 2$ system.

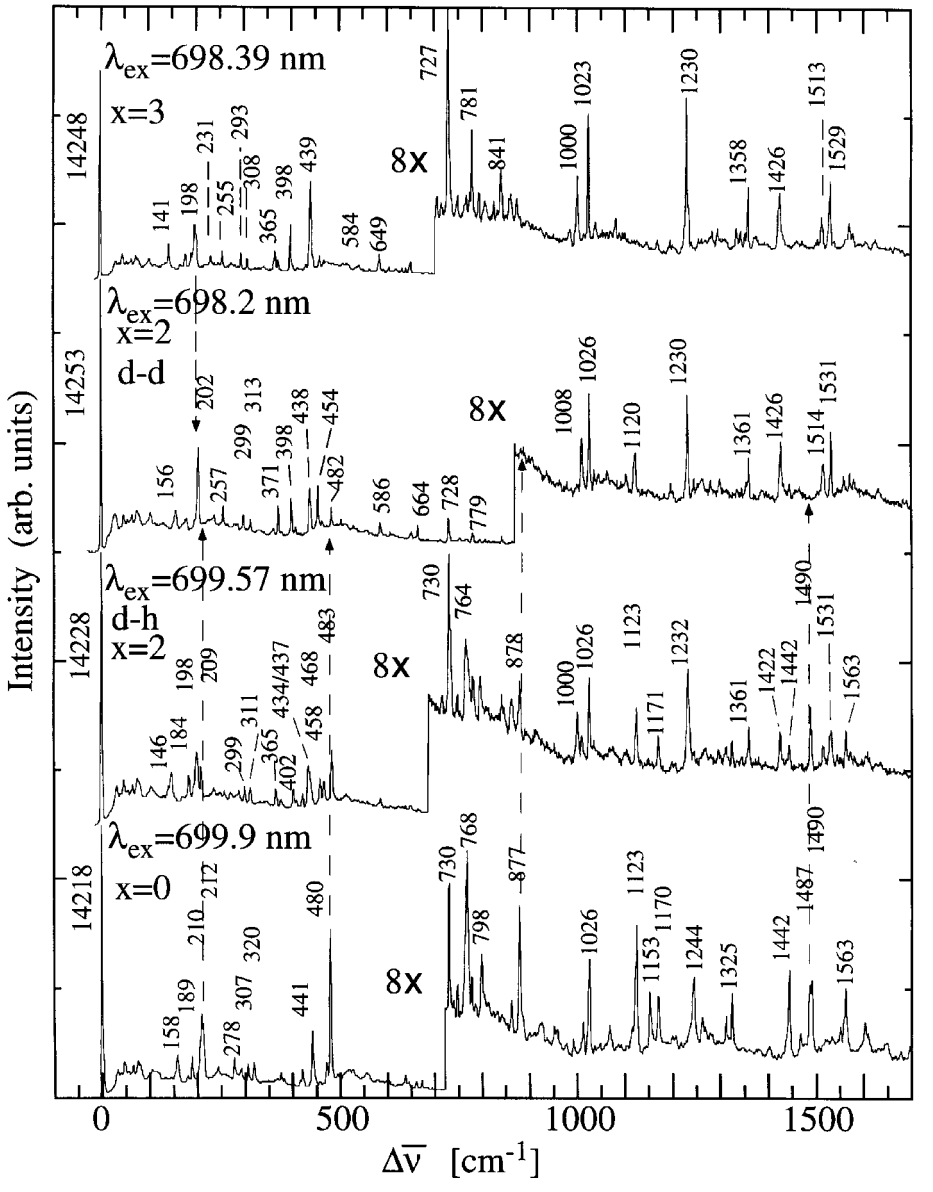

Figure 56. Selectively excited (d-h and d-d) luminescence of $[Os(bpy)(bpy\text{-}d_8)_2]^{2+}$ (x = 2) in $[Zn(bpy)_3](ClO_4)_2$ at 1·8 K in comparison with narrowed luminescence spectra of the x = 0 and x = 3 systems.

Figure 56 presents selectively excited luminescence spectra for the $[Os(bpy)(bpy\text{-}d_8)_2]^{2+}/[Zn(bpy)_3](ClO_4)_2$ system. In this case the lowest-energy exciton is not fully localized by the specific deuteration. A stronger coupling of bpy-h_8 and bpy-d_8 modes in the d-h and d-d emissions respectively, is observed in accord with our assignment of species. As is the case for the corresponding ruthenium(II) systems, the 1490 cm^{-1} bpy-h_8 mode is not evident for the x = 2 complexes which enter the lattice with the bpy-d_8 in the crystallographically equivalent positions. This lack of intensity may be associated with the C2 symmetry of the distinct position as is discussed in section 5.8.

7. Conclusions

The transferred charge in the lowest-excited ^{3}MLCT states of $[Ru(bpy)_3]^{2+}/[Zn(bpy)_3](ClO_4)_2$ and $[Ru(bpy)_3](PF_6)_2$ is localized. The excitation exchange interaction β between metal–ligand subunits in these and related ruthenium(II) diimine systems is less than $\approx 0{\cdot}5\ cm^{-1}$. This value is significantly smaller than the lowest inhomogeneous widths of $\approx 3\ cm^{-1}$. Hence, the static diagonal disorder in equation (5), arising from nanoheterogeneity of the ligands, is much larger than the excitation exchange interaction. Time resolved luminescence line narrowing experiments facilitate direct measurements of the stochastic intramolecular ^{3}MLCT excitation transfer rate.

The appearance of vibrational sidelines associated with spectator ligand(s) cannot, *a priori*, be used as evidence for delocalization or localization. For example, bpy modes are observed in the emission of the $[Ru(bpy)_2(bprid)]^{2+}$ and the $[Ru(bpy)_2(bpz)]^{2+}$ complexes doped in $[Zn(bpy)_3](ClO_4)_2$, although the lowest-excited ^{3}MLCT state is localized on the bprid or the bpz ligands, respectively. The vibrational coupling of the spectator ligand(s) arises as the metal core changes oxidation state in the charge transfer process.

The $[Os(bpy)_3]^{2+}$ complex shows an intramolecular exciton coupling which varies substantially between the $[Ru(bpy)_3](PF_6)_2$ and $[M(bpy)_3](ClO_4)_2$ (M = Ru, Zn) lattices. In the former lattice, which has trigonal symmetry, the excitation exchange interaction β in the lowest-energy levels is $\approx -2\ cm^{-1}$. This excitation exchange interaction leads to Davidov splittings that are comparable to the inhomogeneous width of the electronic origins. Thus the lowest-energy excitations are excitons and involve all three ligands although the coherence, defined in equation (8), is relatively low. Selective deuteration localizes the lowest-excited ^{3}MLCT state on the bpy-h_8 ligand(s) in the $[Os(bpy)_2(bpy\text{-}d_8)]^{2+}$ and $[Os(bpy)(bpy\text{-}d_8)_2]^{2+}$ complexes since the deuteration shift is $\approx 30\ cm^{-1}$.

In the perchlorate salts, substantially larger excitation exchange interactions between the two crystallographically equivalent ligands are observed. As a consequence, partial deuteration does not localize the lowest-energy excitons. In these lattices the coherence of the intramolecular mini-exciton is relatively high. The lowest-excited levels are excitations which involve both crystallographically equivalent ligands.

We have shown that a simple electric dipole–dipole mechanism cannot account for the observed $\beta = -2{\cdot}3\ cm^{-1}$ in the hexafluorophosphate host (Riesen *et al.* 1995c). Nevertheless, there appears to be a scaling of the excitation exchange interaction with the oscillator strength of the transitions involved. The oscillator strengths of the lowest-energy ^{3}MLCT origins in the perchlorate salts are significantly higher than in the hexafluorophosphate crystal.

The charge transfer nature of the lowest excited states is established by Stark measurements which provide, for the first time, excited state dipole moments.

A clear description of the ^{3}MLCT states in metal diimine systems evolves from systematic studies of deuteration and ligand substitution effects, laser line narrowing, transient spectral hole-burning, Stark and Zeeman experiments on the electronic origins. This description encompasses not only overall patterns but subtle details as well.

Acknowledgments

We thank Professor D. P. Craig for his interest in this work and for many valuable suggestions. H. R. thanks the Australian Research Council for a Research Fellowship.

References

Biner, M., Bürgi, H.-B., Ludi, A., and Röhr, C., 1992, *J. Am. chem. Soc.*, **114**, 5197.

Botter, B. J., Nonhof, C. J., Schmidt, J., and van der Waals, J. H., 1976, *Chem. Phys. Lett.*, **43**, 210.

Bradley, P. G., Kress, N., Hornberger, B. A., Dallinger, R. F., and Woodruff, W. H., 1981, *J. Am. chem. Soc.*, **103**, 7441.

Braun, D., Gallhuber, E., Hensler, G., and Yersin, H., 1989, *Molec. Phys.* **67**, 417.

Braun, D., Gallhuber, E., and Yersin, H., 1990, *Chem. Phys. Lett.*, **171**, 122.

Broude, V. L., Rashba, E. I., and Sheka, E. F., 1985, *Spectroscopy of Molecular Excitons* (Berlin: Springer-Verlag).

Burland, D. M., and Zewail, A. H., 1979, *Advances in Chemical Physics*, Vol. 40, edited by I. Prigogine and S. Rice (New York: Wiley), p. 369.

Caroll, P. J., and Brus, L. E., 1987, *J. Am. chem. Soc.*, **109**, 7613.

Caspar, J. V., Westmoreland, T. D., Allen, G. H., Bradley, P. G., Meyer, T. J., and Woodruff, W. H., 1984, *J. Am. chem. Soc.*, **106**, 3492.

Colombo, M. G., Zilian, A., and Güdel, H. U., 1991, *J. Lumin.*, **48 & 49**, 549.

Constable, E. C., Raithby, P. R., and Smit, D. N., 1989, *Polyhedron*, **8**, 367.

Constable, E. C., and Seddon, K. R., 1982, *J. chem. Soc. chem. Comm.*, 34.

Craig, D. P., and Sommer, B.-Sheva, 1973, *Chem. Phys. Lett.*, **22**, 239.

Craig, D. P., and Walmsley, S. H., 1968, *Excitons in Molecular Crystals*, (New York: W. A. Benjamin).

Crutchley, R. J., and Lever, A. B. P., 1982, *Inorg. Chem.*, **21**, 2276.

Danzer, G. D., and Kincaid, J. R., 1990, *J. phys. Chem.*, **94**, 3976.

Danzer, G. D., Golus, J. A., and Kincaid, J. R., 1993, *J. Am. chem. Soc.*, **115**, 8643.

Davidov, A. S., 1962, *Theory of Molecular Excitons* (New York: McGraw-Hill).

DeArmond, M. K., and Carlin, C. M., 1981, *Coord. chem. Rev.*, **36**, 325.

Dhenaut, C., Ledoux, I., Samuel, I. D. W., Zyss, J., Bourgault, M., and Le Bozec, H., 1995, *Nature*, **374**, 339.

Downey, T. M., and Nieman, T. A., 1992, *Anal. Chem.* **64**, 261.

Ferguson, J., Herren, F., Krausz, E. R., Maeder, M., and Vrbanich, J., 1985, *Coord. Chem. Rev.*, **64**, 21.

Forster, M., and Hester, R. E., 1981, *Chem. Phys. Lett.*, **81**, 42.

Frei, G., Zilian, A., Raselli, A., Güdel, H. U., and Bürgi, H.-B., 1992, *Inorg. Chem.*, **31**, 4766.

Friedrich, J., and Haarer, D., 1984, *Angew. Chem. Int. Ed.*, **23**, 113.

Gex, J. N., DeArmond, M. K., and Hanck, K. W., 1987, *Inorg. Chem.*, **26**, 3235.

Glasbeek, M., and Giesbergen, C., 1996, *J. Lumin.*, **66 & 67**, 236.

Glynn, S. P., Azumi, T., and Kinoshita, M., 1969, *Molecular Spectroscopy of the Triplet State* (Englewood Cliffs: Prentice Hall).

Grätzel, M., 1991, *Comments Inorg. Chem.*, **12**, 93.

Harrowfield, J. M., and Sobolev, A. N., 1994, *Aust. J. Chem.*, **47**, 763.

Huber, P., and Yersin, H., 1993, *J. phys. Chem.*, **97**, 12705.

Høg, J. H., Ballhausen, C. J., and Solomon, E. I., 1976, *Molec. Phys.*, **32**, 807.

Juris, A., Balzani, V., Barigelletti, F., Campagna, S., Belser, P., and von Zelewsky, A., 1988, *Coord. chem. Rev.*, **84**, 95.

Kalyanasundaram, K., 1982, *Coord. chem. Rev.*, **46**, 159.

Kato, M., Yamauchi, S., and Hirota, N., 1989, *J. phys. Chem.*, **93**, 3422.

Kitamura, N., Kawanishi, Y., and Tazuke, S., 1983, *Chem. Phys. Lett.*, **97**, 103.

Komada, Y., Yamauchi, S., and Hirota, N., 1986, *J. phys. Chem.*, **90**, 6425.

Krause, R. A., 1987, *Struct. Bond.*, **67**, 1.

Krausz, E., 1987, *Chem. Phys. Lett.*, **135**, 249.

Krausz, E., and Ferguson, J., 1989, *Prog. Inorg. Chem.*, **37**, 293.

Krausz, E., Riesen, H., and Rae, A. D., 1995, *Aust. J. Chem.*, **48**, 929.

Macfarlane, R. M., and Shelby, R. M., 1987, *Spectroscopy of Solids Containing Rare Earth Ions*, edited by A. A. Kaplyanskii and R. M. Macfarlane (Amsterdam: Elsevier), p. 51.

Malone, R. A., and Kelley, D. F., 1991, *J. chem. Phys.*, **95**, 8970.

McClanahan, S., and Kincaid, J., 1984, *J. Raman Spectrosc.*, **15**, 173.

Meyer, T. J., 1984, *Prog. Inorg. Chem.*, **30**, 389.

MOERNER, W. (editor), 1988, *Persistent Spectral Hole-Burning: Science and Applications*, Topics in Current Physics, Vol. 44 (Berlin: Springer).

MURAMATO, T., NAKANISHI, S., and HASHI, T., 1977, *Optics Commun.*, **21**, 139.

OCHS, F. W., PRASAD, P. N., and KOPELMAN, R., 1974, *Chem. Phys.*, **6**, 253.

OH, D. H., and BOXER, S. G., 1989, *J. Am. chem. Soc.*, **111**, 1130.

OH, D. H., SANO, M., and BOXER, S. G., 1991, *J. Am. chem. Soc.*, **113**, 6880.

POGGE, J. L., and KELLEY, D. F., 1995, *Chem. Phys. Lett.*, **238**, 16.

RICHTER, M. M., SCOTT, B., BREWER, K. J., and WILLETT, R. D., 1991, *Acta crystallogr.*, **C47**, 2443.

RIESEN, H., and KRAUSZ, E., 1988, *Chem. Phys. Lett.*, **151**, 71; 1992, *J. chem. Phys.*, **97**, 7902; 1993a, *Comments Inorg. Chem.*, **14**, 323; 1993b, *J. chem. Phys.*, **99**, 7614; 1993c, *Chem. Phys. Lett.*, **212**, 347; 1994a, *J. Lumin.*, **58**, 176; 1994b, *Chem. Phys. Lett.*, **217**, 613; 1995, *Excitonic Processes in Condensed Matter*, Proc. SPIE, Vol. 2362, edited by Jai Singh (Bellingham, WA: SPIE), p. 408; 1996a, *J. Lumin.*, **66&67**, 496; 1996b, *Chem. Phys. Lett.*, **260**, 130.

RIESEN, H., GAO, Y., and KRAUSZ, E., 1994a, *Chem. Phys. Lett.*, **228**, 610.

RIESEN, H., KRAUSZ, E., and PUZA, M., 1988, *Chem. Phys. Lett.*, **151**, 65.

RIESEN, H., RAE, A. D., and KRAUSZ, E., 1994b, *J. Lumin.*, **62**, 123.

RIESEN, H., WALLACE, L., and KRAUSZ, E., 1994c, *Chem. Phys. Lett.*, **228**, 605 (note that the phen transitions in figure (4.c) of this work are incorrectly labelled (I-phen is not visible): correct labelling is shown in figure 26 of the present work); 1995a, *Chem. Phys.*, **198**, 269; 1995b, *J. phys. Chem.*, **99**, 16807; 1995c, *J. chem. Phys.*, **102**, 4823; 1996a, *J. phys. Chem.*, **100**, 4390; 1996b, *Molec. Phys.*, **87**, 1299; 1996c, *J. phys. Chem.*, **100**, 17138.

RILLEMA, D. P., ALLEN, G., MEYER, T. J., and CONRAD, D., 1983, *Inorg. Chem.*, **22**, 1617.

RILLEMA, D. P., JONES, D. S., and LEVY, H. A., 1979, *J. chem. Soc. chem. Commun.*, 849.

SHOEMAKER, R. L., 1979, *Ann. Rev. Phys. Chem.*, **30**, 239.

SMOTHERS, W. K., and WRIGHTON, M. S., 1983, *J. Am. chem. Soc.*, **105**, 1067.

SOLOMON, E. I., BALLHAUSEN, C. J., and HØG, J. H., 1975, *Chem. Phys. Lett.*, **34**, 222.

STRIPLIN, D. R., and CROSBY, G. A., 1994, *Chem. Phys. Lett.*, **221**, 426.

STROMMEN, D. P., MALLICK, P. K., DANZER, G. D., LUMPKIN, R. S., and KINCAID, J. R., 1990, *J. phys. Chem.*, **94**, 1357.

VÖLKER, S., 1989, *Ann. Rev. Phys. Chem.*, **40**, 499.

WALLACE, L., 1996, unpublished results.

YAMAUCHI, S., KOMADA, Y., and HIROTA, N., 1986, *Chem. Phys. Lett.*, **129**, 197.

YEN, W. M., and SELZER, P. M. (editors), 1981, *Laser Spectroscopy of Solids*, *Topics in Applied Physics*, Vol. 49 (Berlin: Springer).

YERSIN, H., GALLHUBER, E., HENSLER, G., and SCHWEITZER, D., 1989, *Chem. Phys. Lett.*, **161**, 315.

ZEWAIL, A. H., SMITH, D. D., and LEMAISTRE, J.-P., 1982, *Excitons*, edited by E. I. Rashba and M. D. Sturge (Amsterdam: North-Holland), p. 665.